

KNOTS AND CHAOS IN THE RÖSSLER SYSTEM

ERAN IGRA

ABSTRACT. The Rössler System is one of the best known chaotic dynamical systems, exhibiting a plethora of complex phenomena - and yet, only a few studies tackled its complexity analytically. In this paper we find sufficient conditions for the existence of chaotic dynamics for the Rössler System at some specific parameter values at which the flow satisfies a certain heteroclinic condition. This will allow us to prove the existence of infinitely many periodic trajectories for the flow, and study their bifurcations in the parameter space of the Rössler system.

Keywords - The Rössler Attractor, Chaos Theory, Heteroclinic bifurcations, Topological Dynamics

1. INTRODUCTION

In 1976, Otto E. Rössler introduced the following system of Ordinary Differential Equations, depending on parameters $A, B, C \in \mathbf{R}^3$ [5]:

$$\begin{cases} \dot{X} = -Y - Z \\ \dot{Y} = X + AY \\ \dot{Z} = B + Z(X - C) \end{cases} \quad (1.1)$$

Inspired by the Lorenz attractor (see [1]), Otto E. Rössler attempted to find the simplest non-linear flow exhibiting chaotic dynamics. This is realized by the vector field above, as it has precisely one non-linearity, XZ in the \dot{Z} component. In more detail, the flow generated by the vector field above models the stretch-and-fold operation of a taffy machine (see [8]) - and as observed by Rössler, the vector field appears to generate a chaotic attractor for $(A, B, C) = (0.2, 0.2, 5.7)$. In more detail, at these parameter values Rössler observed the first return map of the flow has the shape of a horseshoe (i.e., numerically), which is known to be chaotic (see [3]).

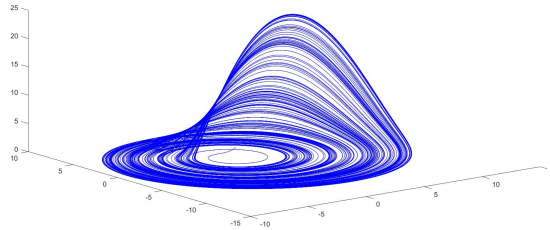


FIGURE 1. The Rössler attractor at $(A, B, C) = (0.2, 0.2, 5.7)$

Since its introduction in 1976, the Rössler system was the focus of many numerical studies - despite the simplicity of the vector field, the flow gives rise to many non-linear phenomena (see, for example: [30], [25], [23], [27], [26]). One particular feature is that varying the parameters A, B, C often leads to a change in the complexity of the system: that is, as the parameters are varied, more and more symbols appear in the first-return map of the flow (for more details, see [30], [25],[14],[28]). In a topological context, several numerical studies noted this variation of parameters changes the topology of the attractor - see, for example, [14],[28].

In contrast to the vast corpus of numerical studies, analytical results on the Rössler system are sparse. For example, in [17], the existence of periodic trajectories at some parameters was established; in [29] the existence of an invariant Torus (and its breakdown) at some parameters was proven; and in [24] the dynamics of the flow at ∞ were analyzed. As far as chaotic dynamics go, their existence at $(A, B, C) = (0.2, 0.2, 5.7)$ was proven with rigorous numerical methods - see [15],[22]. To our knowledge, no studies on the Rössler system attempted to prove its nonlinear phenomena (and in particular, its chaotic dynamics) by analytical tools. It is precisely this gap that this paper aims to address. In this paper we prove analytically, for the first time, sufficient conditions for the existence of complex dynamics in the Rössler system.

To state our main results, given parameter values $p = (A, B, C)$, denote by F_p the corresponding vector field which generates the flow. We first prove the following result about the global dynamics of the Rössler system in Section 2 (see Lemma 2.7 and Th.2.8):

Theorem 1.2. *There exists an open set of parameters $O \subseteq \mathbf{R}^3$ s.t. F_p can be extended to a vector field on S^3 with precisely three fixed points - two saddle-foci P_{In}, P_{Out} (of opposing indices) and a degenerate fixed point at ∞ of index 0. Moreover, both P_{In}, P_{Out} admit heteroclinic trajectories connecting them to ∞ .*

As can be seen, Th.1.2 does not provide us with constraints on the flow which force the existence of complex dynamics. As such, in order to analytically describe the dynamics of the Rössler system we study the dynamics of the Rössler system at a very specific parameter values $p \in P$ - to which we refer as **trefoil parameters** (for the precise formulation, see Def.3.2).

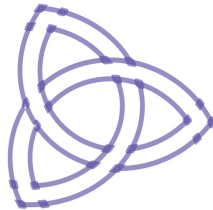


FIGURE 2. A trefoil knot type.

Roughly speaking, trefoil parameters are parameter values (A, B, C) for which the Rössler system generates a heteroclinic trefoil knot Λ in the 3-sphere S^3 , whose knot type is that of the trefoil (see Fig.2). In particular, at trefoil parameters the Rössler system generates a bounded heteroclinic trajectory as in Fig.19 - the existence of such heteroclinic knots for the Rössler system was observed numerically (see Fig.5.B.1 in [30]). Motivated and inspired by both the topology of $S^3 \setminus \Lambda$ and by Th.1 in [19], using Th.1.2 and the Betsvina-Handel Algorithm (see [13]), we prove the following fact in Section 3 (see Th.3.15 in Sect.3):

Theorem 1.3. *Let (A, B, C) be a trefoil parameter. Then, the corresponding Rössler system generates a bounded invariant set in \mathbf{R}^3 , Q , which includes infinitely many periodic trajectories for the flow.*

Once Th.1.3 is proven, we apply it to analyze the dynamical complexity of the flow in and around trefoil parameters. Inspired by [15] and using both Th.1.3 and a Fixed-Point Index argument, we prove the following Theorem in Section 4 (see Th.4.4):

Theorem 1.4. *Let $p = (A, B, C)$ be a trefoil parameter, and choose some $n > 0$. Then, provided $v = (A', B', C')$ is sufficiently close to p , the Rössler system corresponding to v generates at least n -distinct periodic trajectories.*

Theorem 1.4 has the following meaning - the closer a parameter v is to a trefoil parameter p , the more complex are its dynamics. With these ideas in mind, we must remark that when the parameter space of the Rössler system was analyzed numerically, spiral bifurcation structures were observed (see, for example [30], [25], [23] and [27]). In all these studies, these spiral structures always accumulated at some point p_0 , often referred to as a **periodicity hub**, which lies on the Shilnikov homoclinic curve (see [2]). As was observed in [26] (see pg. 430), the dynamics around some periodicity hubs may, in fact, be heteroclinic. This suggests Th.1.3 and 1.4 possibly have a part in explaining the emergence of such complex bifurcation phenomena.

Finally, we also stress that even though our results all relate to the Rössler system, in practice the arguments in Section 3 and 4 are mostly topological. As such, they exemplify the potential of topological methods for explaining the emergence of nonlinear phenomena. Moreover, our results also attest to the importance of bounded heteroclinic trajectories to the emergence of chaotic and complex dynamics in three-dimensional flows. In more detail, it is well-known that heteroclinic trajectories generate chaotic dynamics in the Lorenz system (see, for example, the results of [31] and the references therein). As such, this study and [31] lend further credence to the role of heteroclinic knots in the onset of complex dynamics.

PRELIMINARIES

From now on, given $(a, b, c) \in \mathbf{R}^3$ we switch to the more convenient form of the Rössler system, defined by the following system of ODEs:

$$\begin{cases} \dot{x} = -y - z \\ \dot{y} = x + ay \\ \dot{z} = bx + z(x - c) \end{cases} \quad (1.5)$$

Denote the vector field corresponding to $(a, b, c) \in \mathbf{R}^3$ by $F_{a,b,c}$. This definition is slightly different from the one presented in Eq.1.1 - however, setting $p_1 = \frac{-C + \sqrt{C^2 - 4AB}}{2A}$, it is easy to see that whenever $C^2 - 4AB > 0$, $(X, Y, Z) = (x - ap_1, y + p_1, z - p_1)$ defines a change of coordinates between the vector fields in Eq.1.1 and Eq.1.5.

Before we continue, we introduce the following definition for chaotic dynamics:

Definition 1.1. Chaotic Dynamics Let F be a C^∞ vector field on \mathbf{R}^3 . We say F is **chaotic** or **generates chaotic dynamics** provided there exists a bounded set $B \subseteq \mathbf{R}^3$ which includes infinitely periodic trajectories.

For example, as proven in Th.1.1 in [31], there exist parameter values for which the Lorenz system is chaotic.

Since the vector field in Eq.1.5 depends on three parameters, (a, b, c) , we now specify the region in the parameter space in which we prove our results. The parameter space $P \subseteq \mathbf{R}^3$ we consider throughout this paper is composed of parameters satisfying the following:

- **Assumption 1** - for every parameter $p \in P, p = (a, b, c)$ the parameters satisfy $a, b \in (0, 1)$ and $c > 1$. For every choice of such p , the vector field F_p given by Eq.1.5 always generates precisely two fixed points - $P_{In} = (0, 0, 0)$ and $P_{Out} = (c - ab, b - \frac{c}{a}, \frac{c}{a} - b)$.
- **Assumption 2** - for every $p \in P$ the fixed points P_{In}, P_{Out} are both saddle-foci of opposing indices. In more detail, we always assume that P_{In} has a one-dimensional stable manifold, W_{In}^s , and a two-dimensional unstable manifold, W_{In}^u . Conversely, we always assume P_{Out} has a one-dimensional unstable manifold, W_{Out}^u , and a two-dimensional stable manifold, W_{Out}^s (see the illustration in Fig.7).
- **Assumption 3** - For every $p \in P$, let $\gamma_{In} < 0$ and $\rho_{In} \pm i\psi_{In}, \rho_{In} > 0$ denote the eigenvalues of $J_p(P_{In})$, the linearization of F_p at P_{In} , and set $\nu_{In} = |\frac{\rho_{In}}{\gamma_{In}}|$. Conversely, let $\gamma_{Out} > 0, \rho_{Out} \pm i\psi_{Out}$ s.t. $\rho_{Out} < 0$ denote the eigenvalues of $J_p(P_{Out})$, the linearization at P_{Out} , and define $\nu_{Out} = |\frac{\rho_{Out}}{\gamma_{Out}}|$. We will refer to ν_{In}, ν_{Out} as the respective saddle indices at P_{In}, P_{Out} , and we will always assume $(\nu_{In} < 1) \vee (\nu_{Out} < 1)$ - that is, for every $p \in P$ at least one of the fixed points satisfies the Shilnikov condition.

It is easy to see the parameter space P we are considering is open in the parameter space. In addition, it includes the parameter space for the Rössler system considered in [25],[30] and [23], where many interesting bifurcation phenomena were observed.

In addition, we will also need several results and notions from the theory of two-dimensional surface homeomorphisms. To begin, let D denote a planar disc. Until the end of this section, S would always denote a surface homeomorphic to $D \setminus \{x_1, \dots, x_n\}$, where x_1, \dots, x_n are interior to D and $n \geq 2$. Additionally, $f : S \rightarrow S$ would always denote a homeomorphism which permutes the set $\{x_1, \dots, x_n\}$. We first introduce the following definition:

Definition 1.2. A homeomorphism $f : S \rightarrow S$ is **Pseudo-Anosov** provided there exist two foliations of S , F^u and F^s , transverse to one another throughout S (but not necessarily at the punctures $\{x_1, \dots, x_n\}$ - see the illustration in Fig.3) and some $\lambda > 0$ s.t. the following is satisfied:

- Both F^s and F^u are measured - i.e., if we move some leaf L_1 of F^i to another leaf L_2 of F^i by some isotopy of S (where $i \in \{u, s\}$), the Borel measure on L_2 is the pushforward of the Borel measure on L_1 .
- $f(F^u) = \lambda F^u$ while $f(F^s) = \frac{1}{\lambda} F^s$ - i.e., f stretches uniformly the unstable foliation F^u and squeezes uniformly the stable foliation F^s . We refer to λ as the **expansion constant**.

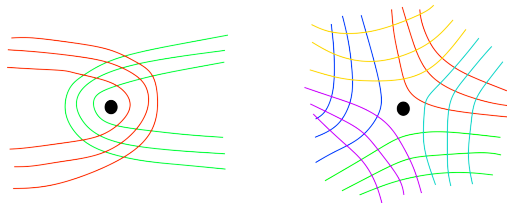


FIGURE 3. Transverse foliations (with singularities) around the punctures of S (i.e. the black discs).

Pseudo-Anosov maps are essentially a generalized form of hyperbolic diffeomorphisms, like Smale's Horseshoe (see [3]) - that is, they contract uniformly in one direction, and expand uniformly in another. The reason we are interested in Pseudo-Anosov maps is because as far as their dynamics are concerned, we have the following result (see Th.7.2 in [12]):

Theorem 1.6. Let $f : S \rightarrow S$ be Pseudo-Anosov - then, the periodic orbits are dense in S .

That is, Pseudo-Anosov maps satisfy a discrete-time version of Def.1.1. In addition, Pseudo-Anosov maps are dynamically minimal in the following sense - if $f : S \rightarrow S$ is a homeomorphism isotopic to a Pseudo-Anosov map $F : S \rightarrow S$, then the dynamics of F are complex at least like those of F . More precisely, we have the following result proven as Th.2 and Remark 2 in [11]:

Theorem 1.7. *Let $F : S \rightarrow S$ be a Pseudo-Anosov map and let $f : S \rightarrow S$ be a homeomorphism isotopic to F . Then, there exists a closed set $Y \subseteq S$ and a continuous, surjective $\pi : Y \rightarrow S$ s.t. $\pi \circ f = F \circ \pi$.*

We are now led to the following question - given a homeomorphism $f : S \rightarrow S$, when is it isotopic to a Pseudo-Anosov map? To introduce the answer to that question, we must first introduce several concepts. We begin with the notion of a spine:

Definition 1.3. *The **spine** of S is a graph Γ embedded in \bar{S} with $n - 1$ vertices and $n - 2$ edges s.t. Γ is a retract of S (see the illustration in Fig.4).*

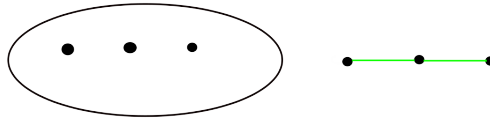


FIGURE 4. *On the left we have a surface S homeomorphic to D punctured at 3 points, and on the right we have its spine, the graph Γ . As can be seen, Γ has two edges and three vertices.*

Now, let us consider a graph map $g : \Gamma \rightarrow \Gamma$, and let us denote by S_1, \dots, S_{n-2} the edges of Γ (see the illustration in Fig.4). We now define a matrix $A = \{a_{i,j}\}_{1 \leq i,j \leq n-2}$ s.t. $a_{i,j}$ is the number of times $g(S_j)$ covers S_i . Finally, let us define the **spectral radius** of A as the maximal eigenvalue for A - and let us further note that since A is a matrix with positive coefficients, its spectral radius is also positive. To continue, note that given a homeomorphism $f : S \rightarrow S$, by retracting S to its spine Γ with edges S_1, \dots, S_{n-2} we can reduce f to a graph map $g : \Gamma \rightarrow \Gamma$, as described in Fig.5. As a consequence, there exists a matrix A generated by g as described above, with a spectral radius γ . Then, we have the following fact, proven in Sections 3.4 and 4.4 of [13]:

Theorem 1.8. *With the notations above, whenever $\gamma > 1$ f is isotopic to a Pseudo-Anosov map $F : S \rightarrow S$. Moreover, if there exists an edges S_i s.t. $g(S_i)$ covers itself at least twice (for some $1 \leq i \leq n - 2$), the dynamics of f in the regions in S collapsed to S_i includes periodic orbits of all minimal periods.*

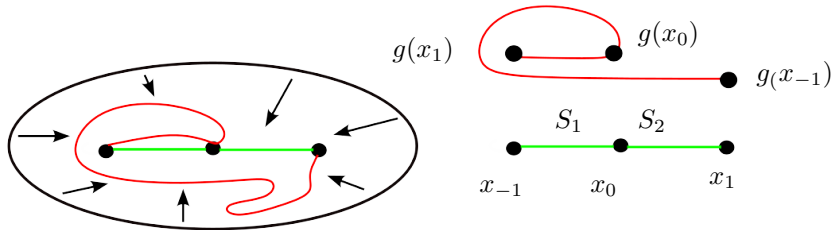


FIGURE 5. *f distorts the graph Γ inside S into the red curve, s.t. $f(x_{-1}) = x_1$, $f(x_1) = x_{-1}$ and $f(x_1) = x_1$ (while the outer circle remains fixed). Consequentially, $g(S_1)$ covers itself twice.*

2. THE GLOBAL DYNAMICS OF THE RÖSSLER SYSTEM.

In this section we perform basic qualitative analysis of the Rössler system for parameters (a, b, c) in the parameter space P - thus establishing certain key facts which will be used throughout this paper. This section is organized as follows: we first consider a cross-section for the flow given by $\{\dot{y} = 0\}$, and study the local dynamics on it. Following that, we study the unbounded dynamics of the flow, and prove Th2.8 (i.e., Th.1.2 from the introduction), with which we conclude this section.

To begin, fix some parameter $p = (a, b, c) \in P$ and recall we denote the vector field generating the corresponding Rössler system by F_p (see Eq.1.5). Now, consider the plane $\{(x, -\frac{x}{a}, z) | x, z \in \mathbf{R}\} = \{\dot{y} = 0\}$, and let $N_p = (1, a, 0)$ denote the normal vector to $\{\dot{y} = 0\}$ (with the velocity \dot{y} taken w.r.t. F_p - see Eq.1.5). By direct computation of the product $F_p(x, -\frac{x}{a}, z) \bullet N_p$ we see F_p is tangent to $\{\dot{y} = 0\}$ precisely at the straight line $l_p = \{(t, -\frac{t}{a}, z) | t \in \mathbf{R}\}$.

Hence, $\{\dot{y} = 0\} \setminus l_p$ consists of two components, both half-planes - let $U_p = \{(x, -\frac{x}{a}, z) | x, z \in \mathbf{R}, -z + \frac{x}{a} < 0\}$ denote the upper half of $\{\dot{y} = 0\} \setminus l_p$, and denote by $L_p = \{(x, -\frac{x}{a}, z) | x, z \in \mathbf{R}, -z + \frac{x}{a} > 0\}$ the lower half (see the illustration in Fig.6).

By the definition of the regions $\{\dot{y} > 0\} = \{(x, y, z) | x + ay > 0\}$, $\{\dot{y} < 0\} = \{(x, y, z) | x + ay < 0\}$ correspond to the regions in front and below $\{\dot{y} = 0\}$ (respectively - see Fig.6) - and by the sign of $F_p(x, -\frac{x}{a}, z) \bullet N_p$ on U_p and L_p we immediately conclude:

- On U_p , the vector field F_p points inside $\{\dot{y} < 0\}$ (see the illustration in Fig.6).
- On L_p , the vector field F_p points inside $\{\dot{y} > 0\}$ (see the illustration in Fig.6).

To continue, given an initial condition s , from now on we always denote its trajectory by γ_s - parameterized s.t. $\gamma_s(0) = s$. As l_p , the tangency set of F_p to $\{\dot{y} = 0\}$ is a straight line, we immediately conclude the following, useful fact:

Lemma 2.1. *Let $s \in \mathbf{R}^3$ be an initial condition that is not a fixed point, whose forward trajectory γ_s is bounded and does not limit to a fixed point - then, γ_s intersects U_p transversely infinitely many times. In particular, every periodic trajectory intersects U_p transversely at least once.*

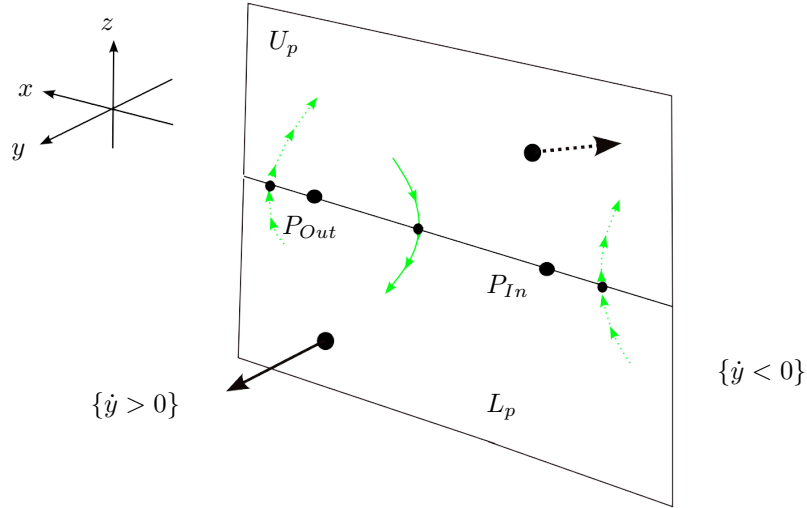


FIGURE 6. The plane $\{\dot{y} = 0\}$ and the cross sections U_p and L_p (and the directions of F_p on them), separated by l_p . The green arcs represent flow lines tangent to $\{\dot{y} = 0\}$ at different arcs on l_p - see Lemma 2.4.

Lemma 2.1 motivates us to introduce the following notations:

Definition 2.1. *From now on throughout the remainder of this dissertation, we always denote by $f_p : \overline{U_p} \rightarrow \overline{U_p}$ the first-return map - wherever defined in $\overline{U_p}$.*

By Lemma 2.1, f_p is defined at least at every initial condition $s \in U_p$ whose forward trajectory is both bounded and does not limit to a fixed point. Continuing in our analysis of the plane $\{\dot{y} = 0\}$, we now prove the following fact:

Lemma 2.2. *Let $p = (a, b, c)$ be some parameter value in P - then, the corresponding two dimensional, invariant manifolds W_{In}^u, W_{Out}^s are transverse to U_p, L_p at both P_{In}, P_{Out} (see the illustration in Fig.7).*

Proof. Let us first consider the tangent vector to the straight line l_p , the tangency curve of F_p to the plane $\{\dot{y} = 0\}$ - as we parameterize l_p by $l_p(x) = (x, -\frac{x}{a}, \frac{x}{a})$, $x \in \mathbf{R}$, the tangent vector to $l_p(x)$ is given $v = (1, -\frac{1}{a}, \frac{1}{a})$. Now, let us consider $J_p(P_{In})$, the Jacobian matrix of F_p at the fixed-point $P_{In} = (0, 0, 0)$, given by the following matrix (see Eq.1.5):

$$\begin{pmatrix} 0 & -1 & -1 \\ 1 & a & 0 \\ b & 0 & -c \end{pmatrix} \quad (2.3)$$

By direct computation, $J_p(P_{In})v = (0, 0, b - \frac{c}{a})$ - as $a, b \in (0, 1)$ and $c > 1$, it follows we always have $ab \neq c$, i.e., $b - \frac{c}{a} \neq 0$, which implies v is not an eigenvector for $J_p(P_{In})$. Let us now remark the plane $\{\dot{y} = 0\}$ is spanned by

$(1, -\frac{1}{a}, \frac{1}{a}) = \nu$ and $(0, 0, 1) = \mu$, and that similarly to the computation above, μ is also not an eigenvalue for $J_p(P_{In})$.

Generalizing these arguments, we now prove that given any non-zero $\nu \in \{\dot{y} = 0\}$, ν does not span an invariant subspace for $J_p(P_{In})$. To do so, recall that every $\nu \in \{\dot{y} = 0\}$ is parameterized by $\nu = (x, -\frac{x}{a}, z)$ (for some $x, z \in \mathbf{R}$). By computation, $J_p(P_{In})\nu = (-z + \frac{x}{a}, 0, bx + z(x - c))$ - which implies that whenever $x \neq 0$, ν is not an invariant direction for $J_p(P_{In})$. When $x = 0$ and $z \neq 0$ we have $\nu = (0, 0, z)$, and consequentially $J_p(P_{In})\nu = (-z, 0, -cz)$ - therefore, again, ν is not an invariant direction for $J_p(P_{In})$. Therefore, all in all, the plane $\{\dot{y} = 0\}$ does not include any invariant directions for the Jacobian matrix $J_p(P_{In})$.

Now, let W denote the two-dimensional unstable invariant subspace for $J_p(P_{In})$ in \mathbf{R}^3 . Recall that since P_{In} is a saddle-focus, W is spanned by the vectors $r_1 = \frac{\omega + \bar{\omega}}{2}$, $r_2 = \frac{\omega - \bar{\omega}}{2i}$, for some $\omega \in \mathbf{C}^3$ which is an eigenvector of $J_p(P_{In})$ (where $\bar{\omega}$ is the complex-conjugate vector to ω). It is easy to see both r_1, r_2 span eigenspaces for $J_p(P_{In})$, which, by the discussion above, implies $r_1, r_2 \notin \{\dot{y} = 0\}$. Consequentially, as W is spanned by r_1 and r_2 , we conclude W and $\{\dot{y} = 0\}$ are transverse to one another. Consequentially, as the two-dimensional unstable manifold W_{In}^u is tangent to W at P_{In} (see Th.2.7.1 in [21]) it follows W_{In}^u must be transverse to $\{\dot{y} = 0\}$ at P_{In} .

Similarly, by considering $J_p(P_{Out})$, the linearization of the saddle focus $P_{Out} = (c - ab, \frac{ab-c}{a}, \frac{c-ab}{a})$, using a similar argument it again follows $\{\dot{y} = 0\}$ does not include any invariant directions under $J_p(P_{Out})$ - therefore, a similar argument prove W_{Out}^s , the two-dimensional stable manifold of P_{Out} , is transverse to $\{\dot{y} = 0\}$ at P_{Out} and Lemma 2.2 now follows (see the illustration in Fig.7). \square

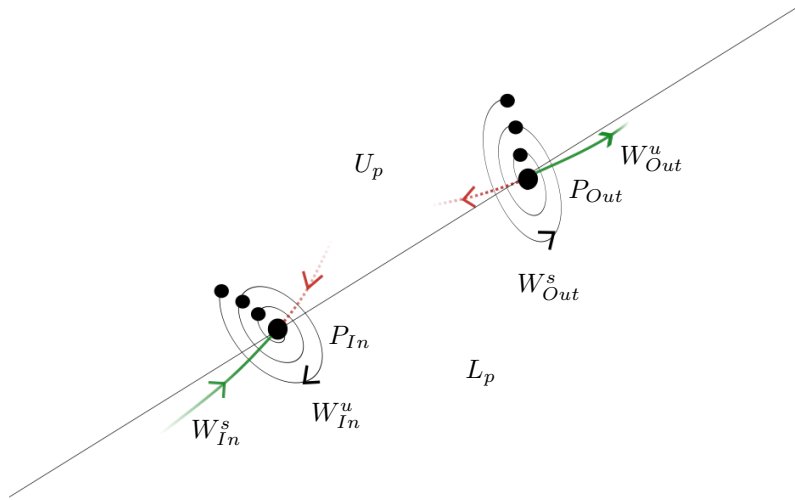


FIGURE 7. The local dynamics around the fixed points. The green and red flow lines are the components of W_{In}^s, W_{Out}^u .

Having proven the invariant manifolds W_{In}^u and W_{Out}^s are transverse to $\{\dot{y} = 0\}$ at the fixed points, we now study the local dynamics of F_p on the tangency line l_p . To do so, first recall that given any $s \in \mathbf{R}^3$, we denote by γ_s its trajectory, parameterized s.t. $\gamma_s(0) = s$ - and furthermore, recall we parameterize l_p by $l_p(x) = (x, -\frac{x}{a}, \frac{x}{a})$, where $x \in \mathbf{R}$. We now prove:

Lemma 2.4. *We have $l_p = \{\dot{x} = 0\} \cap \{\dot{y} = 0\}$. Additionally, given $s \in l_p$, we have the following:*

- For $x < 0$ and $x > c - ab$, there exists some $\epsilon > 0$ s.t. $\gamma_s(t) \in \{\dot{y} < 0\}$ for all $t \neq 0, t \in (-\epsilon, \epsilon)$ (see the illustration in Fig.6).
- Conversely, when $x \in (0, c - ab)$ there exists an $\epsilon > 0$ s.t. for $t \in (-\epsilon, \epsilon), t \neq 0$ we have $\gamma_s(t) \in \{\dot{y} > 0\}$ (see the illustration in Fig.6).

Proof. Note that given $p = (a, b, c)$ by Eq.1.5 we have $\dot{x} = -y - z, \dot{y} = x + ay$ (where $x, y, z \in \mathbf{R}$) - which implies $\{\dot{x} = 0\} \cap \{\dot{y} = 0\}$ is parameterized by the set $\{(x, -\frac{x}{a}, \frac{x}{a}) | x \in \mathbf{R}\}$, i.e., the intersection is given by the line l_p . By computation, we have $F_p(l_p(x)) = (0, 0, bx + \frac{x^2}{a} - \frac{cx}{a})$. Now, let us note $bx + \frac{x^2}{a} - \frac{cx}{a}$ is a quadratic polynomial vanishing precisely at P_{In}, P_{Out} - therefore $F_p(l_p(x))$ points in the positive z -direction precisely when $x < 0$ or $x > c - ab$ (conversely, it points in the negative z direction when $x \in (0, c - ab)$).

On U_p the vector field F_p points into $\{\dot{y} > 0\}$ (see the discussion preceding Lemma 2.1 and the illustration in Fig.6). Since U_p is the upper half-plane, it follows that for $x < 0$ or $x > c - ab$ the trajectory of $s = l_p(x)$ can only arrive at $l_p(x)$ from $\{\dot{y} < 0\}$ (the region behind $\{\dot{y} = 0\}$ in Fig.6). Therefore, by the tangency of F_p to the plane $\{\dot{y} = 0\}$ at s , it follows that forward-trajectory of s enters $\{\dot{y} < 0\}$ upon leaving s (as illustrated in Fig.6) - and it follows that whenever $x < 0$ or $x > c - ab$, there exists an $\epsilon > 0$ (depending on s) s.t. $\gamma_s(t) \in \{\dot{y} < 0\}$ for all $t \neq 0, t \in (-\epsilon, \epsilon)$.

When $x \in (0, c - ab)$, $s = (x, -\frac{x}{a}, \frac{x}{a})$, by the discussion above $F_p(s)$ points in the negative z -direction - which, using a similar argument, implies the backwards trajectory of s arrives from $\{\dot{y} > 0\}$, the region in front of $\{\dot{y} = 0\}$ in Fig.6. By the tangency of F_p to $\{\dot{y} = 0\}$ at s , a similar argument to the one used in the previous paragraph now proves there exists some $\epsilon > 0$ s.t. for $t \neq 0, t \in (-\epsilon, \epsilon)$ we have $\gamma_s(t) \in \{\dot{y} > 0\}$ and Lemma 2.4 now follows. \square

Having concluded our study of the plane $\{\dot{y} = 0\}$, we now begin studying the unbounded dynamics of the Rössler system in \mathbf{R}^3 . We first recall Th.1 in [24], where it was proven that for all $p \in P$, the behaviour of the vector field F_p on $\{(x, y, z) | x^2 + y^2 + z^2 > r\}$ is independent of $r > 0$ (for any sufficiently large r) - which proves one can extend F_p to S^3 by adding ∞ as a fixed point for the flow. In this spirit, we conclude from Th.1 in [24]:

Corollary 2.5. *For every parameter $p \in P$, the Rössler system can be extended to a flow on S^3 - and moreover, ∞ becomes a fixed-point for the flow.*

In the same spirit, we now prove the following fact about the local dynamics around ∞ :

Lemma 2.6. *For every $p \in P$, the index of the fixed-point at ∞ w.r.t. the vector field F_p is 0.*

Proof. Recall $l_p = \{\dot{x} = 0\} \cap \{\dot{y} = 0\}$ (see Lemma 2.4). Now, given $r > 0$ consider $S_r = \{|w| = r, w \in \mathbf{R}^3\}$ - F_p can point on S_r at the $(0, 0, -d), d > 0$ direction only on the intersection $S_r \cap l_p$. Further recall we earlier parameterized l_p by $\{(x, -\frac{x}{a}, \frac{x}{a}), x \in \mathbf{R}\}$, and that by Eq.1.5 we have $F_p(l_p(x)) = (0, 0, bx + \frac{x^2 - xc}{a})$ (see also the proof of Lemma 2.4). For any sufficiently large $|x|$, the polynomial $bx + \frac{x^2 - xc}{a}$ is positive - therefore, given any sufficiently large $r > 0$, F_p cannot point at the $(0, 0, -d), d > 0$ direction on $S_r \cap l_p$. Consequentially, we conclude that provided $r > 0$ is sufficiently large, the function $\frac{F_p}{\|F_p\|} : S_r \rightarrow S^2$ is not surjective - which implies the index of the vector field F_p on the fixed-point at ∞ can only be 0. This implies that given any $p \in P$, as we extend the vector field F_p to ∞ as described above, ∞ is a degenerate fixed point for the Rössler system and the assertion follows. \square

Lemma 2.6 allows us to treat F_p as a vector field on the 3-sphere S^3 with precisely three fixed points - two saddle foci P_{In}, P_{Out} , and a degenerate fixed point at ∞ of index 0. Since the parameter p lies inside the parameter space P , we already know both P_{In} and P_{Out} are saddle-foci, hence hyperbolic - therefore, due to the Hartman-Grobman Theorem we can easily describe the local dynamics around both by reducing them to their linearizations. However, unlike P_{In} and P_{Out} , ∞ is not a hyperbolic fixed-point - which implies the local dynamics around it are potentially much more complicated. In order to study them, we first prove:

Lemma 2.7. *For any parameter $p = (a, b, c) \in P$, the vector field F_p is not C^1 at ∞ . In particular, the Rössler system is not smooth at the fixed point at ∞ .*

Proof. For any $(x, y, z) = v \in \mathbf{R}^3$ consider the linearized vector field $J_p(v)$ at v - namely, the Jacobian matrix of F_p at $v \in \mathbf{R}^3$ (see Eq.1.5). Now, choose some $\lambda \in \mathbf{R}$ and note the equation $\det(J_p(v)) = \lambda$ (where \det denotes the determinant) can be rewritten as $z = \frac{\lambda + c - x - ab}{a}$. This proves the set $S_\lambda = \{\det(J_p(v)) = \lambda\}$ is a plane in \mathbf{R}^3 - which implies that when we extend \mathbf{R}^3 to S^3 we have $\infty \in \partial S_\lambda$ (with ∂S_λ taken in S^3). We conclude that for any $\lambda_1 \neq \lambda_2$, we have $\{\infty\} = \partial S_{\lambda_1} \cap \partial S_{\lambda_2}$ - which proves $\det(J_p(v))$ takes infinitely many values at any neighborhood of ∞ . As such F_p cannot be C^1 at ∞ and the Lemma follows. \square

Lemma 2.7 proves that we cannot extend the Rössler system to a smooth flow on S^3 - which, at least on the surface, could complicate matters. In order to overcome this difficulty, we will now prove throughout our parameter space the vector field F_p always generates two unbounded heteroclinic trajectories: Γ_{In} and Γ_{Out} , which connect P_{In} and P_{Out} to ∞ (respectively). As we will see below, the existence of such unbounded heteroclinic trajectories would allow us to perturb F_p around ∞ to a smooth vector field, with an arbitrarily small loss of dynamical data.

To begin, recall we denote by W_{In}^s the one-dimensional, stable manifold of the saddle-focus P_{In} , and that W_{Out}^u denotes the one-dimensional unstable manifold of P_{Out} (see the illustration in Fig.7). We now prove the following result, with which we conclude this section:

Theorem 2.8. *For every parameter $p \in P$, the corresponding Rössler system generates two heteroclinic trajectories:*

- $\Gamma_{In} \subseteq W_{In}^s$, which connects P_{In}, ∞ in S^3 .
- $\Gamma_{Out} \subseteq W_{Out}^u$, which connects P_{Out}, ∞ in S^3 .

As a consequence, for every sufficiently large $r > 0$, there exists a smooth vector field on S^3 , R_p , s.t.:

- R_p coincides with F_p on the open ball $B_r(P_{In})$.
- R_p has precisely two fixed points in S^3 - namely, the saddle foci P_{In} and P_{Out} .
- R_p generates a heteroclinic trajectory which connects P_{In}, P_{Out} and passes through ∞ .

Proof. We prove Th.2.8 in three stages. The sketch of the proof is as follows:

- In Stage *I* we use the results from Section 2.2 to prove there exists an invariant manifold Γ_{In} , a component of W_{In}^s , which is a heteroclinic connection between P_{In}, ∞ .
- In Stage *II* we prove the existence of Γ_{Out} - a component of W_{Out}^u which forms a heteroclinic connection between P_{Out}, ∞ .
- Finally, in Stage *III* we tie these results together, and conclude the proof of Th.2.8 by constructing the vector field R_p , as described above.

2.1. Stage I - the existence of Γ_{In} . In this subsection we prove the existence of a component $\Gamma_{In} \subseteq W_{In}^s$ which forms an unbounded heteroclinic trajectory, connecting P_{In} and ∞ .

Recall the cross-section $\{y = 0\}$, and that it is composed of three sets: the half-planes U_p and L_p , separated by the line l_p (see the discussion before Lemma 2.1). Additionally, recall that on L_p the vector field F_p points into $\{y > 0\}$, while on U_p it points into $\{y < 0\}$ (see Fig.6 and Fig.8) - while F_p is tangent to $\{y = 0\}$ on l_p . Recall $l_p(x) = (x, -\frac{x}{a}, \frac{x}{a})$, $x \in \mathbf{R}$, and set $l_1 = \{l_p(x) | x < 0\}$. By $l_p(0) = P_{In} = (0, 0, 0)$, it follows l_1 is an unbounded arc in \mathbf{R}^3 which connects the saddle focus P_{In} and ∞ (in S^3).

Now, consider the half-plane $H_1 = \{(x, 0, z) | x < 0, z \in \mathbf{R}\}$ - since the velocity \dot{y} is given by $x - ay$ where the parameter a is positive (see Eq.1.5 and the discussion at page 3), by definition we have $H_1 \subseteq \{\dot{y} < 0\} = \{(x, y, z) | x < -ay\}$. As such, since the normal vector to H_1 is $(0, 1, 0)$, by computation it immediately follows that for $v \in H_1$, the dot product $F_p(v) \cdot (0, 1, 0)$ is negative. Or, in other words, on H_1 the vector field F_v points inside the open region $\{(x, y, z) | y < 0\}$ (see the illustration in Fig.8).

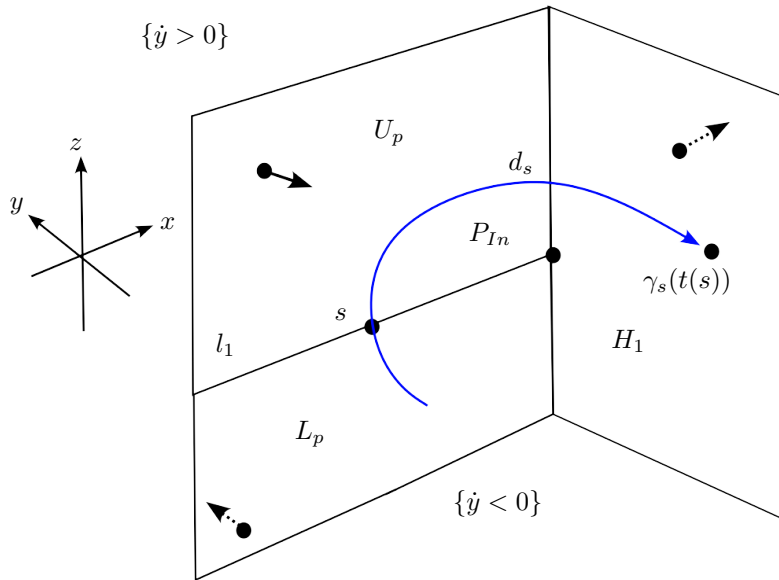


FIGURE 8. The quadrant Q_1 , bounded by H_1, U_p and L_p (and F_p 's directions on them). The vector field is tangent to l_1 , while F_p points into $\{y < 0\}$ on U_p and into $\{y > 0\}$ on L_p , and the flow line from $s \in l_1$ (denoted by d_s) connects to $\gamma_s(t(s))$.

Let us note the two-dimensional set $H_1 \cup \{y = 0\}$ traps a quadrant, $Q_1 = \{y \leq 0\} \cap \{(x, y, z) | y > 0\}$ (see the illustration in Fig.8) - by $l_1 = \{l_p(x) | x < 0\}$ and by $P_{Out} = (c - ab, \frac{ab-c}{a}, \frac{c-ab}{a})$, $c - ab > 0$ (see the discussion in page 3), we conclude both $l_1 \subseteq Q_1$ and $P_{Out} \notin \overline{Q_1}$.

Now, consider some $s \in l_1$ and its trajectory, γ_s (recall we parameterize γ_s s.t. $\gamma_s(0) = s$) - by Cor.2.2 the forward trajectory of s enters the region $\{\dot{y} < 0\}$ immediately upon leaving s (see the illustration in Fig.8). Moreover, let us remark that by definition, given $s \in l_1$ there exists some $x < 0$ s.t. $s = (x, -\frac{x}{a}, \frac{x}{a})$ - which, as the parameter a is positive implies the y -coordinate of s is also positive. Consequentially, it follows the forward trajectory of s cannot be trapped in Q_1 forever - it either escapes Q_1 it by hitting L_p transversely (i.e., entering the region $\{\dot{y} > 0\}$), or by hitting H_1 transversely (i.e., entering the region $\{(x, y, z) | y < 0\}$). Therefore, given $s \in l_1$, we conclude there exists a positive time $t(s) > 0$ s.t. $\gamma_s(t(s))$ is the first intersection point between $H_1 \cup L_p \cup l_1$ and the flow line $\gamma_s(0, t(s)) = d_s$ (see the illustrations in Fig.8 and Fig.11).

This motivates us to define $f : l_1 \rightarrow H_1 \cup L_p \cup l_1$ by $f(s) = \gamma_s(t(s))$ - by the discussion above, f is well-defined. It is easy to see every component of $f(l_1)$ is a curve on the set $H_1 \cup L_p \cup l_1$ (see Fig.11 for an illustration). Now, set V as the collection of flow lines d_s , $s \in l_1$, connecting $f(l_1)$ and l_1 - with these ideas in mind, we are now ready to give an overview for the proof of existence of Γ_{In} . In an ideal scenario, our tactic to prove the existence of the invariant manifold Γ_{In} would be as follows:

- First, we would like to define C_{In} as the region trapped between H_1, L_p and V (see the illustration in Fig.11). Provided C_{In} exists, it is easy to see it would form a topological cone with a tip at P_{In} .
- Second, since by definition $\partial C_{In} \subseteq V \cup H_1 \cup L_p$, for every $s \in \partial C_{In}$ it would follow $F_p(s)$ is either tangent to ∂C_{In} (when $s \in V$) or points into either $\{\dot{y} > 0\}$ or $\{(x, y, z) | y < 0\}$ (when $s \in L_p$ or H_1 , respectively). Since Q_1 is, by definition, a subset of $\{(x, y, z) | \dot{y} < 0, y < 0\}$ it would follow by $C_{In} \subseteq Q_1$ that whenever $s \in \partial C_{In} \setminus V$, $F_p(s)$ points outside of Q_1 . As such, no trajectory can enter C_{In} under the flow.
- Third, since by construction C_{In} is a topological cone with a tip at P_{In} , by considering the linearization of F_p around the saddle-focus P_{In} we conclude it must include some invariant manifold Γ_{In} - as such, since $C_{In} \subseteq Q_1 \subseteq \{\dot{y} \leq 0\}$ (and because no trajectory can escape C_{In} under the inverse flow), by considering the backwards trajectory of $s \in \Gamma_{In}$, it would follow Γ_{In} extends from P_{In} to ∞ .

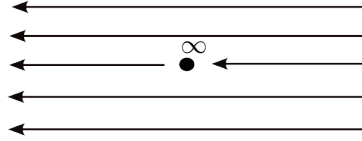


FIGURE 9. A flow around ∞ for the vector fields F_r s.t. ∞ is a 0-index fixed point.

In practice, the argument above has one major flaw - due to Lemma 2.7, the dynamics around ∞ are hard to analyze, i.e., there is no reason to a-priori assume $f(l_1)$ includes an unbounded curve. As such, in order to overcome this difficulty, we first prove:

Proposition 2.9. *For any $p \in P$ and any sufficiently large $r > 0$ we can always deform the vector field F_p to a vector field F_r s.t.:*

- F_p and F_r coincide on the ball of radius r around the origin, $B_r(0)$.
- F_r has precisely two fixed points in \mathbf{R}^3 , the saddle-foci P_{In} and P_{Out} (in particular, F_p and F_r coincide around these fixed points).
- F_r generates an invariant manifold Γ_r for P_{In} , and moreover, Γ_r is trapped inside Q_1 under the flow generated by $-F_r$.

In other words, Prop.2.9 implies that whatever the local dynamics of F_p around the fixed point ∞ may be, in practice, we can always smoothly deform F_p to another vector field, F_r which satisfies the ideal scenario presented above (i.e., F_r does generate a cone with a tip at P_{In}). In particular, the larger r is, the more similar the dynamics of F_r to those of F_p (at least on compact sets in \mathbf{R}^3).

Proof. To begin, consider $r > 0$ sufficiently large s.t. both fixed points P_{In} and P_{Out} are interior to the ball $B_r(0)$ - additionally, let us recall that by Cor.2.6, the index of F_p at its fixed point at ∞ is 0 - hence the flow on $\mathbf{R}^3 \setminus B_r(0)$ can be smoothly deformed to a flow as in Fig.9, without creating any new fixed points. Recall $l_1 = \{l_p(x) | x < 0\}$ (where $l_p(x) = (x, -\frac{x}{a}, \frac{x}{a})$), i.e., it is a curve connecting the fixed point P_{In} and ∞ through the quadrant $\overline{Q_1}$ - similarly, ∞ also lies on the closure of both H_1 and L_p (where the closure in all cases is considered in the 3-sphere S^3). We now define F_r as the following vector field:

- F_r coincides with F_p on $B_r(0)$. Moreover, F_r is a smooth vector field on S^3 .
- ∞ is a fixed point of index 0 for F_r , and the local dynamics around it are as in Fig.10 and Fig.9.

- The sets H_1, L_p, U_p and l_1 remain unchanged for F_r - i.e., the local dynamics on F_r on either one of these sets are orbitally equivalent to the local dynamics of F_p on these sets.
- Additionally, the regions $\{\dot{y} < 0\}$ and $\{\dot{y} > 0\}$ are the same for both F_p and F_r - that is, the quadrant Q_1 is trapped inside $\{\dot{y} \leq 0\}$ w.r.t. both F_p and F_r .

It is easy to see the vector field F_r satisfies the first two assertions of Prop.2.9 - therefore, to conclude the proof we must prove it also generates Γ_r , an invariant manifold trapped forever in Q_1 under the inverse flow. To do so, set $f_r : l_1 \rightarrow H_1 \cup L_p \cup l_1$ as the analogue (w.r.t. the vector field F_r) of the function f defined above - i.e., f_r is the first-hit map for initial conditions on $s \in l_1$ on $H_1 \cup L_p \cup l_1$ w.r.t. F_r . When we smoothen F_p around ∞ to create F_r (as described in the proof of Cor.2.6), using Hopf's Theorem we deform F_p to F_r s.t. the flow moves around ∞ in a specific direction.

The constraints imposed on the flow by the behavior of F_r on the cross-sections H_1, L_p and U_p now imply the trajectories of initial conditions $s \in l_1$ sufficiently close to ∞ collide with $H_1 \cup L_p \cup l_1$ - which allows us to construct F_r s.t. $\lim_{s \rightarrow \infty} f_r(s) = \infty$ (see the illustration in Fig.10). Moreover, the same constraints imply that by slightly bumping flow lines emanating from l_1 outside $B_r(0)$ (if necessary) we ensure that f_r is continuous at some neighborhood of ∞ in l_1 (see the illustration in Fig.10).

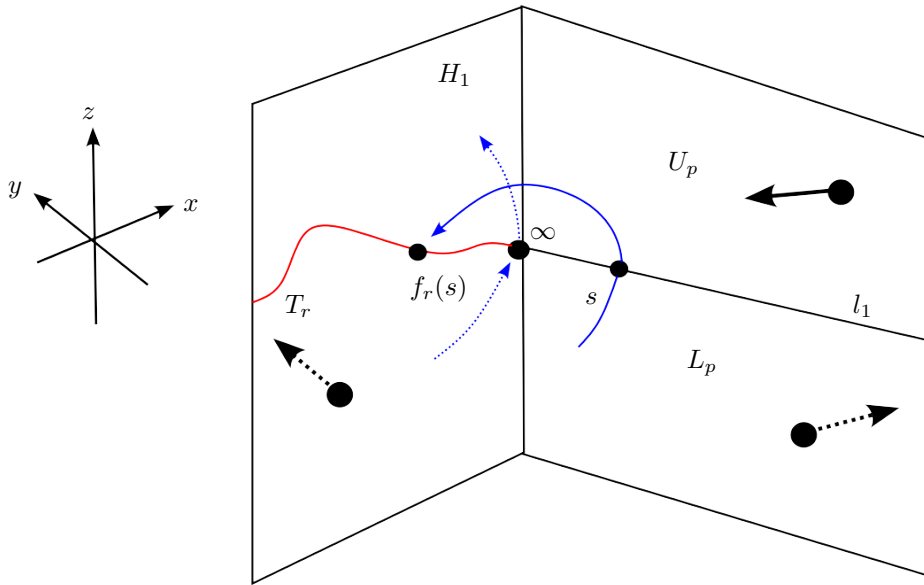


FIGURE 10. The curve $T_r = f_r(l_1)$ and the directions of F_r on H_1, L_p and U_p around ∞ (in S^3). As can be seen, f_r is continuous around ∞ .

Now, set $T_r = f_r(l_1)$ - it is easy to see every component of T_r is a curve $H_1 \cup L_p \cup l_1$ - and by the construction of F_r above, as $\lim_{s \rightarrow \infty} f_r(s) = \infty$ at least one component of T_r is a curve which stretches to ∞ . Moreover, Now, let us note that as P_{In} is a saddle-focus with a two-dimensional unstable manifold W_{In}^u transverse to L_p at P_{In} (see Lemma 2.2), it is easy to see f_r is also continuous around P_{In} and satisfies $\lim_{s \rightarrow P_{In}} f_r(s) = P_{In}$ (see the illustration in Fig.11). Now, set V_r as the collection of flow-lines connecting T_r and l_1 (see the illustration in Fig.11) - we claim:

Lemma 2.10. For every sufficiently large r , F_r generates a three-dimensional body C_{In} trapped between V_r, L_p and H_1 . Moreover, $P_{In} \in \partial C_{In}$.

Proof. Consider $f_r : l_1 \rightarrow H_p \cup L_p \cup l_1$ - either f_1 is continuous on l_1 or it is not. If f_1 is continuous, as it is a first-hit map it follows by the Existence and Uniqueness Theorem, $T_r = f_r(l_1)$ is a simple curve in $H_p \cup L_p \cup l_1$, connecting P_{In} and ∞ . Whenever this is the case, it immediately follows there exists a three dimensional body C_{In} trapped between V_r, L_p and H_1 (see the illustration in Fig.11). Moreover, it is easy to see $P_{In} \in \partial C_{In}$.

Otherwise, f_r is discontinuous at some $s \in l_1$, T_r must include at least two components (as illustrated in Fig.13). Therefore, let T^1 denote the component of T_r beginning at P_{In} - since F_r is transverse to both H_1 and L_p , it terminates at some $s_2 \in l_1$. Or, in other words, there exists a sub-arc $J_1 \subseteq l_1$, beginning at P_{In} and terminating at some finite $s_1 \in l_1$ s.t. $f_r(J_1) = T^1$ and $f_r(s_1) = s_2$ (as illustrated in Fig.12). This implies the flow lines connecting J_1 to $T^1 = f_r(J_1)$ perform a wave-like movement, as sketched in Fig.12 - while $s_3 = f_r(s_2)$ is strictly

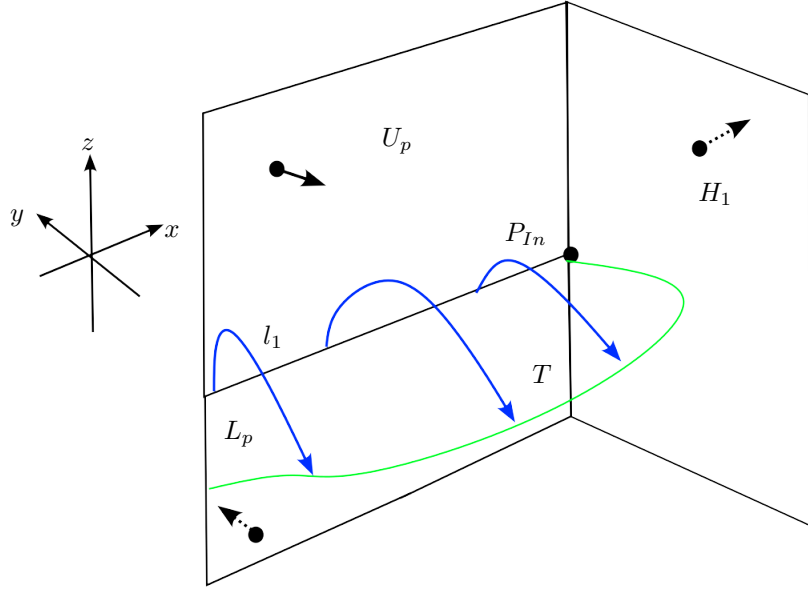


FIGURE 11. The two-dimensional set V (or V_n) is generated by the flow lines connecting T (or T_n) and l_1 . In this case, T (or T_n) is a simple curve, connecting P_{In} and ∞ .

interior to T^1 , as illustrated in Fig.12. In particular, whenever V_r is tangent to l_1 at s_2 , the trajectories of initial conditions $s \in J_2 = l_1 \setminus J_1$ sufficiently close to s_1 slide below the surface connecting J_1 and T^1 , as illustrated in Fig.12 - thus hitting $H_1 \cup L_p$ at the region enclosed between T^1 and l_1 .

Consequentially, given initial conditions $s \in J_2$ sufficiently close to s_1 , $f_r(s)$ lies in the regions on $H_1 \cup L_p$ trapped between J_1 and $T^1 = f_r(J_1)$. Moreover, whenever this is the case T_r is branched (as illustrated in Fig.12).

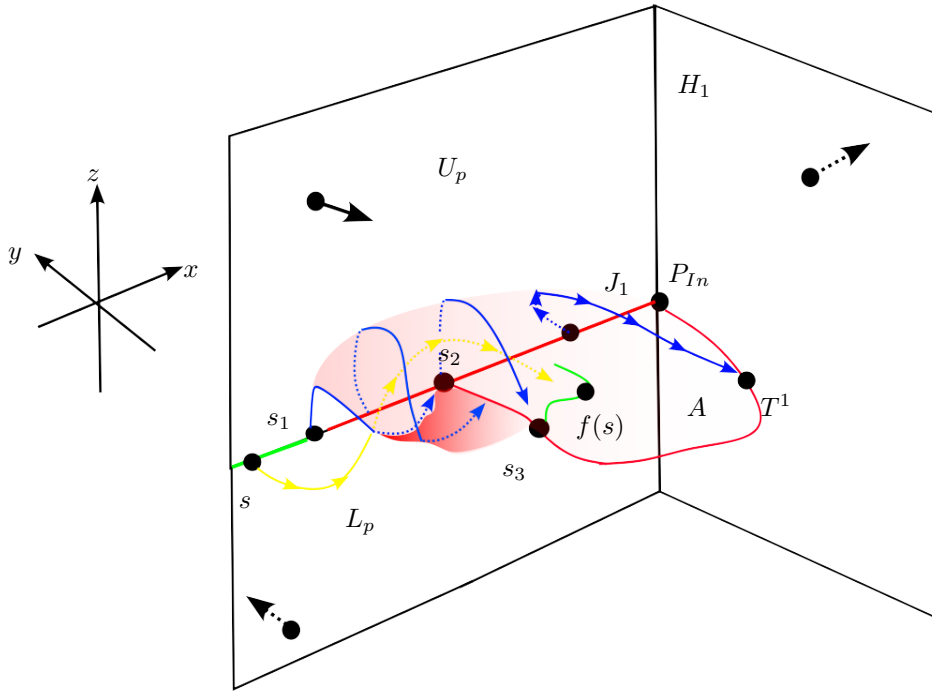


FIGURE 12. The red surface denotes the collection of flow lines connecting J_1 and T^1 . Initial conditions s on J_2 (the green arc) sufficiently close to s_1 flow along the flow line of s_1 below the red surface, thus hitting A (as indicated by the yellow flow line, where $s_2 = f_r(s_1)$, $s_3 = f_r(s_2)$). A denotes the two-dimensional region enclosed by T^1 and l_1 on $H_1 \cup L_p$.

Now, set A as the collection of domains on $L_p \cup H_1$ trapped between T_r and l_1 (see the illustration in Fig.12 and 13). Using a similar argument to the one above it follows that given an initial condition $s \in l_1$ s.t. $f_r(s) \notin \partial A$, then $f_r(s)$ is interior to A . Hence, given an open arc J on l_1 s.t. $f_r(J) \not\subseteq \partial A$, $f_r(J)$ is a collection of arcs in A , each with two endpoints on ∂A - thus, the region trapped between V_r and the flow lines connecting $J, f_r(J)$ is a topological tube with one opening inside A (as sketched in Fig.13) - moreover, the interior of the said tube is a component of $Q_1 \setminus V_r$. As such, it follows $Q_1 \setminus V_r$ includes a component C_{In} , satisfying $P_{In} \in \partial C_{In}$, which lies away from all such tubes - in particular, C_{In} is trapped between V_r, L_p and H_1 .

All in all, regardless of whether f_r is continuous on T_r or not, there always exists a connected three-dimensional region, C_{In} , trapped between V_r and $L_p \cup H_1 \cup l_1$ s.t. $P_{In} \in \partial C_{In}$. The proof of Lemma 2.10 now follows. \square

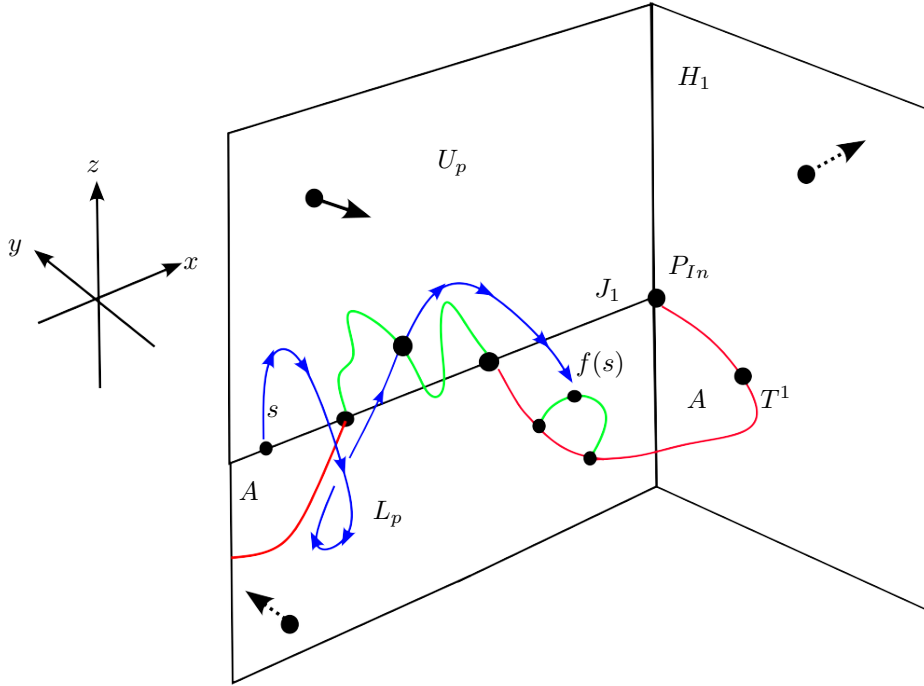


FIGURE 13. In this scenario T_r has two components, where the regions A are trapped between l_1 and the components of T_r . Due to a tangency at the green curve, the points which flow to the green arc eventually flow into A , thus generating a tube connecting the two green arcs (and causing a branching at T_r - as exemplified by the trajectory of s).

We are now ready to conclude the proof of Prop.2.9. To do so, first note that given any F_r (as defined at the beginning of the proof), by construction it follows that the three-dimensional body C_{In} given by Lemma 2.10 is trapped inside the quadrant $Q_1 \subseteq \{(x, y, z) | y \leq 0\}$. As a consequence, by $P_{Out} = (c - ab, \frac{ab-c}{a}, \frac{c-ab}{a})$, $c > 1, a, b \in (0, 1)$ it follows $P_{Out} \notin C_{In}$. Furthermore by construction ∂C_{In} is a subset of the union $V_r \cup H_1 \cup L_p$. Now, note that by definition, F_r is tangent to V_r , and recall F_r and F_p are orbitally equivalent around H_1 and $L_p \subseteq \{y = 0\}$ - as such, since on H_1 and L_p the vector field F_p points into $\{(x, y, z) | y < 0\}$ and $\{y > 0\}$ (respectively), the same is true for F_r on L_p and H_1 . Therefore, since $Q_1 \subseteq \{y \leq 0\} \cap \{(x, y, z) | y < 0\}$ and because $\partial C_{In} \setminus V_r \subseteq L_p \cup H_1$, we conclude that for $s \in \partial C_{In} \setminus V_r$, $F_r(s)$ points out of Q_1 - and hence, outside of C_{In} as well.

Therefore, since $\partial C_{In} \subseteq V_r \cup L_p \cup H_1$ it follows that for any $s \in \partial C_{In}$ $F_r(s)$ is either tangent to ∂C_{In} (when $s \in V_r$), or points outside of C_{In} (when $s \notin V_r$). We may summarize our findings as follows:

- $P_{Out} \notin \overline{C_{In}}$ while $P_{In} \in \partial C_{In}$.
- $C_{In} \subseteq \{\dot{y} \leq 0\}$, where \dot{y} is taken w.r.t. F_r .
- Since F_r is either tangent to ∂C_{In} or points out of C_{In} throughout ∂C_{In} , no trajectory can escape $\overline{C_{In}}$ w.r.t. $-F_n$.

It follows C_{In} forms a topological cone with a tip at P_{In} - therefore, by considering the linearization of F_r it follows there must exist an invariant manifold Γ_r for P_{In} inside C_{In} emanating from P_{In} (w.r.t. the vector field F_r) - see Fig.14. Moreover, if ϕ_t^r denotes the flow generated by F_r , by the discussion above we conclude that given any $s \in \Gamma_r$ and every $t < 0$, $\phi_t^r(s) \in C_{In} \subseteq Q_1$. By this discussion we conclude Γ_r is trapped in Q_1 under the inverse flow generated by $-F_r$, and the proof of Prop.2.9 is now complete. \square

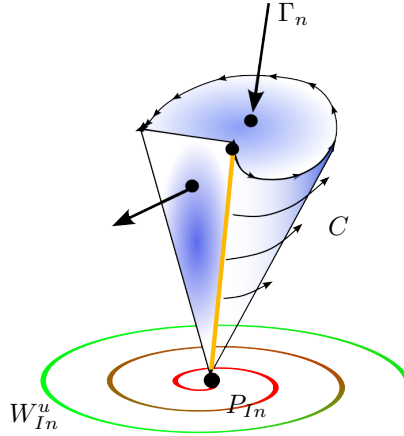


FIGURE 14. By the Hartman-Grobman Theorem, by suspending a l_1 with the flow (the orange curve) we generate a topological cone into which no trajectory can enter. As such, it includes an invariant manifold of P_{In} (w.r.t. F_r).

We now use Prop.2.9 to conclude the proof of Stage I - namely, now prove the existence of an invariant, unbounded, one dimensional manifold Γ_{In} for P_{In} which we do in the following corollary:

Corollary 2.11. *There exists a component $\Gamma_{In} \subseteq W_{In}^s$ - where W_{In}^s is the one-dimensional, stable manifold for the saddle focus P_{In} - s.t. Γ_{In} is a heteroclinic trajectory for F_p in S^3 , connecting the fixed-points P_{In} and ∞ .*

Proof. Choose a sufficiently large $r > 0$ s.t. Prop.2.9 holds, and consider an initial condition $s \in \Gamma_r \cap B_r(0)$. As F_p and F_r coincide on $B_r(0)$ and because $P_{In} \in B_r(0)$, provided s is sufficiently close to P_{In} s is in some invariant manifold Γ_{In} of P_{In} . Now, denote the flow generated by F_p by ϕ_t^p , and consider $\phi_t^p(s)$, for any $t < 0$. Since r can be chosen to be arbitrarily large and because $\Gamma_r \subseteq Q_1 \subseteq \{\dot{y} \leq 0\}$, we conclude that for every $t < 0$ $\phi_t^p(s) \in \{\dot{y} \leq 0\}$ - which implies Γ_{In} is forever trapped in both Q_1 and $\{\dot{y} \leq 0\}$. Recalling the two-dimensional unstable manifold W_{In}^u is transverse to $\{\dot{y} = 0\}$ at P_{In} (see Cor.2.2), it follows the backwards trajectory of every initial condition on W_{In}^u fluctuates infinitely many times between $\{\dot{y} > 0\}$ and $\{\dot{y} < 0\}$ - therefore, $\Gamma_{In} \cap W_{In}^u = \emptyset$. Consequentially, Γ_{In} can only be a component of the one-dimensional invariant manifold W_{In}^s .

Furthermore, since $P_{Out} = (c - ab, \frac{ab-c}{a}, \frac{c-ab}{a})$, $c - ab > 0$ (see the definition of the parameter space P at page 3), by $Q_1 \subseteq \{(x, y, z) | x \leq 0\}$ it follows $P_{Out} \notin \overline{Q_1}$. Therefore, given any $s \in \Gamma_{In}$, $P_{Out} \neq \lim_{t \rightarrow -\infty} \phi_t^p(s)$, i.e., Γ_{In} is not a heteroclinic trajectory connecting P_{In} and P_{Out} . Therefore, since for every $s \in \Gamma_{In}$ and every $t < 0$ we have $\phi_t^p(s) \in \{\dot{y} \leq 0\}$, it follows $\lim_{t \rightarrow -\infty} \phi_t^p(s) = \infty$ and Cor.2.11 now follows. \square

2.2. Stage II - the existence of Γ_{Out} . Having proven the existence of Γ_{In} , we now prove the analogous result for P_{Out} - namely, we now prove the existence of a heteroclinic trajectory Γ_{Out} , a component of the one-dimensional unstable manifold W_{Out}^u , which connects P_{Out}, ∞ . Despite some slight differences, in practice the proof will be almost symmetric to the one in Stage I.

To begin, recall $P_{Out} = (c - ab, \frac{ab-c}{a}, \frac{c-ab}{a})$, where $c - ab > 0$ (see page 3) and that $l_p(c - ab) = P_{Out}$ - where l_p is the tangency curve of the vector field F_p to the plane $\{\dot{y} = 0\}$, parameterized by $l_p(x) = (x, -\frac{x}{a}, \frac{x}{a})$, $x \in \mathbf{R}$ (see the illustration in Fig.6 and Fig.7). Now, set $l_2 = \{l_p(x) | x > c - ab\}$ (see the illustration in Fig.15) - we prove the existence of Γ_{Out} by making an analogous argument to the one used to prove the existence of Γ_{In} . To begin, consider the half-plane $H_2 = \{(x, \frac{ab-c}{a}, z) | x < c - ab, z \in \mathbf{R}\}$ (see the illustration in Fig.15). Again, by $\dot{y} = x + ay$ it follows, $H_2 \subseteq \{\dot{y} < 0\}$ - and since the normal vector to H_2 is $(0, 1, 0)$ by considering $F_p(x, \frac{ab-c}{a}, z) \bullet (0, 1, 0) = x + ab - c$ it immediately follows that on H_2 the vector field F_p points into the region $\{(x, y, z) | y < c - ab\}$ (see the illustration in Fig.15).

Consequentially, $H_2 \cup \{\dot{y} = 0\}$ traps a quadrant $Q_2 = \{\dot{y} \leq 0\} \cap \{(x, y, z) | y < \frac{ab-c}{a}\}$ (see the illustration in Fig.15) - by $l_2 = \{l_p(x) | x > c - ab\}$, we conclude $l_2 \subseteq \partial Q_2$. Now, consider some $s \in l_2$ and its backwards trajectory. Recall that by Lemma 2.2 the backwards trajectory of s enters $\{\dot{y} < 0\}$ immediately upon leaving s (see the illustration in Fig.15) - moreover, let us remark that by definition, given $s \in l_2$, it is given by the coordinates $s = (x, -\frac{x}{a}, \frac{x}{a})$ (for some $x > c - ab$) - hence, its y -coordinate is greater than $\frac{ab-c}{a}$. As such, the backwards trajectory of s cannot be trapped in Q_2 forever - i.e., it either escapes by hitting the half-plane U_p transversely (i.e., entering $\{\dot{y} > 0\}$) - see the illustration in Fig.15, or by hitting H_2 transversely (i.e., entering $\{(x, y, z) | y > \frac{ab-c}{a}\}$).

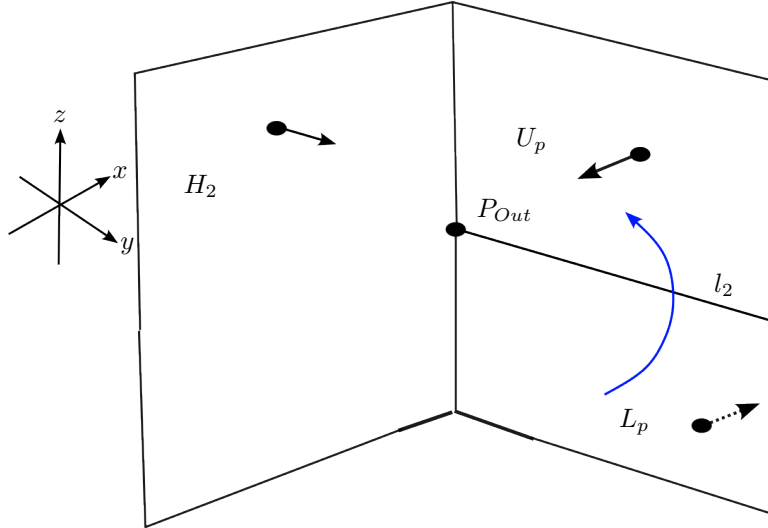


FIGURE 15. The quadrant Q_2 along with a flow line tangent to l_2 (and the directions of F_p on U_p, L_p and H_2).

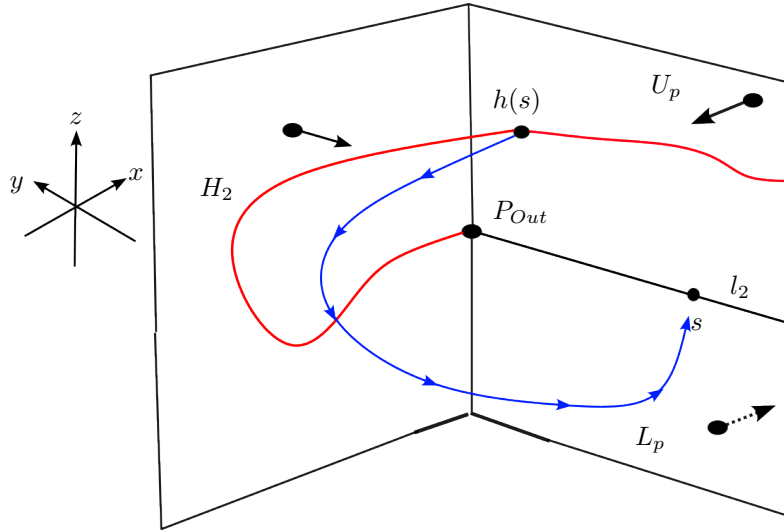


FIGURE 16. The quadrant Q_2 along with a flow line connecting a point $h(s) = \gamma_s(j(s))$ (or conversely, $h_n(s)$) in $J = h(l_2)$, the red curve, and $s \in l_2$. In this scenario J is homeomorphic to an unbounded straight line.

Therefore, given $s \in l_2$, there exists a strictly negative time $j(s) < 0$ s.t. $\gamma_s(j(s))$ is the first intersection point between the two-dimensional set $H_2 \cup U_p \cup l_2$ and the backwards trajectory of s (see the illustration in Fig,15). Now, define $h : l_2 \rightarrow H_2 \cup U_p \cup l_2$ by $h(s) = \gamma_s(j(s))$ - that is, h is the first-hit map w.r.t. the inverse flow for initial conditions in l_2 in $H_2 \cup U_p \cup l_1$.

Therefore, replacing the flow generated by F_p with the inverse flow generated by $-F_p$, and replacing f and $f(l_1)$ with h and $h(l_2)$, using similar arguments to those used to prove Prop.2.9 we conclude :

Proposition 2.12. For any $p \in P$ and every sufficiently large $r > 0$ we can always deform the vector field $-F_p$ to a vector field G_r s.t.:

- $-F_p$ and G_r coincide on $B_r(0)$, the ball of radius r around the origin.
- G_r has precisely two fixed points in \mathbf{R}^3 - the saddle-foci P_{In} and P_{Out} as saddle-foci (in particular, $-F_p$ and G_r coincide around the fixed points).
- G_r generates an invariant manifold Γ_r for P_{Out} which is trapped in Q_2 under the flow generated by the vector field $-G_r$.

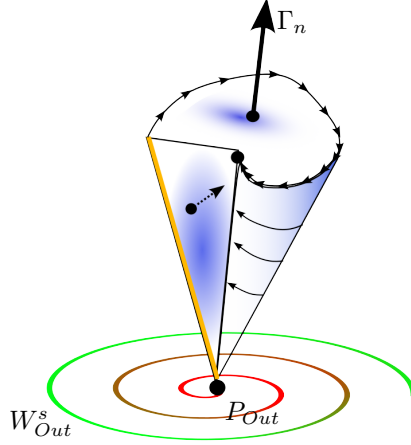


FIGURE 17. Similarly to the argument used to prove Prop.2.9, by suspending a l_2 (the orange curve) with G_r and considering the Hartman-Grobman Theorem we generate a topological cone with a tip at P_{Out} which traps an invariant manifold of P_{Out} .

We are now ready to conclude Stage II of the proof - i.e., to prove the existence of Γ_{Out} , which we do using a symmetric argument to the one used to prove Cor.2.2. Replacing F_p with $-F_p$ and F_r with G_r in the proof of Cor.2.2, we conclude:

Corollary 2.13. *There exists a component Γ_{Out} of the one-dimensional, unstable invariant manifold of P_{Out} , W_{Out}^u , s.t. Γ_{Out} is a heteroclinic trajectory connecting P_{Out}, ∞ .*

2.3. Stage III - constructing R_p and concluding the proof. Having proven the existence of $\Gamma_{In}, \Gamma_{Out}$, invariant, unbounded one-dimensional manifolds in W_{In}^s, W_{Out}^u , respectively, we can now conclude the proof of Th.2.8. Namely, we will now use the fact Γ_{Out} and Γ_{In} connect at ∞ to prove the existence of a smooth vector field on S^3, R_p , s.t. the following conditions are satisfied:

- For every sufficiently large $r > 0$, we can construct R_p s.t. it coincides on $\{(x, y, z) | x^2 + y^2 + z^2 < r\}$ with F_p , the original vector field given by Eq.1.5.
- R_p has precisely two fixed points in $S^3 - P_{In}, P_{Out}$.
- R_p generates an unbounded heteroclinic trajectory, connecting P_{In}, P_{Out} .

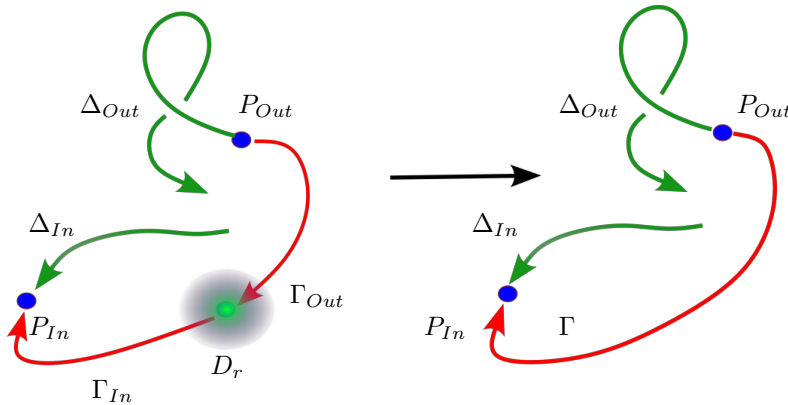


FIGURE 18. The smooth deformation of F_p to R_p - F_p remains unchanged in $\mathbf{R}^3 \setminus D_r$. $\Delta_{In}, \Delta_{Out}$ denote the respective components of $W_{In}^s \setminus \Gamma_{In}, W_{Out}^u \setminus \Gamma_{Out}$. D_r is the region $\{(x, y, z) | x^2 + y^2 + z^2 \geq r^2\}$.

Let us recall that by Lemma 2.6, the index of the vector field F_p at ∞ is 0 - hence, by Hopf's Theorem (see pg. 51 in [20]), for every sufficiently large r , F_p is homotopic on the set $D_r = \{w \in \mathbf{R}^3 | |w| \geq r\}$ to a vector field which generates a tubular flow (that is, a flow given by the vector field $F(x, y, z) = (1, 0, 0)$). Applying Hopf's Theorem, for any sufficiently large r we now smoothly deform F_p inside D_r by some smooth homotopy which removes the fixed point at ∞ . As the index at ∞ is 0, we can do so s.t. no new fixed points are generated in D_r . More importantly, because $\infty \in \overline{\Gamma_{In}} \cup \overline{\Gamma_{Out}}$, we construct this perturbation s.t. $\Gamma_{In}, \Gamma_{Out}$ connect to a heteroclinic connection passing through ∞ - the curve Γ (see the illustration in Fig.18).

Now, denote the vector field constructed above by R_p - by construction it is a smooth vector field in S^3 , and by the paragraphs above it satisfies the following:

- Given a sufficiently large $r > 0$, we can construct R_p s.t. it coincides with the vector field F_p (i.e., with the Rössler system) on $\{(x, y, z) | x^2 + y^2 + z^2 > r\}$.
- R_p has precisely two fixed points in S^3 - P_{In} and P_{Out} , both saddle foci (of opposing indices).
- P_{In} and P_{Out} are connected by Γ , a heteroclinic trajectory passing through ∞ .

All in all, Th.2.8 is now proven. □

Remark 2.14. In [30] it was observed a component of W_{Out}^u always tends to infinity. Th.2.8 (and in particular, Cor.2.13) is an analytic proof of this numerical observation.

3. CHAOTIC DYNAMICS AND TREFOIL KNOTS

Having characterized the global dynamics of the flow in Th.2.8, we now turn our gaze to prove a sufficient condition for the chaoticity of the flow (per Def.1.1). In more detail, in this section we prove that in a specific type of parameters $p \in P$ (to which we refer as trefoil parameters), the flow behaves chaotically - i.e., it creates a bounded, infinite collection of periodic trajectories. In order to give an outline of all that lies ahead, we first motivate and then rigorously define the said notion of a trefoil parameter.

To begin, recall that given a parameter $p = (a, b, c) \in P$, we denote by W_{In}^s and by W_{Out}^u the respective one-dimensional invariant manifolds for the saddle-foci P_{In}, P_{Out} (see the discussion in page 3). We first define:

Definition 3.1. Consider $p \in P$ for which there exists a bounded heteroclinic trajectory for the corresponding Rössler system in $W_{In}^s \cap W_{Out}^u$, connecting P_{In}, P_{Out} . In that case we say p is a **heteroclinic parameter** - see the illustration at Fig.19.

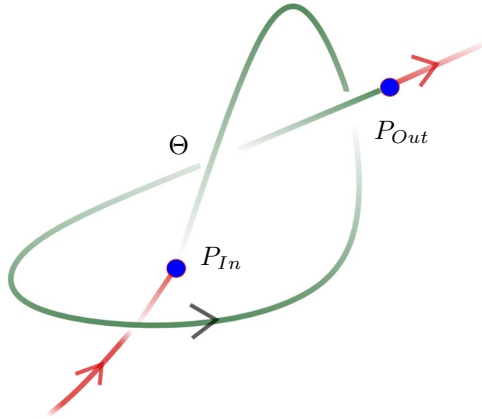


FIGURE 19. A heteroclinic trefoil knot for the Rössler system (see Def.3.2). Θ denotes the bounded heteroclinic connection.

Having defined heteroclinic parameters for the Rössler system, we now aim to introduce trefoil parameters as an idealized form of the Rössler system - and in order to do so in a meaningful way, we first recall the results of the numerical studies. As observed numerically in [30], there exists a partition of the parameter space P to three subsets: S_1, S_2 , and S_3 , on which the dynamics is characterized as follows:

- For parameters $p \in S_1$, the corresponding Rössler system generates an attractor (not necessarily chaotic). Moreover, it was observed throughout S_1 that the two-dimensional W_{Out}^s appears to shield trajectories from escaping to ∞ - while a bounded component of the one-dimensional W_{Out}^u repels them towards the attractor (see the discussion in Section V in [30]). Additionally, the attractor intersects transversely with some cross section, on which the first-return map is well-defined.
- For parameters $p \in S_2$, the dominant behavior is unbounded. In more detail, the two-dimensional W_{Out}^u does not shield trajectories from diverging to ∞ - and consequentially, most trajectories appear to diverge to ∞ .
- For parameters $p \in S_3$, the attractor coincides with the two-dimensional manifold W_{Out}^s . In addition, S_3 forms a bifurcation set between S_1 and S_2 .

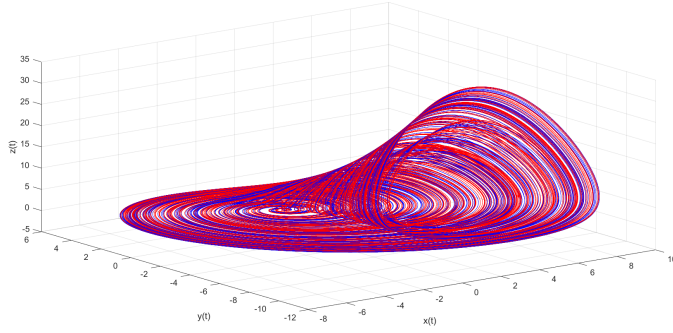


FIGURE 20. The attractor at parameter values $(a, b, c) \approx (0.468, 0.3, 4.615)$, sketched in Matlab. In these parameter values the vector field was observed numerically to generate a heteroclinic trefoil knot as in Fig.19 (see Fig.B.1 [30]).

These numerical observations are too general to work with analytically - therefore, in order to rigorously study the dynamics of the Rössler system we now introduce another, more specific topological constrain on the dynamics.

To do so, recall that as observed numerically there exists a parameter $p = (a, b, c) \in S_1$, $(a, b, c) \approx (0.468, 0.3, 4.615)$ at which the Rössler system generates a bounded heteroclinic trajectory Θ as in Fig.19 (see Fig.5.B.1 in [30]). By numerical approximation, the attractor at the said parameters is inseparable from the fixed-points P_{In}, P_{Out} , and appears to be wrapped around Θ (see the illustration in Fig.20). Now, recall the invariant one-dimensional manifolds Γ_{In} and Γ_{Out} given by Th.2.8 - it is easy to see that whenever such a Θ exists, it is not linked with Γ_{In} and Γ_{Out} . Consequentially, $\Lambda = \Gamma_{In} \cup \Gamma_{Out} \cup \Theta \cup \{P_{In}, P_{Out}, \infty\}$ forms a heteroclinic trefoil knot in S^3 (see the illustration in Fig.19).

We now combine the existence of a heteroclinic trefoil knot with the general numerical observations above to define trefoil parameters:

Definition 3.2. Let $p = (a, b, c) \in P$ be a heteroclinic parameter for the Rössler system. We say p is a **trefoil parameter** provided the following three conditions are satisfied by the corresponding vector field F_p :

- There exists a bounded heteroclinic trajectory Θ as in Fig.19. Therefore, Λ (as defined above) forms a trefoil knot in S^3 .
- The two-dimensional manifolds W_{In}^u and W_{Out}^s coincide. This condition implies $\overline{W_{In}^u} = \overline{W_{Out}^s}$ forms the boundary of an open topological ball - which, from now on, we always denote by B_α . It is easy to see $\Theta \subseteq B_\alpha$, while $\Gamma_{In}, \Gamma_{Out} \not\subseteq B_\alpha$ (see the illustration in Fig.21).
- $\Theta \cap \overline{U_p} = \{P_0\}$ is a point of transverse intersection - see the illustration at Fig.22 and Fig.32.

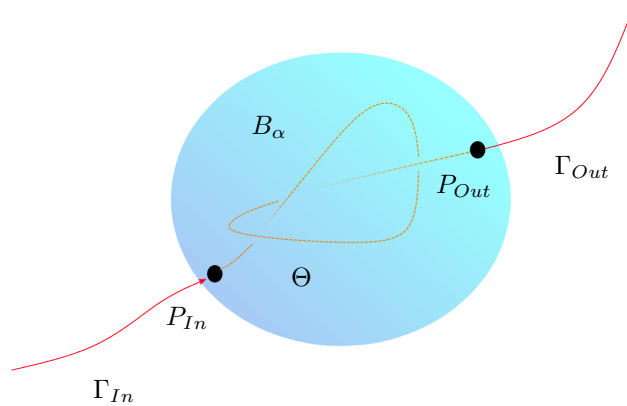


FIGURE 21. The heteroclinic trajectory Θ trapped inside the topological ball B_α , sketched as the blue sphere.

We now claim the definition of trefoil parameters captures key aspects of the numerical observations mentioned above. To see why, first of all, at trefoil parameters the Rössler system generates a bounded heteroclinic trajectory Θ as in Fig.19 (while Λ forms a heteroclinic trefoil knot). Second, the existence of B_α implies W_{Out}^s forces the existence of bounded dynamics for the flow around the heteroclinic trajectory Θ (see Fig.21). Moreover, as we will prove later on, the set $B_\alpha \cap U_p$ forms a cross-section on which the first-return map is well-defined. As such, it is easy to see trefoil parameters can be thought of as some idealized form of the Rössler system.

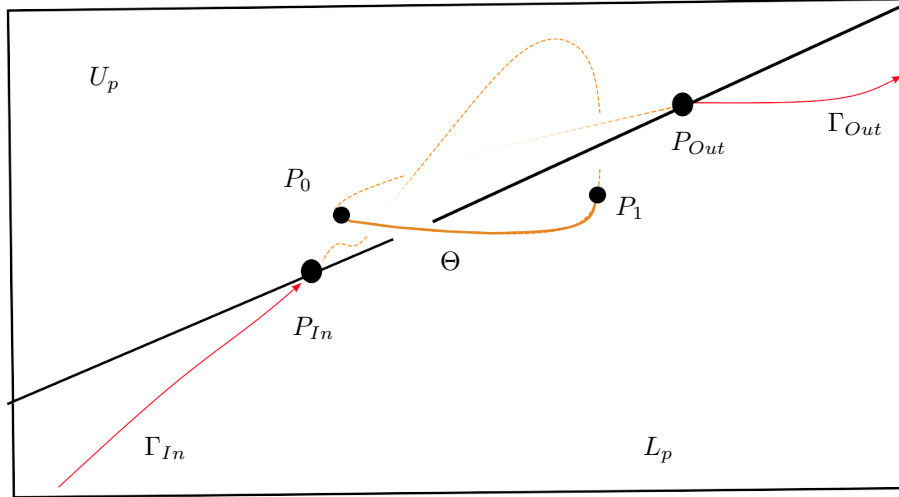


FIGURE 22. The heteroclinic trajectory Θ winds once around P_{In} - hence it intersects the half-plane U_p at P_0 and the half-plane L_p at P_1 .

Having defined trefoil parameters, let us give a brief overview of what lies ahead. In subsection 3.1 we study the basic properties (as well as existence) of the first-return map on the set $D_\alpha = B_\alpha \cap U_p$. Following that, in subsection 3.2 we study the discontinuities of the first-return map in D_α . Finally, in subsection 3.3 we prove Th.3.15 - where we establish that at trefoil parameters the first-return map has infinitely many periodic orbits in D_α , thus implying chaotic behavior for the flow.

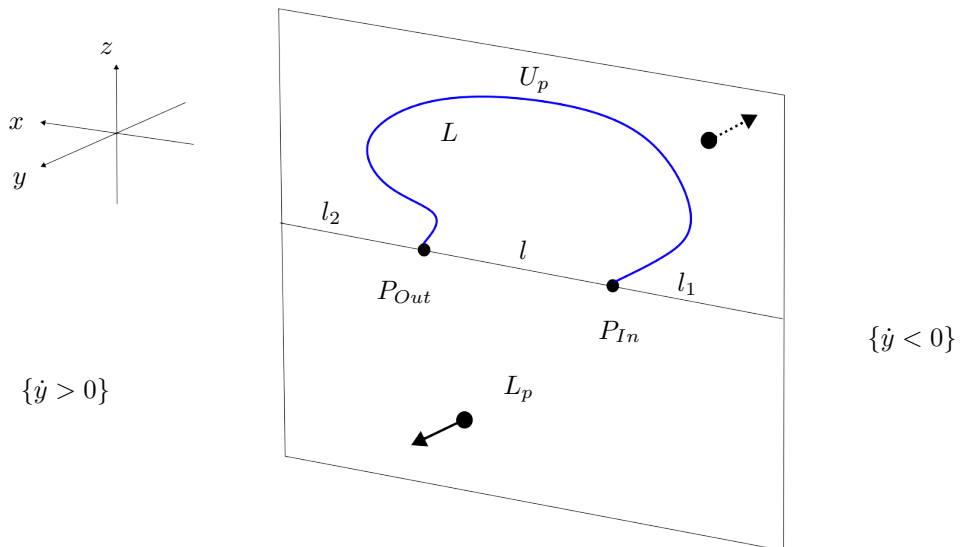


FIGURE 23. The curves l_1, l_2 and l on $\{y = 0\}$ along with the directions of F_p on the plane $\{y = 0\}$ - these curves are all sub-arcs of l_p , the tangency set of the vector field F_p to $\{y = 0\}$. In this illustration, we have $\beta_{In} = \beta_{Out} = L$, while $s_{In} = P_{Out}$, $s_{Out} = P_{In}$.

3.1. The first-return map at trefoil parameters. Let $p \in P$ be a trefoil parameter for the Rössler system, and consider the open topological ball B_α given by Def.3.2. Recall the cross-section U_p is an open half plane (see the discussion before Lemma 2.1), and set $D_\alpha = B_\alpha \cap U_p$ (see the illustration in Fig.37) - we first prove:

Lemma 3.1. *Let $p \in P$ be a trefoil parameter - then, the set D_α is non-empty, P_0 is interior to D_α , and $P_{In}, P_{Out} \in \partial D_\alpha$.*

Proof. Recall Lemma 2.2, where we proved W_{In}^u, W_{Out}^s are both transverse to U_p at the fixed-points P_{In}, P_{Out} (respectively). Since $p \in P$ is a trefoil parameter, by $\partial B_\alpha = W_{In}^u \cup \{P_{In}, P_{Out}\} = W_{Out}^s \cup \{P_{In}, P_{Out}\}$, it follows $U_p \setminus W_{In}^u$ intersects both components of $\mathbf{R}^3 \setminus \partial B_\alpha$ - which proves $D_\alpha = U_p \cap B_\alpha \neq \emptyset$. We similarly conclude $P_{In}, P_{Out} \in \partial B_\alpha \cap \partial U_p$, i.e., $P_{In}, P_{Out} \in \partial D_\alpha$.

To conclude the proof it remains to show P_0 is interior to D_α . Because $\Theta \subseteq B_\alpha$ and because by Def.3.2 P_0 is interior to the cross-section $\overline{U_p}$ (see the illustrations in Fig.21 and Fig.22), it follows P_0 is in $\overline{D_\alpha}$. Note that $\partial D_\alpha \subseteq \partial U_p \cap \partial B_\alpha$ - therefore, since P_0 is interior to both U_p and B_α it follows P_0 is also interior to D_α and Lemma 3.1 now follows (see the illustration in Fig.37). \square

Set $S = W_{In}^u = W_{Out}^s$ - by $\partial B_\alpha = \{P_{In}, P_{Out}\} \cup S$ it follows ∂B_α is invariant under the flow, which implies $\overline{B_\alpha}$ is also invariant under the flow. Therefore, since $\overline{B_\alpha}$ is bounded, given any $s \in \overline{B_\alpha}$, its trajectory is bounded as well. Combining this fact with Lemma 2.1, we now prove:

Lemma 3.2. *Let $p \in P$ be a trefoil parameter for the Rössler system. Then, the first-return map $f_p : \overline{D_\alpha} \setminus \{P_0\} \rightarrow \overline{D_\alpha} \setminus \{P_0\}$ is well-defined - and conversely, so is its inverse $f_p^{-1} : \overline{D_\alpha} \setminus \{P_0\} \rightarrow \overline{D_\alpha} \setminus \{P_0\}$. Moreover, whenever $s \in \overline{D_\alpha} \setminus \{P_0\}$ is not a fixed point, $f_p(s)$ is also not a fixed-point.*

Proof. Recall the forward trajectory of an initial condition $s \in \overline{D_\alpha}$ tends to a fixed-point precisely when $s \in W_{In}^s \cup W_{Out}^s$ - and that $(W_{In}^s \cup W_{Out}^s) \cap B_\alpha = W_{Out}^s \cup \Theta$, where Θ is the heteroclinic trajectory given by Def.3.2.

We now prove Lemma 3.2, in three short steps. To begin, consider $s \in W_{Out}^s$, the stable two-dimensional, invariant manifold of the saddle focus P_{Out} . By Lemma 2.2, W_{Out}^s is transverse to U_p at P_{Out} - which implies the forward trajectory of s hits the cross-section $\overline{U_p}$ transversely infinitely many times as it spirals to P_{Out} (see the illustration in Fig.7). Consequentially, by $\partial B_\alpha = W_{Out}^s \cup \{P_{In}, P_{Out}\}$ it follows that given $s \in \partial B_\alpha$ which is not a fixed-point, its forward trajectory hits $\overline{U_p}$ transversely infinitely many times - and each such intersection point between the trajectory of s and $\overline{U_p}$ is not a fixed point.

Now, consider an initial condition $s \in B_\alpha \setminus \Theta$ - as s is interior to B_α , it is not a fixed point itself. Moreover, since B_α is an open topological ball in \mathbf{R}^3 , by $\partial B_\alpha = W_{Out}^s \cup \{P_{In}, P_{Out}\}$ we conclude $s \notin W_{Out}^s$, hence its trajectory does not limit to P_{Out} - and by $\Theta = W_{In}^s \cap \overline{B_\alpha}$ it follows the forward trajectory of s does not limit to P_{In} either. Therefore, since B_α is bounded and invariant under the flow, so is the forward trajectory of s : which, by Lemma 2.1, proves the forward trajectory of s hits $\overline{U_p}$ transversely infinitely many times. Moreover, because s is not a fixed point (and doesn't get attracted to one through some stable manifold) every intersection point between its trajectory and $\overline{U_p}$ is not fixed point.

We conclude that for all $s \in \overline{B_\alpha} \setminus (\Theta \cup \{P_{In}, P_{Out}\})$ its forward trajectory hits the cross-section $\overline{U_p}$ transversely infinitely many times - and moreover, every point of intersection between the said trajectory and $\overline{U_p}$ is not a fixed point. Recalling $D_\alpha = B_\alpha \cap U_p$, because $\overline{B_\alpha}$ is invariant under the flow the trajectory of any initial condition $s \in \overline{D_\alpha} \setminus \Theta$ returns to $\overline{U_p}$ precisely at $\overline{D_\alpha} \setminus \Theta$. Since $\overline{D_\alpha} \cap \Theta = \{P_0\}$, it now follows the first-return map $f_p : \overline{D_\alpha} \setminus \{P_0\} \rightarrow \overline{D_\alpha} \setminus \{P_0\}$ is well defined - and whenever $s \in \overline{D_\alpha} \setminus \{P_0\}$ is not a fixed point, neither is $f_p(s)$. Using a similar argument applied to the inverse flow, we conclude the inverse first-return map $f_p^{-1} : \overline{D_\alpha} \setminus \{P_0\} \rightarrow \overline{D_\alpha} \setminus \{P_0\}$ is also well-defined and Lemma 3.2 now follows. \square

Remark 3.3. *Using the invariance of B_α under the flow, the argument used to prove Lemma 3.2 implies both $f_p(\overline{D_\alpha} \setminus \{P_0\}) = \overline{D_\alpha} \setminus \{P_0\}$ and $f_p^{-1}(\overline{D_\alpha} \setminus \{P_0\}) = \overline{D_\alpha} \setminus \{P_0\}$.*

We conclude this section by proving the set D_α is a topological disc in the half-plane U_p . To do so, first recall the curve l_p is parameterized by $l_p(x) = (x, -\frac{x}{a}, \frac{x}{a})$, $x \in \mathbf{R}$ (see Lemma 2.4 and the illustrations in Fig.6 and Fig.7). In particular, recall l_p is the tangency curve of F_p to the plane $\{\dot{y} = 0\}$, and that $\{\dot{y} = 0\} \setminus l_p$ is composed of two components - the half planes U_p and L_p (see the discussion preceding Lemma 2.1, and the illustration in Fig.23). As shown immediately before the proof of Lemma 2.1, on U_p the vector field F_p points into $\{\dot{y} < 0\}$ (the region in front of $\{\dot{y} = 0\}$), while on L_p , F_p points into $\{\dot{y} > 0\}$ (the region behind $\{\dot{y} = 0\}$) - see the illustration in Fig.23.

Additionally, we will also need to recall some notations from Section 2 - and introduce two new ones:

- From now on, we always denote by l the set $\{l_p(x) | x \in (0, c - ab)\}$ - that is, l is the sub-arc on l_p connecting P_{In}, P_{Out} (see Fig.32 and Fig.23).

- Similarly to what we did in Sect.2, we define $l_1 = \{l_p(x)|x < 0\}$, and $l_2 = \{l_p(x)|x > c - ab\}$ (see the illustration in Fig.23).
- Finally, we set $L = W_{In}^u \cap U_p = W_{Out}^s \cap U_p = \partial B_\alpha \cap U_p$ (see the illustration in Fig.23 and .32). Since $W_{In}^u = W_{Out}^s = S \subseteq \partial B_\alpha$, by $D_\alpha = B_\alpha \cap U_p$ it follows $L \subseteq \partial D_\alpha$.

With these ideas in mind, we now prove:

Proposition 3.4. *Let $p \in P$ be a trefoil parameter. Then, the set L is a curve in U_p , with one endpoint at P_{In} and another at P_{Out} , as illustrated in both Fig.32 and Fig.23. Consequentially, D_α is a open topological disc on the half-plane U_p , satisfying $\partial D_\alpha = L \cup l \cup \{P_{In}, P_{Out}\}$ - see the illustrations in Fig.32 and Fig.23.*

Proof. As we assume $p \in P$ is a trefoil parameter, by definition we have $W_{In}^u = W_{Out}^s$ - and therefore also $\partial B_\alpha = W_{Out}^s \cup \{P_{In}, P_{Out}\} = W_{In}^u \cup \{P_{In}, P_{Out}\}$ (we will use both these representations throughout the proof). The proof of Prop.3.4 is rather technical and based on directly analyzing the local dynamics of the vector field F_p in \mathbf{R}^3 .

To give an outline of our argument, note that that by Lemma 2.2, ∂B_α is transverse to U_p at both fixed-points. This implies there exists a component $\beta_{In} \subseteq W_{In}^u \cap U_p$ which is a curve beginning at P_{In} and terminates at some point $s_{In} \in l_p$ - similarly, there also exists a component $\beta_{Out} \subseteq W_{Out}^s \cap U_p$ which begins at P_{Out} and terminates at some $s_{Out} \in l_p$ (see the illustrations in Fig.24 and 26, respectively). We now sketch the proof of Prop.3.4 - where l, l_1 and l_2 are the components of $l_p \setminus \{P_{In}, P_{Out}\}$ as defined above:

- First, we prove $s_{In} \notin l_1 \cup l$ (see Lemma 3.5).
- Second, we prove - using an almost symmetric argument - that $s_{Out} \notin l_2 \cup l$ (see Lemma 3.6).
- Finally, we tie these results together and conclude $s_{In} = P_{Out}, s_{Out} = P_{In}$, from which Prop.3.4 would follow.

To begin, recall we denote by $f_p : \overline{D_\alpha} \setminus \{P_0\} \rightarrow \overline{D_\alpha} \setminus \{P_0\}$ the first-return map, and recall f_p is defined throughout $\partial B_\alpha \cap \overline{U_p} \subseteq \partial D_\alpha$ (see Lemma 3.2). Per the outline above, we first prove:

Lemma 3.5. *With the notations and definitions above, whenever $p \in P$ is a trefoil parameter, $s_{In} \notin l_1 \cup l$.*

Proof. We prove Lemma 3.5 by contradiction - we first rule out the possibility $s_{In} \in l_1$, after which we rule out $s_{In} \in l$, using similar arguments.

To begin, assume $s_{In} \in l_1$, which implies β_{In} is a curve in U_p whose closure connects P_{In} and l_1 as in Fig.24. Since by definition $\beta_{In} \subseteq W_{In}^u \cap U_p$, as W_{In}^u is the unstable invariant manifold of P_{In} it follows both $f_p(\beta_{In}) \not\subseteq \beta_{In}$ and $\beta_{In} \subseteq f_p(\beta_{In})$. This proves there exists an initial condition s_1 , strictly interior to β_{In} , s.t. $f_p(s_1) = s_{In}$ as illustrated in Fig.24. Since by Lemma 2.4 the trajectory of s_1 flows to s_{In} through $\{y \leq 0\}$, the y -coordinate of s_1 is strictly greater than that of s_{In} (see the illustration in Fig.24).

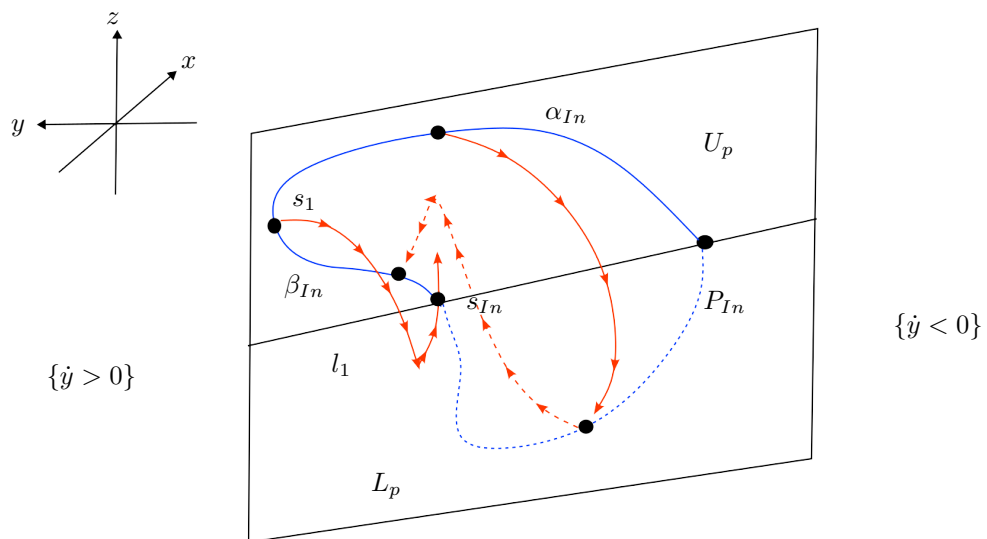


FIGURE 24. The curve β_{In} when $s_{In} \in l_1$. The sub-arc α_{In} flows to β_{In} by hitting L_p , while the y -coordinate of s_1 is greater than that of s_{In} . This scenario will imply a contradiction.

Now, let $\alpha_{In} \subseteq \beta_{In}$ denote the sub-arc of β_{In} connecting P_{In} and s_1 , and let us consider the two-dimensional set V generated by the collection of flow-lines connecting α_{In} to β_{In} (as illustrated in Fig.24) - around P_{In} , V

forms the boundary of a topological cone C with a tip at P_{In} . Moreover, V and the plane $\{y = 0\}$ trap between them a topological cap $\mu = C \cap \{y \geq 0\}$, as illustrated in Fig.24. As a consequence, one can enter the cone C only through the (closed) region $\{y \leq 0\}$. Now, write $s_{In} = (x_{In}, y_{In}, z_{In})$ and consider the half-plane $H = \{(x, y_{In}, z) | x + ay_1 < 0\}$ - by the discussion above, writing $s_1 = (x_1, y_1, z_1)$ we know $y_1 > y_{In}$, which, as s_1 flows to s_{In} implies V intersects $H \cup L_p$ in a collection of curves connecting α_{In} and s_{In} , as illustrated in Fig.25.

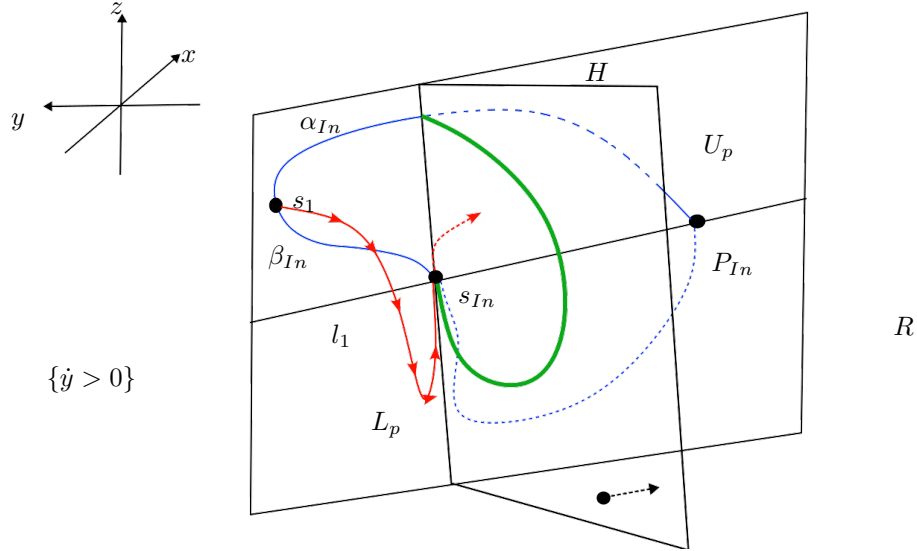


FIGURE 25. The intersection of the cone C with H , sketched as the dark green curve, along with the directions of F_p on H . The trajectory of s_{In} enters the region $R = \{(x, y, z) | \dot{y} < 0, y < y_{In}\}$ immediately after leaving s_{In} .

The normal vector to H is $(0, 1, 0)$, therefore, given $s \in H$, $s = (x, y_{In}, z)$, by definition $F_p(s) \cdot (0, 1, 0) = \dot{y} = x + ay_{In} < 0$ (see the illustration in Fig.25) - therefore, on H the vector field F_p points into the region $\{(x, y, z) | y < y_{In}, \dot{y} < 0\}$. Consequentially, because $s_{In} \in l_1$, we know $F_p(s_{In})$ is tangent to the plane $\{y = 0\}$ (see Lemma 2.4) - which implies the trajectory of s_{In} enters the region $C \cap \{(x, y, z) | y < y_{In}, \dot{y} < 0\}$ upon leaving s_{In} (as illustrated in Fig.25). Since s_{In} lies on the trajectory of s_1 , the trajectory of every $s \in W_{In}^u$ sufficiently close to s_1 also enters $C \cap \{y < y_{In}, \dot{y} < 0\}$ along the trajectory of s_1 (see the illustration in Fig.26).

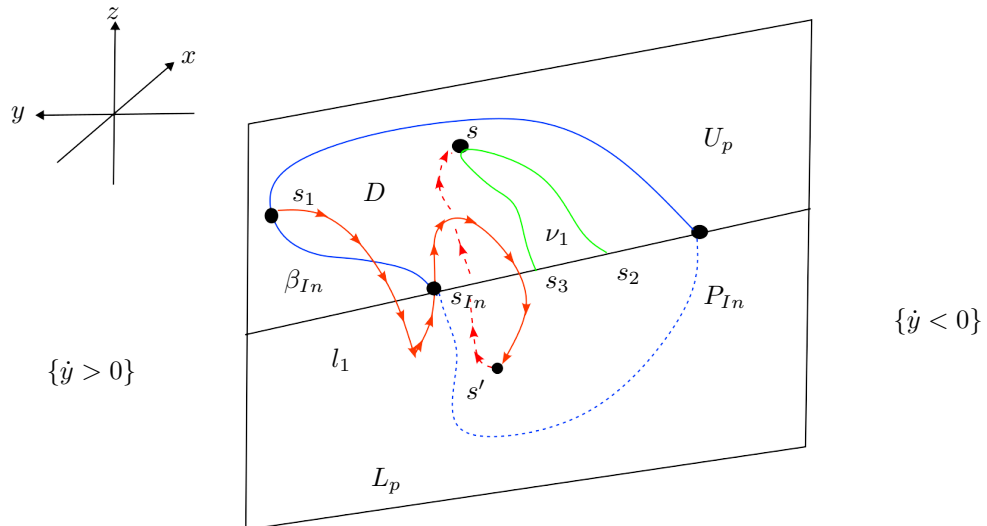


FIGURE 26. The trajectory of s_1 flows to some $s' \in L_p$, after which it hits D transversely at s . Consequentially, there exists a component ν_1 of $W_{In}^u \cap U_p$ in D . We use this to generate a contradiction.

Now, set $D = C \cap U_p$ - by definition, D is a Jordan domain on U_p , trapped between the curves β_{In} and l_1 (as illustrated in Fig.26). As the trajectory of s_1 enters C upon leaving s_{In} , by Lemma 3.2 and by $f_p(s_1) = s_{In}$ there

must exist some minimal $k > 1$ s.t. $f_p^k(s_1) \in D$ - which implies there exists a component ν_1 of $W_{I_n}^u \cap U_p$ in D (see the illustration in Fig.26). Since $W_{I_n}^u$ is a surface and both ν_1 and β_{I_n} are components of the transverse intersection $W_{I_n}^u \cap U_p$, we have $\nu_1 \cap \beta_{I_n} = \emptyset$ - therefore, we conclude ν_1 is a curve in D with two endpoints in $l_1 \cap \partial D_1$, which we denote by s_2 and s_3 (see Fig.26). As there are no homoclinic trajectories in $W_{I_n}^u$ per assumption (as p is a trefoil parameter), both s_2 and s_3 are not P_{I_n} , and are also distinct from one another (as illustrated in Fig.27).

To continue, let us suspend ν_1 with the flow - as $s_2, s_3 \in l_1 \cap \partial D$, using a similar argument to the one used to prove the trajectory of s_{I_n} enters C , it follows the forward trajectories of s_2 and s_3 remain trapped in C until hitting D transversely. Therefore, $f(\nu_1) = \nu_2$ is also a collection of curves inside D , which lie on components of $W_{I_n}^u \cap D$. Let us note every component of $W_{I_n}^u \cap D$ is a curve with two endpoints on $l_1 \cap \partial D_1$ (as illustrated in Fig.27). Additionally, we have $\nu_1 \cap \nu_2 = \emptyset$, $\nu_2 \cap \beta_{I_n} = \emptyset$.

Repeating this process, as every component of $W_{I_n}^u \cap D$ has two endpoints on $l_1 \cap \partial D$, it follows ν_2 flows through the cone C to $\nu_3 = f_p(\nu_2)$, another collection of curves trapped inside D - and again, every component of ν_3 lies on some component of $W_{I_n}^u \cap D$, hence the same is true for $\nu_4 = f_p(\nu_3)$. Repeating this suspension over and over, we conclude the sequence $\{\nu_n\}_n$, $\nu_n = f_p(\nu_{n-1})$, $n > 2$ satisfies the following:

- For every n , the trajectories of initial conditions in ν_{n-1} flow to ν_n through the cone C .
- For every n , we have $\nu_n \subseteq D = C \cap U_p$.

Since D is a Jordan domain trapped between β_{I_n} and l_1 , it follows by $s_{I_n} \neq P_{Out}$ that $P_{Out} \notin \bar{D}$ (see the illustration in Fig.27). This implies that given any initial condition $s \in \nu_1 \subseteq W_{I_n}^u \cap U_p$, by $f_p^n(s) \in \nu_{n+1}$ we have $\lim_{n \rightarrow \infty} f_p^n(s) \neq P_{Out}$. However, because $p \in P$ is a trefoil parameter, by Def.(3.2) we must have $W_{I_n}^u = W_{Out}^s$ - which implies that for every $s \in W_{I_n}^u \cap U_p$ we have $\lim_{n \rightarrow \infty} f_p^n(s) = P_{Out}$. This is a contradiction, from which we conclude $s_{I_n} \notin l_1$, i.e., $\bar{\beta}_{I_n}$ cannot connect P_{I_n} with l_1 through U_p .

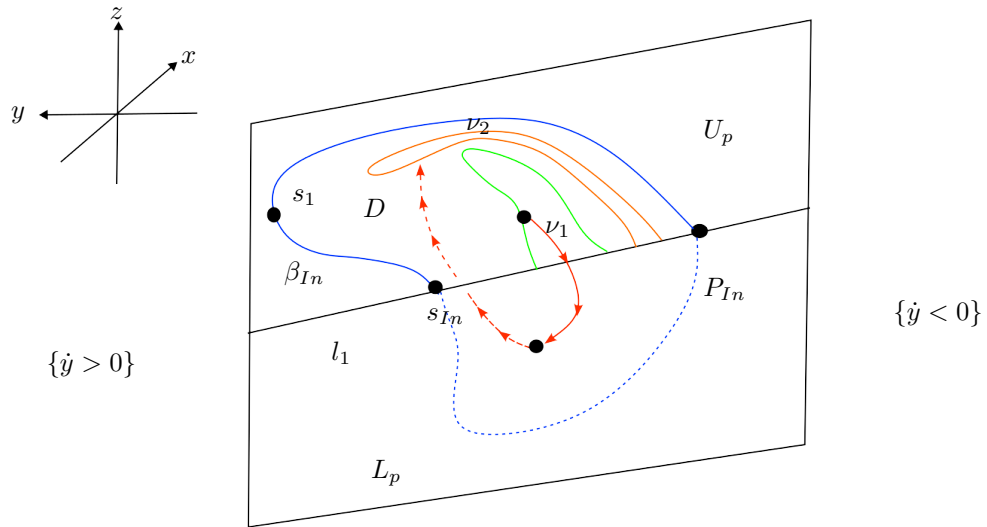


FIGURE 27. The sequence of curves ν_n which flow to one another and remain trapped in D . This yields a contradiction.

Having proven $s_{I_n} \notin l_1$, we now prove $s_{I_n} \notin l$ using a similar argument - thus concluding the proof of Lemma 3.5. To this end, assume by contradiction $s_{I_n} \in l$, as illustrated in Fig.28. Recalling Lemma 2.2, again we conclude there exists some interior $s_1 \in \beta_{I_n}$ s.t. $f_p(s_1) = s_{I_n}$, and some sub-arc $\alpha_{I_n} \subseteq \beta_{I_n}$ connecting P_{I_n} and s_1 (as illustrated in Fig.28) s.t. $f_p(\alpha_{I_n}) = \beta_{I_n}$. Note that V , the collection of flow lines connecting α_{I_n} and β_{I_n} traps a topological cone C - which intersects L_p in a curve ρ_{I_n} , as indicated in Fig.28 (it is easy to see $P_{Out} \notin \bar{C}$). By definition, the trajectory of s_1 flows through $\{y < 0\}$ to some $s \in \rho_{I_n}$ after which it flows through $\{y > 0\}$ to s_{I_n} . This implies the y -component of s is smaller than that of s_{I_n} (see the illustration in Fig.28).

Similar arguments to those used before prove the flow lines connecting ρ_{I_n} and β_{I_n} and the plane $\{y = 0\}$ trap between them a topological cap $\mu' \subseteq \{y \leq 0\}$ - moreover, setting $s_{I_n} = (x_{I_n}, y_{I_n}, z_{I_n})$ and considering the half-plane $H' = \{(x, y_{I_n}, z) | x + ay_{I_n} > 0\}$, using similar arguments we conclude the trajectory of s_{I_n} enters the region $C \cap \{(x, y, z) | y > y_{I_n}, \dot{y} > 0\}$ upon leaving s_{I_n} . Again, the trajectories of initial conditions $s \in W_{I_n}^u$ sufficiently close to s_1 also enter C - and similarly to the previous arguments, after entering C the trajectories of such s can

hit U_p transversely only in the region $C \cap U_p$ (i.e., the analogue of D from before). Using a similar argument we again derive a contradiction from which we conclude $s_{In} \notin l$ - and Lemma 3.5 now follows. \square

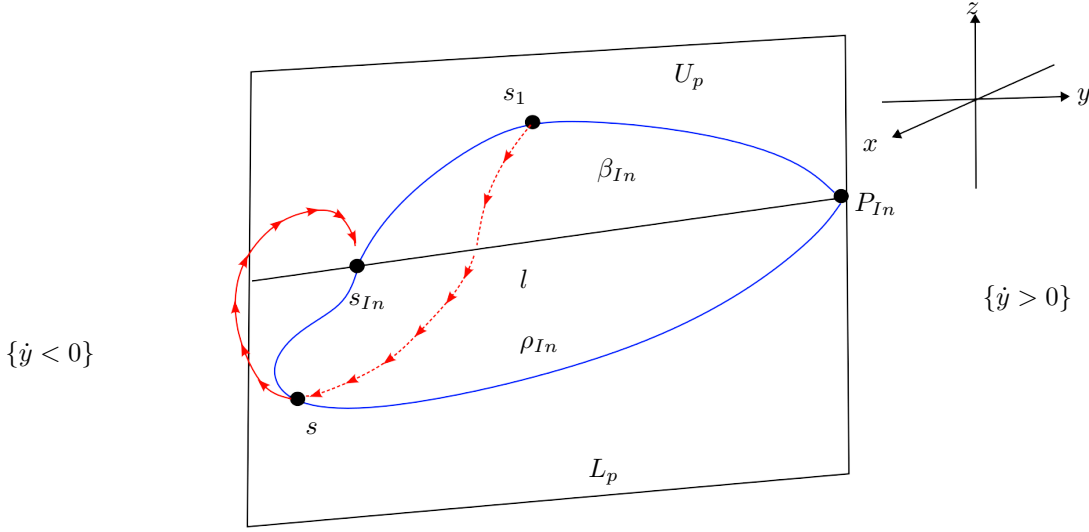


FIGURE 28. The case where $s_{In} \in l$ - as can be seen, there still exists some $s_1 \in \beta_{In}$ which flows to $s \in L_p$, after which it flows to $s_{In} = f_p(s_1)$. The y -coordinate of s is lesser than that of s_{In} - which implies a contradiction.

Having proven Lemma 3.5, we now prove its analogue for β_{Out} - the component of $W_{Out}^s \cap U_p$ which begins at P_{Out} (see the illustration in Fig.23 and Fig.29). To do so, recall we denote by s_{Out} the termination point of $\overline{B_{Out}}$ on l_p , s.t. $s_{Out} \neq P_{Out}$ (see the illustration in Fig.23 and Fig.29), and recall $l_2 = \{l_p(x) | x > c - ab\}$ (see the discussion immediately before Prop.3.4). We now prove:

Lemma 3.6. *Whenever $p \in P$ is a trefoil parameter, we have $s_{Out} \notin l_2 \cup l$.*

Proof. We prove Lemma 3.6 using similar arguments to those used to prove Lemma 3.5 - again, we first prove $s_{Out} \notin l_2$, after which we prove $s_{Out} \notin l$ (both by contradiction).

To begin, assume by contradiction $s_{Out} \in l_2$, as illustrated in Fig.29. Since $\beta_{Out} \subseteq W_{Out}^s \cap U_p$, because W_{Out}^s is the two-dimensional stable manifold of P_{Out} we conclude there exists some $s_1 \in \beta_{Out}$ s.t. $f_p^{-1}(s_1) = s_{Out}$ - and by Lemma 2.4 we know the backwards trajectory of s_1 arrives at s_{Out} through $\{y \leq 0\}$ (passing first through the half-plane L_p , as indicated in Fig.29). Similarly to the proof of Lemma 3.5, let α_{Out} denote the sub-arc of β_{Out} beginning at P_{Out} and terminating at s_1 - again, using similar arguments, it follows the inverse flow lines connecting α_{Out} and β_{Out} trap a topological cone C (see the illustration in Fig.29). It is easy to see $P_{In} \notin \overline{C}$.

Now, set $s_{Out} = (x_{Out}, y_{Out}, z_{Out})$ and $H = \{(x, y_{Out}, z) | x + ay_{Out} < 0\}$. Using a similar argument to the one used to prove Lemma 3.5 (applied to the inverse flow) it follows the backward trajectories of initial conditions $s \in W_{Out}^s$ sufficiently close to s_1 enter $C \cap \{(x, y, z) | y > y_{Out}\}$ under the inverse flow, and never escape it. By $P_{In} \notin \overline{C}$, we conclude that for $s \in W_{Out}^s$ sufficiently close to s_1 we have $\lim_{n \rightarrow \infty} f_p^{-n}(s) \neq P_{In}$ - and by $W_{Out}^s = W_{In}^u$, we again derive a contradiction which implies $s_{Out} \notin l_2$.

To conclude the proof of Lemma 3.6, it remains to prove $s_{Out} \notin l$. To do so, assume by contradiction we have $s_{Out} \in l$ - then, again, suspending β_{Out} with the inverse flow (as indicated in Fig.30) we conclude there exists some $s_1 \in \beta_{Out}$ s.t. $f_p^{-1}(s_1) = s_{Out} = (x_{Out}, y_{Out}, z_{Out})$. Defining $\alpha_{Out} \subseteq \beta_{Out}$ analogously, we again generate a topological cone C with a tip at P_{Out} - again, $P_{In} \notin \overline{C}$ (see the illustration in Fig.30).

As the backwards trajectory connecting s_1 to s_{Out} arrives from $\{y \geq 0\}$, using symmetric arguments, it follows the backward trajectories of initial conditions $s \in W_{Out}^s$ sufficiently close to s_1 eventually enter $C \cap \{(x, y, z) | y > 0, y < y_{Out}\}$ - and remain trapped in it forever. Again, by $W_{Out}^s = W_{In}^u$ we have a contradiction - which implies $s_{Out} \notin l$ as well and Lemma 3.6 now follows. \square

From Lemmas 3.5 and 3.6, we conclude the points s_{In} and s_{Out} lie outside of $l_1 \cup l$ and $l_2 \cup l$ (respectively). We can almost prove $\beta_{In} = \beta_{Out}$ - before doing so, we will also need the following fact, a corollary of both Lemma 3.5 and Lemma 3.6:

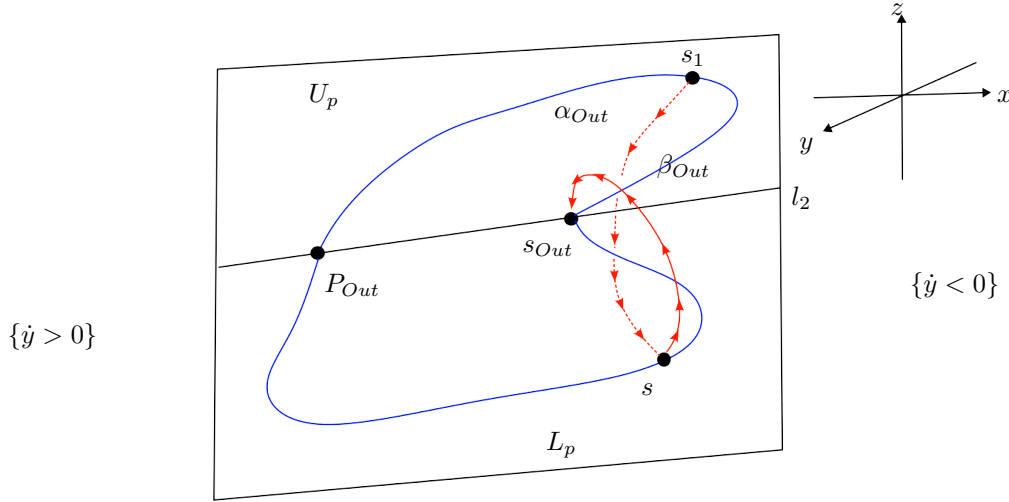


FIGURE 29. By $s_{Out} \in l_2$ there exists some $s_1 \in \beta_{Out}$ which flows to $s \in L_p$, after which it flows (under the inverse flow) to $s_{Out} = f_p^{-1}(s_1)$ (the arc α_{Out} satisfies $f_p^{-1}(\alpha_{Out}) = \beta_{Out}$). As s flows to s_{Out} through $\{y < 0\}$ under the inverse flow, the y -coordinate of s_{Out} is greater than that of s - from which, using similar arguments we again derive a contradiction.

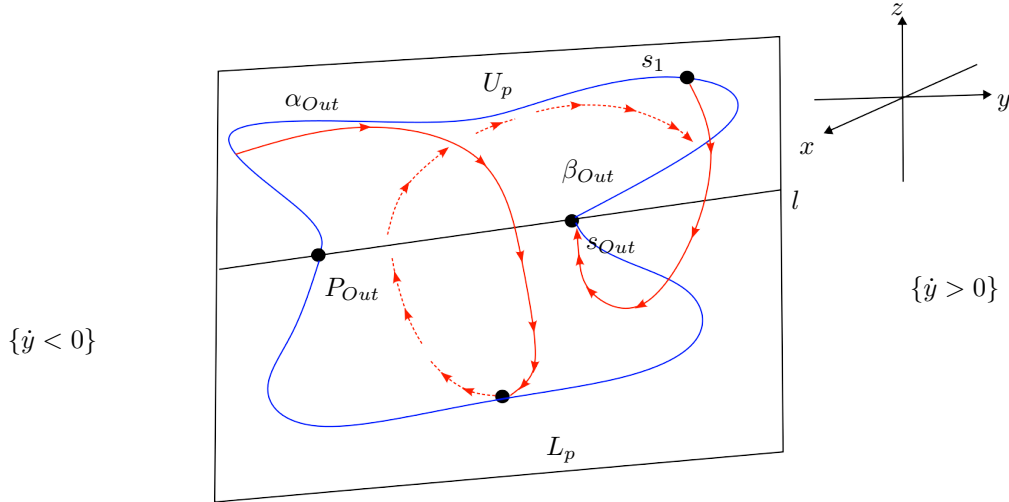


FIGURE 30. The case where $s_{Out} \in l$ - again, there must exist some $s_1 \in \beta_{Out}$ which flows to $s_{Out} = f_p^{-1}(s_1)$ under the inverse flow (the arc α_{Out} satisfies $f_p^{-1}(\alpha_{Out}) = \beta_{Out}$). The y -coordinate of s_{Out} is greater than that of s_1 - which implies a contradiction.

Corollary 3.7. $s_{In} \notin l_2$ and $s_{Out} \notin l_1$.

Proof. We prove Cor.3.7 by contradiction. If $s_{In} \in l_2$, it immediately follows β_{In} separates β_{Out} from l_1 (see the illustration in Fig.31). This implies $\overline{\beta_{Out}}$ connects P_{Out} and some $s_1 \in l \cup l_2$, or, in other words, $s_{Out} \in l \cup l_2$. Since this is impossible by Lemma 3.6, we must have $s_{In} \notin l_2$. Using a symmetric argument we conclude $s_{Out} \notin l_1$ and the assertion follows. \square

Having proven Lemmas 3.5, 3.6 and Cor.3.7, we now conclude the proof of Prop.3.4. To do so, let us first remark that since $p \in P$ is a trefoil parameter there are no homoclinic trajectories - which implies β_{In} cannot be a closed loop which begins and terminates at P_{In} . Consequentially, as $\overline{\beta_{In}}$ cannot connect P_{In} through U_p with either l_1, l_2, l or P_{In} , the only possibility is that it terminates at P_{Out} , i.e., $s_{In} = P_{Out}$. This immediately implies $L = \beta_{In} = \beta_{Out} = W_{In}^u \cap U_p = W_{Out}^s \cap U_p$ is a simple curve in U_p , connecting P_{In} and P_{Out} through U_p , as illustrated in Fig.23 and Fig.32.

It now immediately follows the union $T = L \cup l \cup \{P_{In}, P_{Out}\}$ is a Jordan curve on $\overline{U_p}$, which implies $U_p \setminus T$ consists of two components - a bounded and an unbounded set. As B_α is bounded we conclude the bounded set is $D_\alpha = B_\alpha \cap U_p$ which implies D_α is a topological disc on U_p as illustrated in Fig.32. The proof of Prop.3.4 is now complete. \square

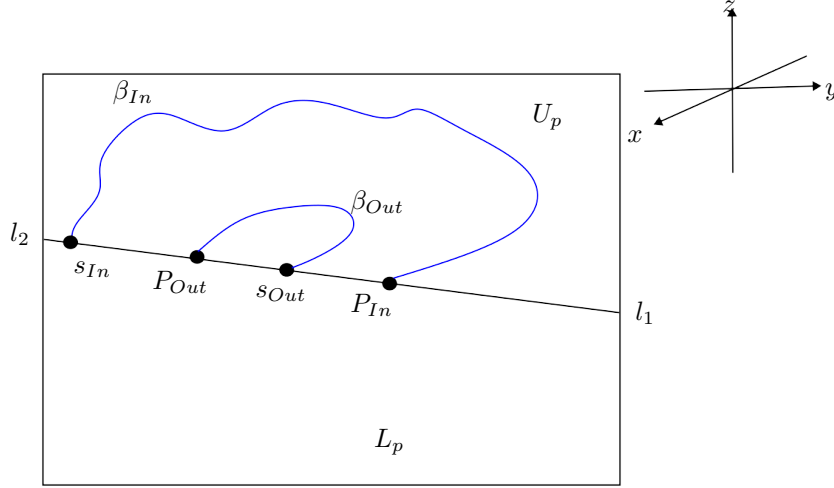


FIGURE 31. The case where $s_{In} \in l_2$ - as β_{In} would then separate β_{Out} and l_1 , it would force s_{Out} to be in either l_2 or l (where l is the open arc connecting P_{In} and P_{Out}). This contradicts Lemma 3.6.

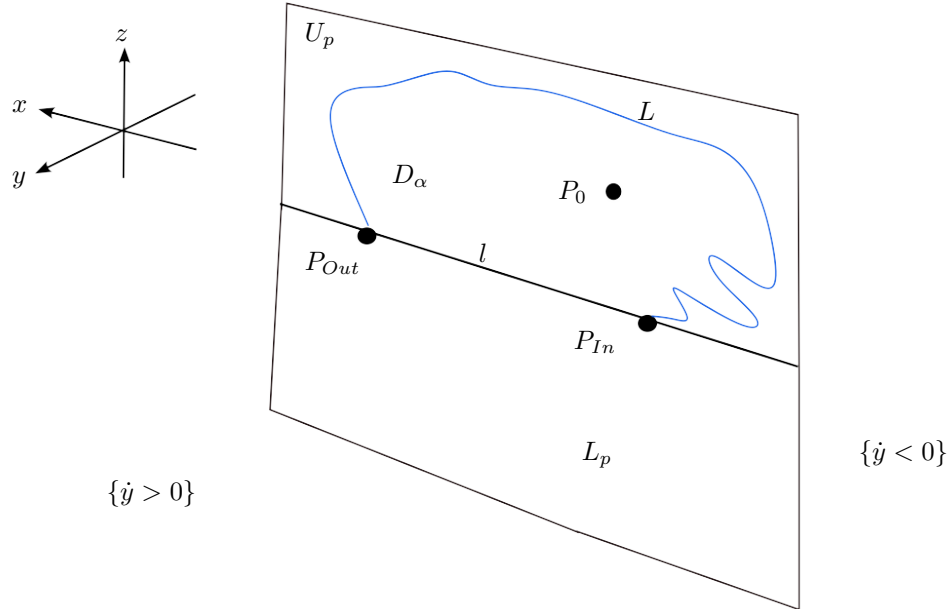


FIGURE 32. The Jordan domain $D_\alpha \subseteq U_p$, bounded by the blue curve $L = \partial B_\alpha \cap U_p$ (see Def.3.2), the fixed points, and the boundary arc l . l lies on the line l_p , the tangency set of F_p to $\{\dot{y} = 0\}$ which separates L_p from U_p .

3.2. The discontinuity properties of the first-return map. Having proven the existence of the first-return map $f_p : \overline{D_\alpha} \setminus \{P_0\} \rightarrow \overline{D_\alpha} \setminus \{P_0\}$ at trefoil parameters and that D_α is a topological disc, in this subsection we now study its continuity and discontinuity properties of f_p .

To begin, let $p \in P$, $p = (a, b, c)$ be a trefoil parameter. Recall the heteroclinic trefoil knot intersects the cross-section U_p at a single point, P_0 , interior to the topological disc D_α (see the illustration in Fig.32). We begin with the following technical result, where we characterize the discontinuity set of f_p in the punctured disc $D_\alpha \setminus \{P_0\}$:

Proposition 3.8. *Let $p \in P$ be a trefoil parameter for the Rössler system. Then, the first-return map $f_p : \overline{D_\alpha} \setminus \{P_0\} \rightarrow \overline{D_\alpha} \setminus \{P_0\}$ is continuous at the fixed-point P_{In} and on the curve L - moreover, the discontinuities of f_p in the punctured topological disc $D_\alpha \setminus \{P_0\}$, denoted by $Dis(f_p)$, are given by $f_p^{-1}(l) \cap D_\alpha$. In addition, there exists a curve $\delta \subseteq Dis(f_p)$ satisfying:*

- δ is a component of $Dis(f_p)$, and it is homeomorphic to an open interval.
- δ has two endpoints: P_0 and some point $\delta_0 \in \bar{l}$. Moreover, $\delta_0 \neq P_{In}$.

- $P_{In} \in \overline{f_p(\delta)}$.
- If ρ is a component of $Dis(f_p)$ s.t. $\rho \neq \delta$, it is a curve with (at least) two endpoints on \bar{l} . Moreover, $P_0 \notin \bar{\rho}$.

Proof. First, recall that since p is a trefoil parameter the two-dimensional invariant manifolds W_{In}^u, W_{Out}^s coincide. Moreover, recall that by Prop.3.4 D_α is an open topological disc bounded by the Jordan curve $l \cup L \cup \{P_{In}, P_{Out}\}$ - and that $L = W_{In}^u \cap U_p$ is a curve connecting P_{In} and P_{Out} through U_p (see the illustration in Fig.32). By the invariance of W_{In}^u under the flow we have $f_p(L) = L$.

We now prove f_p is continuous on L . To see why, note that by $L \subseteq U_p$ it follows L lies away from l_p , the tangency curve of the vector field F_p to the plane $\{y = 0\}$ - see the illustration in Fig.32. Therefore, for every $s \in L$ the flow line connecting s to $f_p(s) \in L$ is transverse to the cross-section U_p at $f_p(s)$. Consequentially, the first-return map f_p is continuous throughout L .

Using a similar argument, we now prove f_p is continuous around P_{In} (in $\overline{D_\alpha}$) - to do so, recall that by Lemma 2.2 W_{In}^u , is transverse to $\overline{U_p}$ at P_{In} . Therefore, since P_{In} is a saddle-focus initial conditions on the arc l_p sufficiently close to P_{In} are mapped inside U_p by f_p (see the illustration in Fig.33). By the orientation-preserving property of the flow and because both $f_p(L) = L$ and $f_p(P_{In}) = P_{In}$, it follows f_p squeezes some sector in $\overline{D_\alpha}$ trapped between L and l inside $\overline{D_\alpha}$ (see the illustration in Fig.33). Consequentially, f_p is continuous on some neighborhood of P_{In} in $\overline{D_\alpha}$.

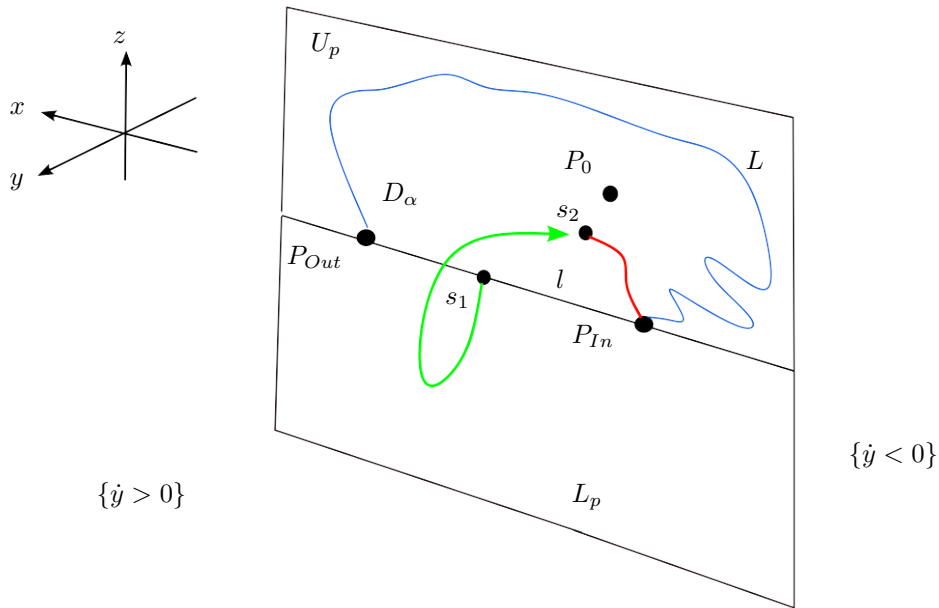


FIGURE 33. The trajectory of an initial condition $s_1 \in l$ which is sufficiently close to P_{In} - because P_{In} is a saddle-focus, the trajectory of s_1 hits the cross-section transversely. The red curve is the image under f_p of the arc connecting P_{In} and s_1 .

We now prove $Dis(f_p) = f_p^{-1}(l) \cap D_\alpha$. We first prove that for an initial condition $s \in D_\alpha \setminus \{P_0\}$ to be a discontinuity point for f_p , a necessary condition is that $f_p(s)$ lies in l . To see why this is so, recall the following facts:

- By Lemma 3.1, the fixed points P_{In} and P_{Out} lie in ∂D_α . As such, any $s \in D_\alpha \setminus \{P_0\}$ is not a fixed point for the flow - hence, by Lemma 3.2 $f_p(s) \neq P_{In}, P_{Out}$.
- By the continuity of f_p on $L \subseteq \partial D_\alpha$, there are no discontinuity points for f_p on L .
- Since the vector field F_p is transverse to U_p it is also transverse to the (open) punctured disc $D_\alpha \setminus \{P_0\} \subseteq U_p$ - which proves that whenever $f_p(s) \in D_\alpha \setminus \{P_0\}$, f_p is continuous at s .

By $\overline{D_\alpha} \setminus \{P_0\} = L \cup l \cup \{P_{In}, P_{Out}\} \cup (D_\alpha \setminus \{P_0\})$ we conclude that whenever f_p is discontinuous at $s \in D_\alpha \setminus \{P_0\}$, the only possibility is $f_p(s) \in l$. Now, recall $l \subseteq l_p$ - where l_p is the tangency set of F_p to $\overline{U_p}$ (see the discussion immediately before Lemma 2.1). This implies that given $s \in D_\alpha \setminus \{P_0\}$ whose trajectory is tangent to $\overline{D_\alpha}$ at $f_p(s) \in l$, there exists a two-dimensional disc on D_α , centered at s , whose image under f_p is torn in two as

illustrated in Fig.34. In other words, whenever $s \in D_\alpha \setminus \{P_0\}$ satisfies $f_p(s) \in l$, f_p is discontinuous at s .

Therefore, since the condition $f_p(s) \in l$ is both sufficient and necessary for an initial condition $s \in D_\alpha \setminus \{P_0\}$ to be a discontinuity for f_p , we conclude the discontinuity set of f_p in $D_\alpha \setminus \{P_0\}$ is given by $f_p^{-1}(l) \cap D_\alpha = Dis(f_p)$. Furthermore, by $l \cap L = \emptyset$ and by the invariance of L it is also immediate that L does not intersect the closure of $Dis(f_p)$.

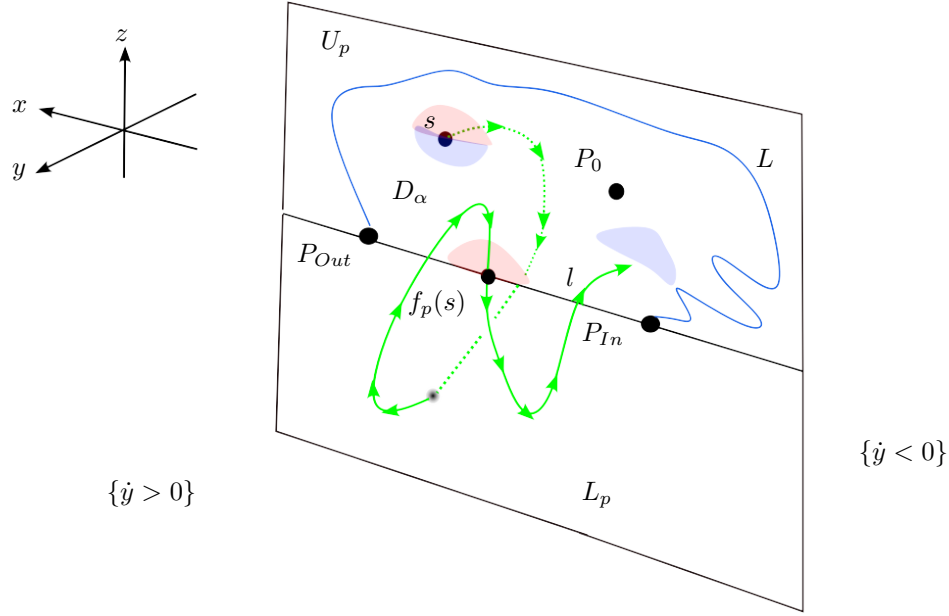


FIGURE 34. The trajectory of an interior point $s \in D_\alpha$ s.t. $f_p(s) \in l$. Typically, this would mean there are nearby trajectories that hit D_α in its interior when the trajectory of s hits the boundary at $f_p(s)$, and other trajectories which continue with the trajectory of s and hit the interior of D_α around $f_p^2(s)$.

We now prove the existence of the discontinuity curve δ as posited above. To do so, consider some closed loop ζ in D_α surrounding P_0 . Since p is a trefoil parameter, the trajectory of P_0 flows to P_{In} in infinite time without ever hitting $\overline{D_\alpha}$ along the way (see Def.3.2) - hence, f_p cannot be continuous on ζ : for if it were continuous on ζ , $f_p(\zeta)$ would be a closed curve in $\overline{D_\alpha}$ surrounding P_{In} . Because this is impossible by $P_{In} \in \partial D_\alpha$, from the discussion above we conclude there must exist a discontinuity point $\zeta_0 \in \zeta$ - i.e., there exists some $\zeta_0 \in \zeta$ s.t. $f_p(\zeta_0) \in l$.

Varying the loop ζ continuously in D_α we construct an open arc δ of discontinuity points, whose closure $\bar{\delta}$ is a curve connecting P_0 and some unique point δ_0 in \bar{l} (see the illustration in Fig.37 and Fig.35). As $\overline{P_0}$ tends to P_{In} in infinite time, it follows $f_p(\delta)$ is an arc on l s.t. $P_{In} \in \overline{f_p(\delta)}$ - similarly, we also have $f_p^j(\delta_0) \in \overline{f_p(\delta)} \subseteq \bar{l}$ for some $j \geq 1$ (see the illustration in Fig.35). It is easy to see that because f_p is continuous around P_{In} , it follows $\delta_0 \neq P_{In}$ - and moreover, by $Dis(f_p) \cap L = \emptyset$ we have $L \cap \delta = \emptyset$.

We now prove that $f_p^{-2}(l) \cap \delta = \emptyset$, which we will later use to prove δ is a component of $Dis(f_p)$. To do so, first note that for any $s \in l$ the flow line connecting $s, f_p(s)$ lies strictly inside $\{y \geq 0\}$ (see the illustration in Fig.35). This proves that for $s \in l$, the y -coordinate of $f_p(s)$ is strictly greater than that of s - and by $f_p(\delta) \subseteq l$ we conclude that for $s \in \delta$, the y -coordinate of $f_p^2(s)$ is greater than that of $f_p(s)$. Second, by $\delta \subseteq D_\alpha$ and $f_p(\delta) \subseteq \partial D_\alpha$, as D_α is an open topological disc we conclude $f_p(\delta) \cap \delta = \emptyset$ - which further yields $f_p^2(\delta) \cap f_p(\delta) = \emptyset$ (see the illustration in Fig.35).

Now, recall we parameterize l by $(x, -\frac{x}{a}, \frac{x}{a})$, $x \in (0, c - ab)$ - by $P_{In} = (0, 0, 0)$ it follows the y -coordinate on l increases monotonically as $s \in l$ tends to P_{In} . Therefore, because $\overline{f_p(\delta)}$ is an arc with one endpoint at P_{In} , given $v \in l \setminus \overline{f_p(\delta)}$ and $\mu \in \overline{f_p(\delta)}$ the y -coordinate of v is smaller than that of μ - and since by previous paragraph for every $s \in \delta$ the y -coordinate of $f_p^2(s)$ is greater than that of $f_p(s)$, we conclude $f_p^2(\delta) \cap l \setminus \overline{f_p(\delta)} = \emptyset$. Combined with $f_p(\delta) \cap f_p^2(\delta) = \emptyset$, it follows $f_p^2(s) \notin l$, i.e., $\delta \cap f_p^{-2}(l) = \emptyset$ (see the illustration in Fig.35).

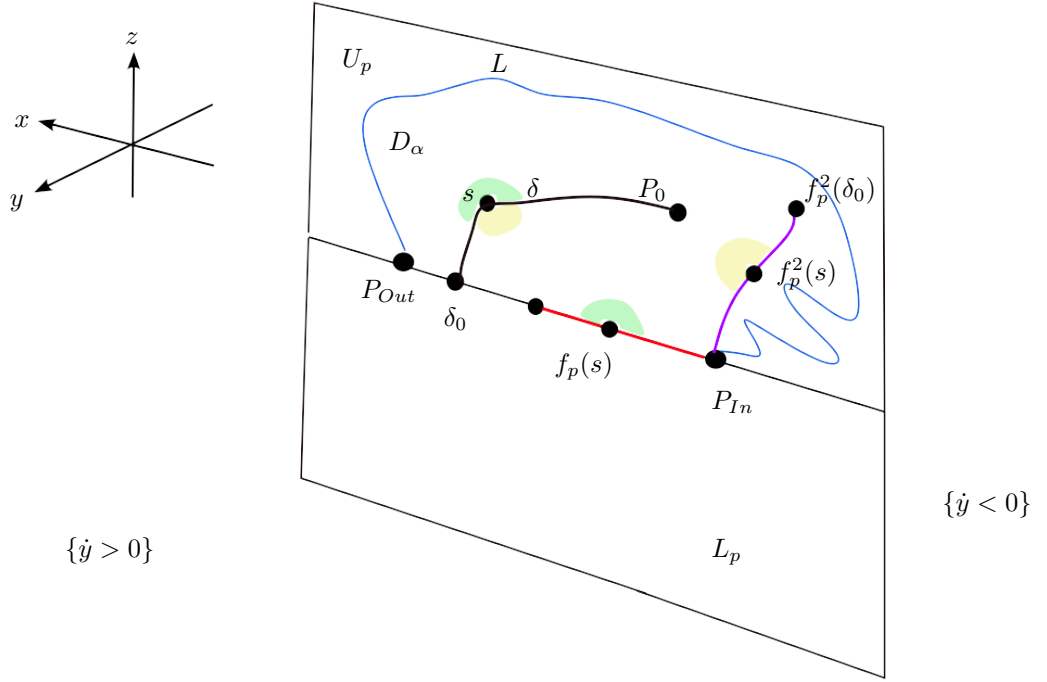


FIGURE 36. The trajectories on initial conditions $s \in \delta$ - the green region hits the green half-disc above $f_p(\delta)$ (denoted by the red arc), while the yellow half-disc hits close to $f_p^2(s)$ (which lies on $f_p^2(\delta)$, denoted by the purple arc).

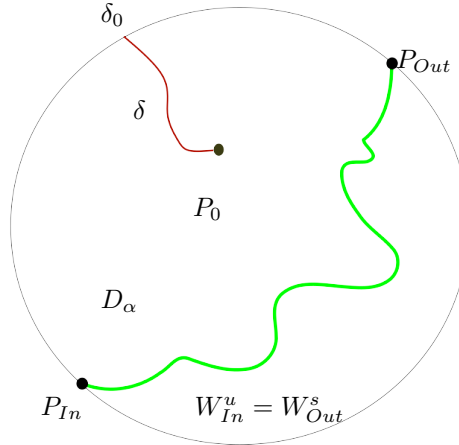


FIGURE 37. The geography of the cross-section U_p for a trefoil parameter $p \in P$, sketched as a disc for simplicity (with the curve δ sketched in red). The green arc denotes $W_{In}^u \cap \overline{U_p} = W_{Out}^s \cap \overline{U_p}$. The set D_α corresponds to $B_\alpha \cap \overline{U_p}$.

D_α , that endpoint can only be P_0 .

To conclude the proof, recall that since both ρ and δ are components of $Dis(f_p)$ we have $f_p(\rho), f_p(\delta) \subseteq l$ - recalling l is an open arc on ∂D_α whose endpoints are P_{In}, P_{Out} , since P_0 lies in $\overline{\rho} \cap \overline{\delta}$ and because P_0 tends to P_{In} in infinite time, we conclude $P_{In} \in \overline{f_p(\delta)} \cap \overline{f_p(\rho)}$. As both $f_p(\delta), f_p(\rho)$ are arcs on l with an endpoint at P_{In} , it follows $f_p(\rho) \cap f_p(\delta) \neq \emptyset$ - therefore, by the Existence and Uniqueness Theorem $\rho = \delta$. Consequentially, if ρ is a component of $Dis(f_p)$ s.t. $\rho \neq \delta$, then ρ has two endpoints in l . A similar argument proves that whenever $\rho \neq \delta$ we have $P_0 \notin \rho$ and Prop.3.8 follows (see Fig.39 for an illustration). \square

Remark 3.9. Given $s \in l$, the same arguments used above also imply that whenever $f_p(s)$ is interior to D_α , f_p is continuous on a neighborhood of s in $\overline{D_\alpha}$.

The main takeaway from Prop.3.8 is that the point P_0 generates a discontinuity curve δ which, due to the existence of the heteroclinic trefoil, is associated with the fixed point P_{In} . However, this does not imply the

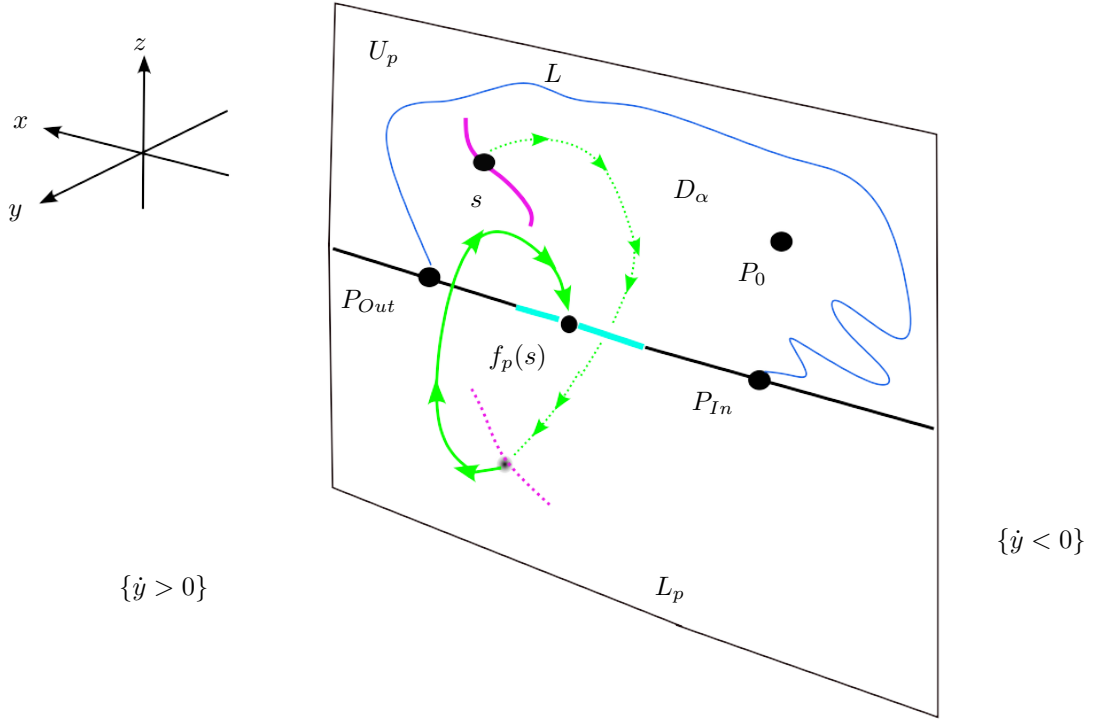


FIGURE 38. $\gamma \subseteq \text{Dis}(f_p)$, the pink curve, flows towards l , passes through L_p at the dashed pink curve, after which it hits l at $\theta = f_p(\gamma)$, the cyan arc. As can be seen, if $f_p(s)$ is interior to θ , s is interior to γ (and vice versa).

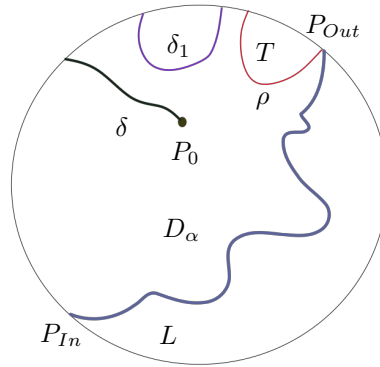
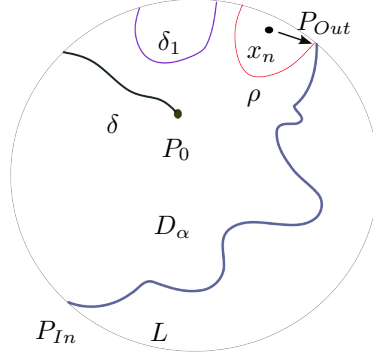


FIGURE 39. The discontinuity curves for f_p in D_α - δ, ρ , and δ_1 , another possible discontinuity curve. In this sketch, U_p is drawn for simplicity as a disc. T is the sector trapped between l and ρ .

first-return map is continuous at the second fixed point, P_{Out} . Using the same notations and ideas used to prove Prop.3.8 we now prove:

Corollary 3.10. *Let $p \in P$ be a trefoil parameter. Then, there exists a unique curve $\rho \subseteq \text{Dis}(f_p)$ s.t. $P_{Out} \in \bar{\rho}$. Moreover, there exists a bounded sector T , trapped between ρ and l with a tip at P_{Out} , s.t. $P_0 \in \partial f_p(T)$ (see Fig.39 and Fig.41 for illustrations).*

Proof. Let us recall the two-dimensional stable manifold for P_{Out} , W_{Out}^s , is transverse to the cross-section U_p at P_{Out} (see Lemma 2.2 and the illustration in Fig.7). This implies the backwards trajectories of initial conditions on the arc l sufficiently close to P_{Out} all hit U_p transversely - or, in other words, there exists a curve $\rho \subseteq \text{Dis}(f_p)$, $P_{Out} \in \bar{\rho}$, s.t. $f_p(\rho)$ is an arc on l with an endpoint at P_{Out} (see the illustration in Fig.41) - that is, the flow pushes ρ over the arc $f_p(\rho)$ - it is easy to see that by the Existence and Uniqueness Theorem, ρ is unique. Now, let T denote the open sector trapped between ρ and l (see the illustration in Fig.40 and Fig.41), and let us consider a sequence $\{x_n\}_n \subseteq T$ s.t. $x_n \rightarrow P_{Out}$.


 FIGURE 40. x_n tends to P_{Out} from inside the sector T .

Now, recall the heteroclinic trajectory Θ given by Def.3.2 flows from P_{Out} to P_{In} , while hitting D_α transversely at P_0 along the way. Additionally, note that since the first-return map pushes ρ down on $f_p(\rho)$, it follows $f_p(T) \cap T = \emptyset$, hence $f_p(x_n) \not\rightarrow P_{Out}$. Therefore, because $\{x_n\}_n$ tends to P_{Out} it follows that for n sufficiently large x_n leaves D_α and travels along the bounded heteroclinic trajectory Θ until hitting D_α (see the illustration in Fig.41). Hence, since $x_n \rightarrow P_{Out}$ and because Θ hits D_α transversely at P_0 we have $f_p(x_n) \rightarrow P_0$ and Cor.3.10 now follows (see the illustration in Fig.40 and Fig.41). \square

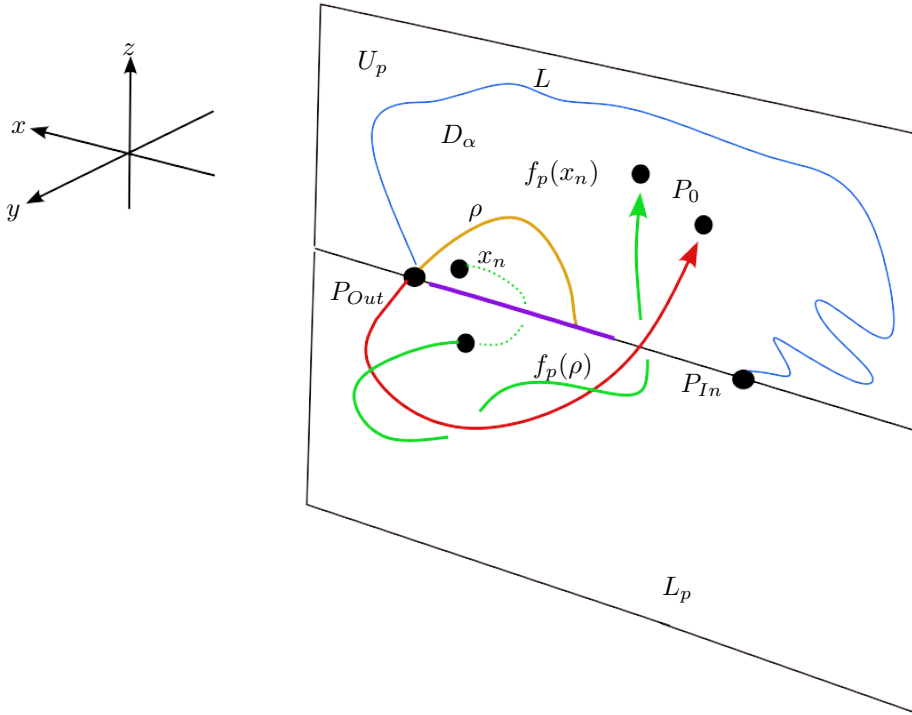


FIGURE 41. The flow line connecting x_n and $f_p(x_n)$, spiralling along the heteroclinic trajectory (the red curve). The purple arc denotes $f_p(\rho)$ - it is easy to see that since the flow pushes ρ on l , ρ is the unique curve of $Dis(f_p)$ s.t. $P_{Out} \in \bar{\rho}$.

To continue, having studied the discontinuity properties of f_p in Prop.3.8 and Cor.3.10, we now study the continuity properties of the first-return map f_p . To do so, consider the set $I = (\overline{D_\alpha} \setminus \{P_0\}) \setminus \cup_{n>0} f_p^{-n}(l)$ - that is, I is the (maximal) invariant set of f_p in $(\overline{D_\alpha} \setminus \{P_0\}) \setminus l$. We now prove the following corollary of Prop.3.8:

Corollary 3.11. *Let C be a component of I . Then, for every $n > 0$, f_p^n is continuous on C - and moreover, I is dense in $\overline{D_\alpha}$.*

Proof. By Prop.3.8 it immediately follows that given C as above and any $n > 0$, f_p^n is continuous on C . Therefore, it remains to prove I is dense in $\overline{D_\alpha}$. To do so, recall f_p is a first-return map generated by a smooth flow - hence

given any $n \in \mathbf{N}$, $f_p^{-n}(l)$ is a collection of smooth curves (some of which are possibly singletons - see the illustration in Fig.42). As such, for every $n \geq 0$, $I_n = \overline{D_\alpha} \setminus (\cup_{0 \leq k \leq n} \overline{f_p^{-k}(l)})$ is dense in $\overline{D_\alpha}$ and open in $\overline{D_\alpha}$. $\overline{D_\alpha}$ is a complete and separable metric space, hence, by the Baire Category Theorem it follows $I = \cap_{n \geq 1} I_n$ is dense in $\overline{D_\alpha}$ and Cor.3.11 follows. \square

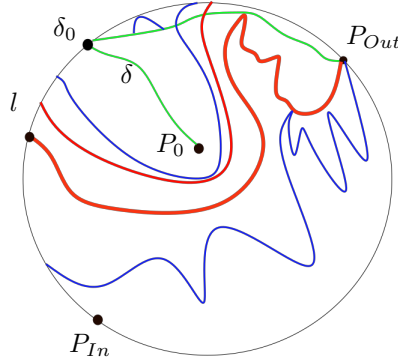


FIGURE 42. The set I_3 inside the disc D_α - the green curves correspond to $f_p^{-1}(l)$, the red to $f_p^{-2}(l)$, and the blue to $f_p^{-3}(l)$.

Having proven Prop.3.8, Cor.3.10 and Cor.3.11, we now study the question of how the curves in $f_p^{-1}(l)$ (and by extension, $Dis(f_p)$) are configured inside the cross-section $\overline{D_\alpha}$. The reason we are interested in this question is because the configuration of $f_p^{-1}(l)$ dictates how the first-return map f_p can (and cannot) behave. As we will now soon prove, there are precisely three ways in which $f_p^{-1}(l)$ can be configured inside the cross-section D_α . To do so, we first prove the following technical Lemma:

Lemma 3.12. *Let p be a trefoil parameter, let δ be the curve given by Prop.3.8, and let ρ be as in Cor.3.10. Then there exists a cross section H_p , a component of $(\overline{D_\alpha} \setminus \{P_0\}) \setminus f_p^{-1}(l)$, satisfying:*

- H_p is a topological disc, and f_p is continuous on H_p .
- P_{In} , L , ρ and P_{Out} all lie in ∂H_p (see the illustration in Fig.43).
- Either $\delta \subseteq \partial H_p$, or $\bar{\delta} \cap \partial H_p \subseteq \{\delta_0\}$ (see the illustrations in Fig.44).

Proof. By Prop.3.8, every component of $f_p^{-1}(l) \cap D_\alpha$ is either the curve δ , or alternatively, a curve with at least two endpoints on l . Consequentially, as $D_\alpha \setminus \{P_0\}$ is homeomorphic to an open punctured disc and because $P_0 \in \bar{\delta}$, every component of $(D_\alpha \setminus \{P_0\}) \setminus f_p^{-1}(l)$ is an open topological disc. Recalling that by Prop.3.8 the discontinuities of f_p in $D_\alpha \setminus \{P_0\}$ are given by $f_p^{-1}(l) \cap D_\alpha$, it follows the components of $(D_\alpha \setminus \{P_0\}) \setminus f_p^{-1}(l)$ are the continuity sets of f_p inside $D_\alpha \setminus \{P_0\}$.

Since by Prop.3.8 f_p is continuous on a neighborhood of P_{In} in D_α , there exists a neighborhood of P_{In} in $\overline{D_\alpha}$ which lies away from $f_p^{-1}(l)$ (see the illustration in Fig.33). Consequentially, there exists a unique component of $(D_\alpha \setminus \{P_0\}) \setminus f_p^{-1}(l)$, which we denote by H_p , s.t. $P_{In} \in \partial H_p$. By the discussion above, f_p is continuous on H_p , and H_p is a topological disc (see the illustration in Fig.43).

We now prove that in addition to the fixed-point P_{In} , the sets L , P_{Out} and ρ also lie in ∂H_p . To do so, recall the curve L is the intersection of the cross-section U_p with the two-dimensional, unstable, invariant manifold W_{In}^u (see the illustration in Fig.43) - as proven in Prop.3.4, L is curve in $\partial D_\alpha \cap U_p$ with endpoints P_{In} , P_{Out} . Since by Prop.3.8 f_p is continuous at both L and a neighborhood of P_{In} in $\overline{D_\alpha}$, we conclude $\bar{L} \subseteq \partial H_p$. Therefore, by $P_{Out} \in \bar{L}$ it follows P_{Out} is also in ∂H_p (see the illustration in Fig.47 or 57). Finally, since by Cor.3.10 $\rho \subseteq f_p^{-1}(l)$ is the unique curve in $f_p^{-1}(l) \cap D_\alpha$ with an endpoint at P_{Out} , it follows $\rho \subseteq \partial H_p$ as well (see Fig.43). That is, we have just proven L , P_{Out} and ρ are all subsets of ∂H_p .

To prove Lemma 3.12 it remains to prove either $\delta \subseteq \partial H_p$ or $\bar{\delta} \cap \partial H_p \subseteq \{\delta_0\}$ - where $\delta \subseteq f_p^{-1}(l) \cap D_\alpha$ is the curve given by Prop.3.8, and δ_0 is the endpoint of δ on l (see the illustration in Fig.43). As H_p is a component of $D_\alpha \setminus f_p^{-1}(l)$, by $\delta \subseteq f_p^{-1}(l)$ we already know $\delta \cap H_p = \emptyset$ - which proves δ intersects \bar{H}_p at most in ∂H_p . Now, let us recall ∂H_p is composed of arcs in ∂D_α and in $f_p^{-1}(l)$ - therefore, since every $s \in \delta$ is interior to D_α , and because δ is also a component of $f_p^{-1}(l) \cap D_\alpha$ homeomorphic to an open interval, it follows that if $\delta \cap \partial H_p \neq \emptyset$ the only possibility is $\delta \subseteq \partial H_p$. Consequentially, whenever $\delta \not\subseteq \partial H_p$, the only possibility is $\partial H_p \cap \bar{\delta} \subseteq \{\delta_0\}$ (see the illustration in Fig.44 or 47). The proof of Lemma 3.12 is now complete. \square

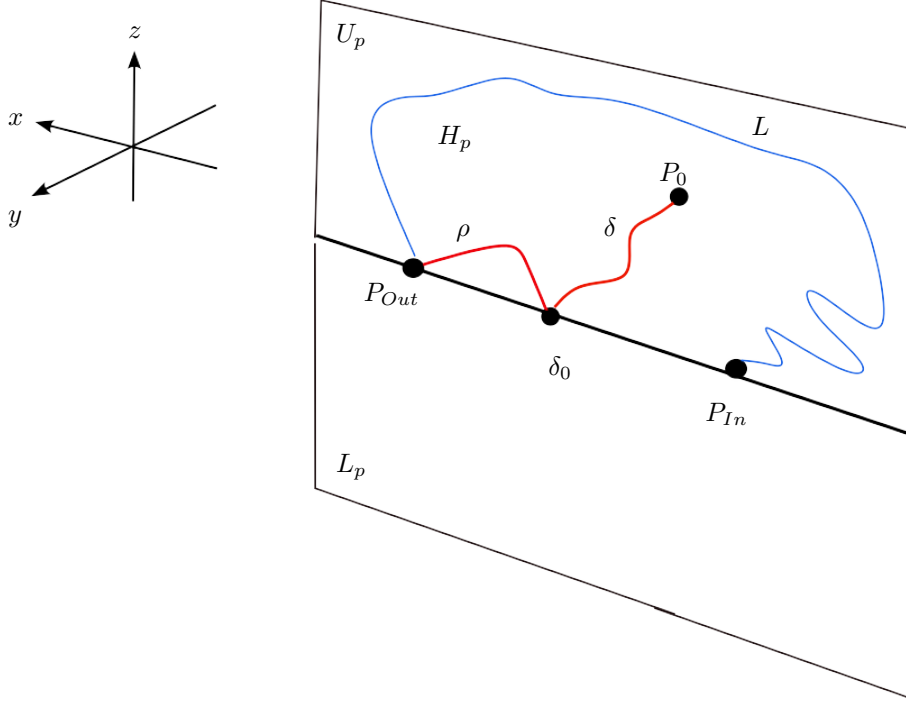


FIGURE 43. The cross-section $H_p \subseteq D_\alpha$ (where D_α is the Jordan domain trapped between L and l), trapped between $f_p^{-1}(l)$, l , and L - where l is the interval connecting P_{In} and P_{Out} , and $f_p^{-1}(l)$ is the red curve (in this illustration, ρ is the red arc connecting P_{Out} and δ_0). It follows H_p is an open topological disc.

We are now ready to prove that given a trefoil parameter $p \in P$, there are precisely three options as to how the collection of curves $f_p^{-1}(l)$ can be arranged inside D_α - and we do so by considering the possible topology of ∂H_p (as dictated by Lemma 3.12). First, whatever the case, by Lemma 3.12 the fixed points P_{In} and P_{Out} and the arcs L and ρ are inside ∂H_p . Additionally, by Prop.3.8 either $\delta_0 = P_{Out}$ or δ_0 is interior to l . Therefore, given any trefoil parameter $p \in P$ there are precisely three possibilities as to how δ , δ_0 and the cross-section H_p can be arranged inside $\overline{D_\alpha}$ (see Fig.44):

- The first possibility is $P_{Out} = \delta_0$. Since δ_0 is the unique intersection point of $\bar{\delta}$ with l (see Prop.3.8), whenever $\delta_0 = P_{Out}$ the curve δ is an arc in the open disc D_α - with one endpoint at P_0 and another at P_{Out} (see the illustration in Fig.44 and 66). By $f_p(P_{Out}) = P_{Out}$ and because the trajectory of P_0 tends to P_{In} we have $f_p(\delta) = l$ - i.e. $f_p^{-1}(l) = \delta = \rho$. This implies $H_p = D_\alpha \setminus \delta$, hence H_p is homeomorphic to a slit disc (see the illustration in Fig.44 and Fig.66). We refer to this scenario as **Case C**.
- The second case we consider is the scenario where $\delta \subseteq \partial H_p$ and $\delta_0 \neq P_{Out}$ (see the illustration in Fig.44 and Fig.57). As δ is a component of $f_p^{-1}(l) \cap D_\alpha$, it again follows H_p is homeomorphic to a slit disc. We refer to this scenario as **Case B**.
- The third (and final) possibility is that $\bar{\delta} \cap \partial H_p \subseteq \{\delta_0\}$ (as illustrated in both Fig.44 and Fig.47). In light of the discussion above, whenever $\bar{\delta} \cap \partial H_p \subseteq \{\delta_0\}$ we have $\delta_0 \neq P_{Out}$ - we refer to this scenario as **Case A**.

It is easy to see that by Lemma 3.12, there are no other possible configurations of ∂H_p . Summarizing our results, we obtain:

Corollary 3.13. *Let $p \in P$ be a trefoil parameter - then, the configuration of ∂H_p in $\overline{D_\alpha}$ falls into either Case A, Case B or Case C.*

Despite its technical nature, Cor.3.13 will be of extreme importance to the proof of chaoticity for the Rössler system at trefoil parameters in the next section - primarily because each scenario forces the first-return map $f_p : H_p \rightarrow \overline{D_\alpha}$ to behave somewhat differently.

Before we conclude this subsection and move to prove Th.3.15, let us remark all the results proven so far study only the bounded dynamics of the flow - therefore, before concluding this section, for the sake of completeness we study the unbounded dynamics at trefoil parameters. To do so, recall that given a parameter $p \in P$, we always denote by F_p the corresponding vector field. Inspired by Th.2.8 from and Shilnikov's Homoclinic Bifurcation Theorem, we now prove:

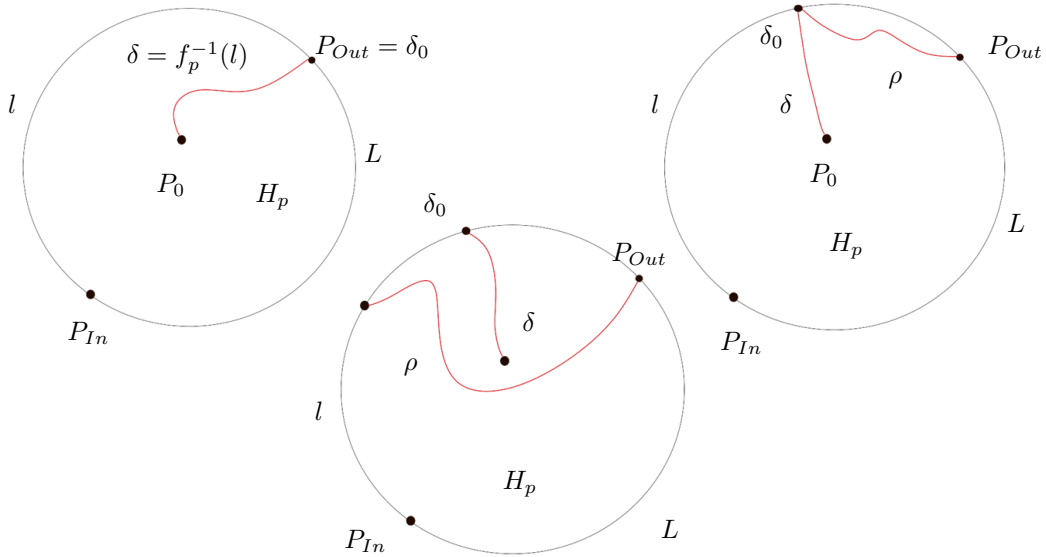


FIGURE 44. The three possibilities for the topology of ∂H_p inside D_α (for convenience, we sketch D_α as a topological disc). In Case C (upper left), $\delta = f_p^{-1}(l) = \rho$, and $P_{Out} = \delta_0$. In Case B (upper right) we have $\delta_0 \neq P_{Out}$ and $\delta \subseteq \partial H_p$, while in Case A (lower-center) we have $\bar{\delta} \cap \partial H_p \subseteq \{\delta_0\}$.

Proposition 3.14. *Let $p \in P$ be a trefoil parameter. Then, there exists a sequence of smooth vector fields $\{K_n\}_n$ on S^3 s.t.:*

- Given any compact $K \subseteq \mathbf{R}^3$, $K_n \rightarrow F_p$ on K (w.r.t. the C^∞ metric).
- Every K_n generates an unbounded set of periodic trajectories.

Proof. Let $p \in P$ be a trefoil parameter. By Th.2.8, we can always perturb F_p into a smooth vector field on S^3 , R_p s.t. the following is satisfied:

- R_p coincides with F_p around the fixed points.
- Given any compact $K \subseteq \mathbf{R}^3$, we can choose R_p s.t. it coincides with F_p on K .
- R_p generates an unbounded heteroclinic trajectory Γ which flows from P_{Out} towards P_{In} (in infinite time).

Since $p = (a, b, c)$ lies in the parameter space P , per our assumption on the parameter space, at least one of the fixed points P_{In} and P_{Out} always satisfies the Shilnikov Condition (see the discussion in page 3). Assume first that P_{Out} satisfies the Shilnikov condition - since R_p is a smooth vector field on S^3 , we can smoothly deform R_p around the fixed point P_{In} by connecting Γ and some trajectory on $S = W_{In}^u = W_{Out}^s$ to generate ζ , a homoclinic trajectory to P_{Out} - in particular, we choose this perturbation s.t. R_p and K_n coincide around P_{Out} . Since Γ is unbounded, so is ζ .

Denote by K_n the vector field described above - it is easy to see K_n is a smooth vector field on S^3 , and that we can choose it s.t. its C^∞ distance from R_p is arbitrarily small. Therefore, given any compact $K \subseteq \mathbf{R}^3$, since R_p can be chosen to coincide with F_p on K , K_n can be chosen to be arbitrarily close to F_p on K (in the C^∞ metric).

Since P_{Out} satisfies the Shilnikov Condition w.r.t. F_p and R_p , by our construction of K_n it also satisfies it w.r.t. K_n . Therefore, as P_{Out} satisfies the Shilnikov Condition and because K_n generates a homoclinic trajectory ζ to P_{Out} , from Shilnikov's Theorem K_n generates Ω - a collection of periodic trajectories which are dense around ζ (see [2] or Th.13.8 in [18]). As such, since ζ is unbounded so is Ω . When P_{In} satisfies the Shilnikov Condition, similar arguments (when applied to the inverse flow) imply the same result and Prop.3.14 now follows. \square

Let us remark Prop.3.14 correlates with the results of some numerical studies. To see how, let us assume $v \in P$ is a parameter (not necessarily a trefoil parameter) at which F_v generates a stable, attracting periodic trajectory T - which attracts an open, unbounded set of initial conditions in \mathbf{R}^3 . As observed numerically in [25], whenever this is the case, the trajectory of a generic initial condition $s \in \mathbf{R}^3$ behaves a-periodically for a long duration of time - at least until it gets sufficiently close to T , after which it settles down and tends to T relatively orderly.

This strange numerical behavior was termed **Transient Chaos** in [25] - and Prop.3.14 is a possible analytic explanation for the existence of these transient chaotic dynamics. To see why, assume $p \in P$ is a trefoil parameters, and that the periodic trajectories given by Prop.3.14 persist for the vector field F_p , and also persist in some form

under sufficiently small perturbations of F_p in the parameter space. In that case, provided the parameter v above is sufficiently close to p , we would expect the unbounded dynamics of F_v to be complex as well - i.e., we would expect F_v to also generate a collection of periodic trajectories (which may or may not be unbounded), which would force the trajectories generic initial conditions to have transient chaotic dynamics.

3.3. Chaotic dynamics at trefoil parameters. In this subsection we prove the Rössler system at trefoil parameter generates complex dynamics (which we do in Th.3.15). In more detail, we will prove that given a trefoil parameter, its dynamics include infinitely many periodic trajectories - which manifest as periodic orbits for the first-return map f_p , of all minimal periods.

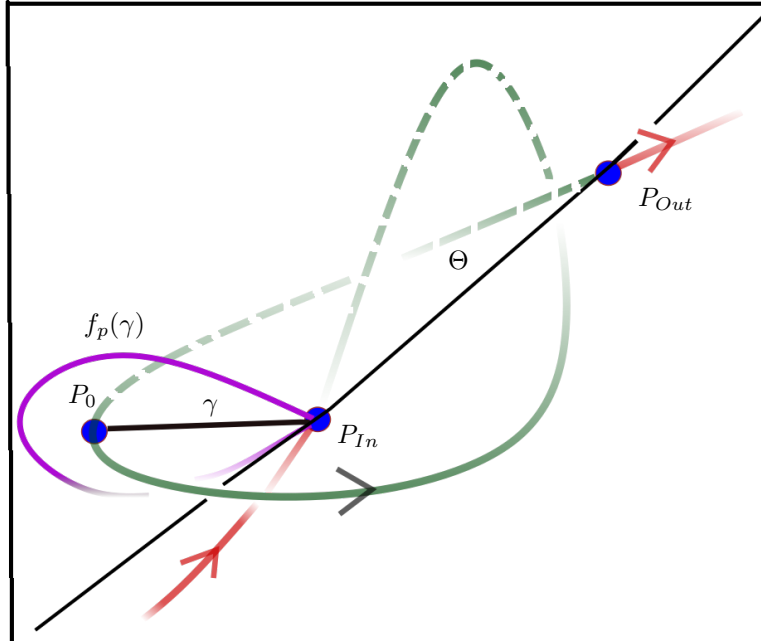


FIGURE 45. Flowing γ along the trefoil. Θ is the green trajectory.

The motivation behind the proof is relatively simple. To introduce it, consider a scenario as described in Fig.45. That is, given a trefoil parameter $p \in P$ and the corresponding bounded heteroclinic trajectory Θ , choose some curve $\gamma \subseteq U_p$ s.t. γ connects the fixed point P_{In} and P_0 on the cross-section U_p .

Now, let us suspend the curve γ along Θ , the bounded component of the heteroclinic trefoil knot (see the illustration in Fig.45). By the topology of the heteroclinic trefoil knot, we conclude it constrains γ to return to U_p as in Fig.45 - that is, heuristically, $f_p(\gamma)$, the image under the first-return map is a closed loop on the cross-section U_p which begins and terminates at the fixed point P_{In} . Therefore, we can impose $f_p(\gamma)$ on U_p roughly as in Fig.46 - which, heuristically, implies the existence of a rectangle $R \subseteq U_p$ s.t. f_p is Smale Horseshoe map on R . As such, it should follow the dynamics of F_p must include infinitely many periodic trajectories in R .

In practice, due to Prop.3.8 and Cor.3.10 the heuristic described above is far from obvious. Namely, the assumption we can choose a curve $\gamma \subseteq U_p$ s.t. $f_p(\gamma)$ is a closed loop is far from trivial: recalling both Prop.3.8 and Cor.3.10, it is easy to see one cannot assume $f_p(\gamma)$ is even connected in $\overline{D_\alpha}$. However, as we will see below, provided we are sufficiently careful, this heuristic becomes a rigorous proof.

Theorem 3.15. *Let $(a, b, c) = p \in P$ be a trefoil parameter, and denote by $\sigma : \{1, 2\}^{\mathbb{N}} \rightarrow \{1, 2\}^{\mathbb{N}}$ the one-sided shift. Then, there exists a bounded set $V \subseteq \mathbf{R}^3$ s.t. the corresponding Rössler system has infinitely many periodic trajectories in V . Moreover, these periodic trajectories are in a surjective correspondence to the set of periodic orbits for σ in $\{1, 2\}^{\mathbb{N}}$.*

Before presenting the proof, let us remark the formalism above has the following meaning: that at trefoil parameters the dynamics of the Rössler system inside the set V are complex at least like those of a suspended Smale Horseshoe map. In particular, Th.3.15 proves the flow is chaotic w.r.t. Def.1.1.

Proof. To begin, recall the bounded cross-section $D_\alpha \subseteq U_p$, $D_\alpha = B_\alpha \cap U_p$ (where B_α is the topological ball generated by the equality $W_{In}^u = W_{Out}^s$ - see Def.3.2). Additionally, recall the first-return map $f_p : \overline{D_\alpha} \setminus \{P_0\} \rightarrow$

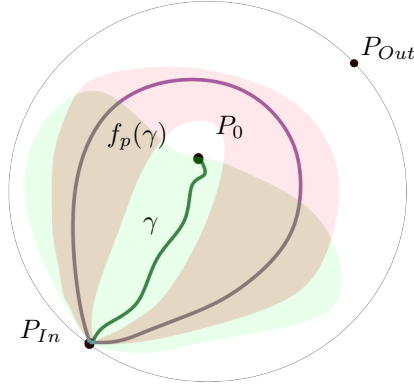


FIGURE 46. Imposing $f_p(\gamma)$ on U_p - since $f_p(\gamma)$ is a closed loop, heuristically, there exists a degenerate rectangle R (the green region) with sides AB, CD corresponding to P_{In}, P_0 (respectively) s.t. $f_p(R)$ (the red region) looks like a singular Smale Horseshoe.

$\overline{D_\alpha} \setminus \{P_0\}$ - as proven in Prop. 3.4 D_α is a bounded Jordan domain on the half-plane U_p (see the illustration in Fig.32), and the first-return map f_p is well-defined throughout the punctured (topological) disc $\overline{D_\alpha} \setminus \{P_0\}$ (see Lemma 3.2). Additionally, recall we denote by H_p is the component of $\overline{D_\alpha} \setminus f_p^{-1}(l)$ s.t. $P_{In} \in \partial H_p$ (see Lemma 3.12). Our strategy of proof is as follows - we prove the existence of a set Q inside the cross-section $\overline{H_p}$ s.t. the following is satisfied:

- f_p is continuous on Q .
- There exists a continuous $\pi : Q \rightarrow \{1, 2\}^{\mathbb{N}}$ s.t. $\pi \circ f_p = \sigma \circ \pi$.
- $\pi(Q)$ includes any periodic $s \in \{1, 2\}^{\mathbb{N}}$ - and if the minimal period of s is k , $\pi^{-1}(s)$ includes a periodic point for f_p of minimal period k .

Now, set Per as the set of periodic trajectories for the flow intersecting Q . It is easy to see that since $Q \subseteq \overline{H_p} \subseteq \overline{D_\alpha} \subseteq \overline{B_\alpha}$, because $\overline{B_\alpha}$ is bounded Per is bounded as well - and that π gives us the continuous and surjective map between Per and the periodic orbits for σ in $\{1, 2\}^{\mathbb{N}}$. As such, to prove Th.3.15 it would suffice to prove the assertions above.

To do so, recall that per Cor.3.13, given a trefoil parameter $p \in P$ it falls into either Case A , Case B or Case C , s.t. in each case the topology of the cross-section H_p is somewhat different. Therefore, we will prove Th.3.15 for each of these cases separately - despite the subtle differences in the arguments, the proof in each case would be essentially the same. As we will see, in each case we extend the first-return map $f_p : \overline{H_p} \rightarrow \overline{D_\alpha} \setminus \{P_0\}$ to a homeomorphism of the disc which we isotope to a Pseudo-Anosov homeomorphism, G , which acts as a Smale Horseshoe map on some rectangle. The existence of G would suffice to imply Th.3.15 - because, as we will prove below, all the periodic orbits for G persist when we continuously deform it back to f_p . As such, since we will prove G acts as a Smale Horseshoe map on some disc, Th.3.15 would follow.

3.3.1. *Stage I - proving Th.3.15 for Case A:* As stated above, we begin by proving Th.3.15 for Case A - that is, in Case A , we have $\partial H_p \cap \bar{\delta} \subseteq \{\delta_0\}$. To begin, let us recall the first-return map $f_p : \overline{D_\alpha} \setminus \{P_0\} \rightarrow \overline{D_\alpha} \setminus \{P_0\}$ is continuous around P_{In} (see Prop.3.8) - which implies there exists a maximal arc $l_1 \subseteq l$, beginning at P_{In} and terminating at some $r_0 \in l \cap f_p^{-1}(l)$ s.t. $l_1 \subseteq \partial H_p$ (see the illustration in Fig.47) - consequentially, f_p is continuous in l_1 (in particular, r_0 is the closet point in $f_p^{-1}(l) \cap l$ to the fixed-point P_{In}). Therefore, for every $s \in l_1$ which is strictly interior to l_1 , $s \notin f_p^{-1}(l)$ - i.e., for such s , $f_p(s)$ is interior to $\overline{D_\alpha}$. Since by definition $r_0 \in f_p^{-1}(l) \cap l$ it follows $f_p(l_1)$ is an arc in D_α with endpoints $r_1 = f_p(r_0) \in l$ and P_{In} , which implies $\overline{f_p(l_1)} \cap \partial D_\alpha = \{P_{In}, r_1\}$ (see the illustration in Fig.48).

Additionally, since the flow line connecting r_0, r_1 lies in $\{\dot{y} \geq 0\}$ and since r_0, r_1 are both in l , recalling l is parameterized by $l(x) = (x, -\frac{x}{a}, \frac{x}{a})$, $x \in (0, c - ab)$ and that $P_{In} = (0, 0, 0)$, it follows r_1 is closer to P_{In} than r_0 (as illustrated in Fig.48). Since $r_0 \neq P_0$, it follows $r_1 \neq P_{In}$ - that is, $\overline{f_p(H_p)}$ misses an arc on l which begins at P_{In} (see the illustration in Fig.48).

Now, recall that P_0 has no pre-images, as it lies on the heteroclinic trefoil. Now, recall the curve ρ from Cor.3.10, and that by Lemma 3.12 the curve ρ also lies in ∂H_p , we conclude by Cor.3.10 there exists no $\{x_n\} \in \overline{H_p}$ s.t. $f_p(x_n) \rightarrow P_0$ (or, in other words, the sector T given by Cor.3.10 lies outside of H_p - see the illustration in Fig.47). Consequentially, we have $P_0 \notin f_p(\overline{D_\alpha} \setminus \{P_0\})$. Moreover, let us note that as H_p is a component of $D_\alpha \setminus f_p^{-1}(l)$, by

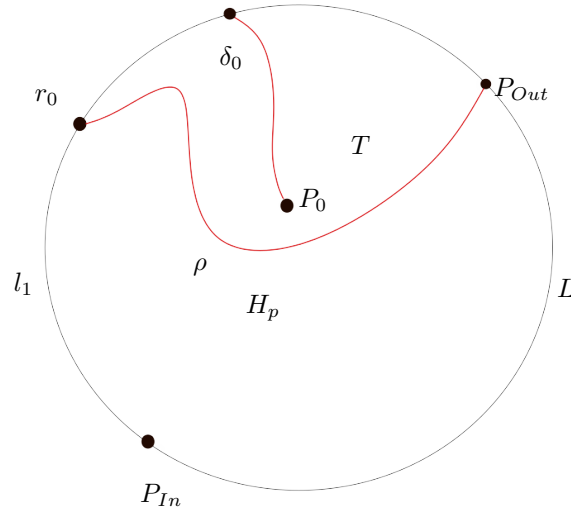


FIGURE 47. Case A - δ lies away from $\overline{H_p}$ - in particular, $\delta_0 \neq P_{Out}$.

Prop.3.8 it follows the first-return map is continuous on $\overline{H_p}$, hence all in all we conclude $P_0 \notin \overline{f_p(H_p)}$. Now, consider the set Γ of curves γ in D_α which connect P_{In} and P_0 , we see $\Gamma \cap H_p$ foliates H_p . Finally, recall that for every $\gamma \in \Gamma$, as we suspend γ with the flow, γ loops around the heteroclinic trajectory - as depicted in Fig.45. As such, since $\Gamma \cap H_p$ foliates H_p , all in all, as $P_0 \notin \overline{f_p(H_p)}$ and since r_1 is closer to P_{In} than r_0 , we conclude $f_p(H_p)$ can be imposed on D_α like a crescent-shaped figure with one tip at P_{In} and another at r_1 (see the illustration in Fig.48).

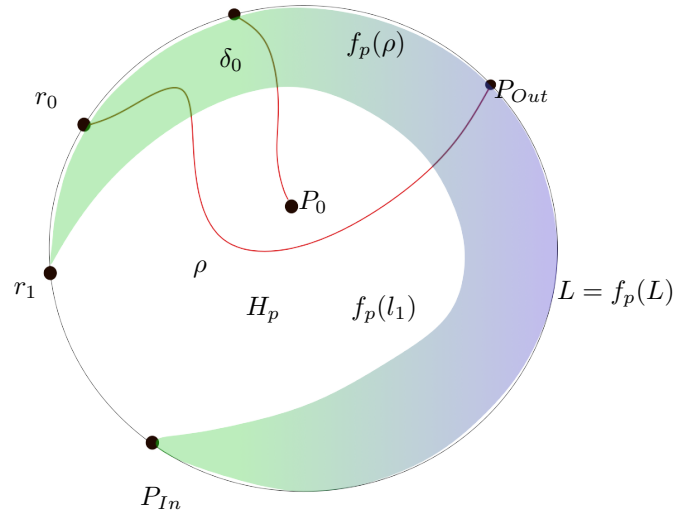


FIGURE 48. Imposing $f_p(H_p)$ on D_α in Case A. $f_p(l_1)$ is the arc connecting P_{In} and r_1 .

There is not much that can be said on the invariant set of f_p in $\overline{H_p}$ from Fig.48 alone - let alone factor its dynamics to those of the one-sided shift $\sigma : \{1, 2\}^{\mathbb{N}} \rightarrow \{1, 2\}^{\mathbb{N}}$ (let us remark, however, that it is easy to see it is non-empty - by definition, it includes both fixed points and the arc L). In order to say something smart about it, let us first extend it as follows - first, let us sketch D_α as a half-disc instead of a disc or a half plane, and let us glue to D_α another half-disc, C_α , at the curve l , s.t. $V_\alpha = \overline{D_\alpha} \cup C_\alpha$ forms a disc (see the illustration in Fig.49).

Now, choose some P_1 , an interior point to C_α (as illustrated in Fig.49), and let $F : V_\alpha \rightarrow V_\alpha$ be some homeomorphism s.t. the following is satisfied (see the illustration in Fig.50):

- $F|_{\overline{H_p}} = f_p$, i.e., F coincides with f_p on $\overline{H_p}$ (we allow F to differ from f_p on $\overline{D_\alpha} \setminus \overline{H_p}$).
- $F(D_\alpha \setminus H_p)$ includes an region in V_α , connecting P_1 and l .
- $F(\partial V_\alpha) = \partial V_\alpha$, and in particular - $F(P_{In}) = P_{In}$, while $F(P_0) = P_1$ and $F(P_1) = P_0$.

Our strategy of proof now is as follows: we first consider the surface $S = V_\alpha \setminus \{P_0, P_1\}$, as illustrated in Fig.50, after which we study the isotopy class of F in S . That is, we consider the isotopy class of all maps F' isotopic to F in S , s.t. $F'(P_{In}) = P_{In}$, $F'(P_0) = P_1$, and $F'(P_1) = P_0$. As we will now prove, this isotopy class

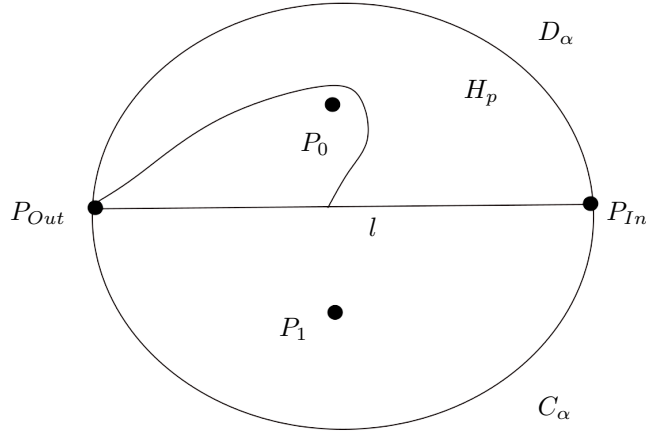


FIGURE 49. D_α is the upper half disc, glued to C_α , the lower half disc at the curve l - together, they constitute V_α .

includes a Pseudo-Anosov map whose periodic orbits are all isotopy stable - from which the conclusion would follow.

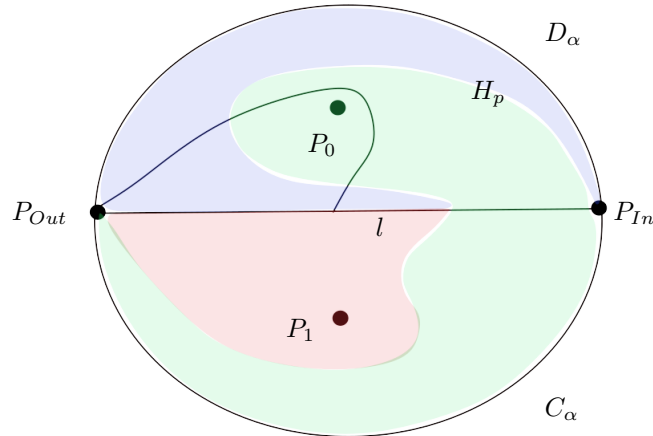


FIGURE 50. The action of F on V_α - the blue region corresponds to $F(H_p)$, the red to $F(D_\alpha \setminus H_p)$, and the green to $F(C_\alpha)$.

To begin, per the outline in Sect.1 of the Betsvina-Handel Algorithm (for more details, see [13] or [12]), let us choose a spine for S , i.e., a graph embedded in S , which is a retract of S - in particular, we choose a graph $T \subseteq S$, with vertices at P_{In}, P_0 and P_1 , with two edges: T_1 connecting P_0 to P_{In} and T_2 , connecting P_1 to P_{In} (see the illustration in Fig.52). Now, consider $F(T)$ - recalling $f_p(H_p)$ lies away P_0 and that $F|_{\overline{H_p}} = f_p$, by $F(P_{In}) = P_{In}$, $F(P_0) = P_1$ and $F(P_1) = P_0$ we conclude $F(T)$ looks as in Fig.51.

Consequently, $F(T_1)$ begins at P_{In} , surrounds T_1 from both sides, and then stretches along T_2 until terminating at P_1 - conversely, $F(T_2)$ is an edge connecting P_{In} to P_0 , stretching along T_1 (see the illustration in Fig.51). Now, let us retract F as described in Fig.52 to a graph map $g : T \rightarrow T$, and consider the matrix $A = \{a_{i,j}\}_{1 \leq i,j \leq 2}$, where $a_{i,j}$ denotes the times the curve $g(T_i)$ covers the side T_j - it is easy to see A is simply the matrix:

$$\begin{pmatrix} n & 1 \\ 1 & 0 \end{pmatrix}$$

Where $n \geq 2$. That is - $g(T_1)$ covers T_1 at least twice, while covering T_2 only once (conversely, $g(T_2)$ only covers T_1 once) . By computation, the spectral radius of A is $\frac{\sqrt{n^2+4+n}}{2}$ (i.e., its maximum positive eigenvalue), with a corresponding eigenvector $(\frac{\sqrt{n^2+4+n}}{2}, 1)$. As $n \geq 2$, by $\sqrt{n^2+4} > 2 - n$ it follows $\frac{\sqrt{n^2+4+n}}{2} > 1$ which proves the spectral radius is greater than 1.

Now, let us begin applying the Betsvina-Handel Algorithm to F - namely, going over steps 1 - 7 in [13] we deform F isotopically s.t. the graph map g is "straightened" - i.e., we deform F isotopically in S which ensures the

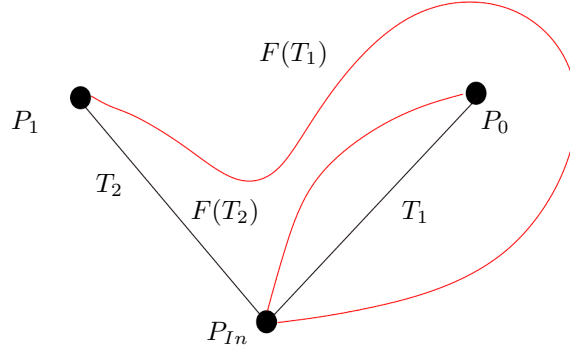


FIGURE 51. The graph T with vertices P_{In}, P_0 and P_1 (in black), and its image under F (in red).

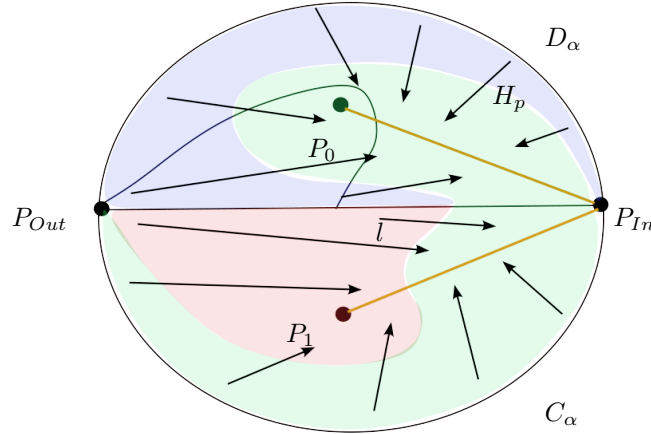


FIGURE 52. Collapsing F to a graph map - as can be seen, H_p and $f_p(H_p)$ are collapsed on T_1 , the edge connecting P_{In} and P_0 .

resulting graph map g is injective on every edge in T (see the illustration in Fig.54). In particular, let us remark that all the dynamics of F in H_p (and consequentially, those of the first-return map f_p in H_p) are collapsed by the deformation precisely to $g(T_1) \cap T_1$ - and moreover, any point in the invariant set of g in T_1 corresponds under the deformation to some point in the invariant set of F in $\overline{H_p}$, i.e., to that of f_p in $\overline{H_p}$. Consequentially, provided we prove F has infinitely many periodic orbits in $\overline{H_p}$, we're done.

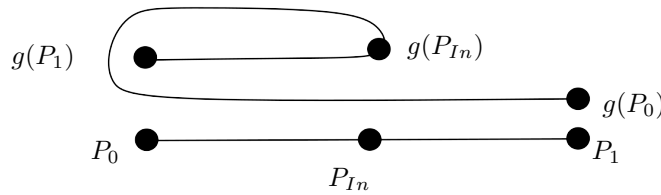


FIGURE 53. As can be seen, g acts on T as follows - $g(T_1)$ covers T_1 twice and stretched towards P_1 , while $g(T_2)$ covers T_1 .

To do so, following Ch.3.4 and Ch.4.4 in [13], as the spectral radius of the matrix A is $\frac{\sqrt{n^2+4+n}}{2} > 1$, it follows $F : S \rightarrow S$ can be isotopically deformed to a Pseudo-Anosov homeomorphism $G : S \rightarrow S$. Consequentially, since $g(T_1)$ covers T_1 twice, it follows by the argument given in Ch.3.4 and Ch.4.4 of [13] (see also Th.1.8) that there exists a G -invariant set, $I \subseteq S$ which includes infinitely many periodic orbits - moreover, by Th.1.8, the set I lies precisely in the regions of S which are retracted to T_1 , that is, in $\overline{H_p}$. In fact, it is easy to see that on $\overline{H_p}$, G acts as a Smale Horseshoe map (see the illustration in Fig.54). Namely, we have just proven:

Corollary 3.16. g has periodic orbits of all minimal periods in T_1 - consequentially, so does G in $\overline{H_p}$, which from now on we denote by $ABCD$. In particular, $G : ABCD \rightarrow ABCD$ is a Smale Horseshoe map.

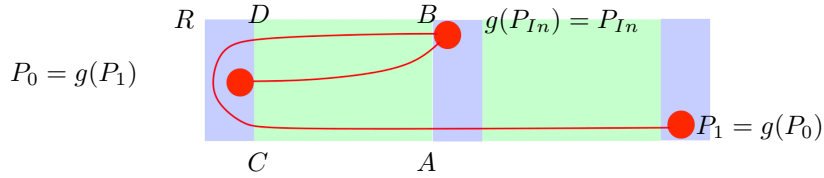


FIGURE 54. The red curve is $g(T)$ embedded in S - due to these properties, G acts on $ABCD$ as a Smale Horseshoe map (which is continuously deformed to a subset of $\overline{H_p}$ by the isotopy). The region R lies in S outside $ABCD$.

Now, let us recall that by definition, G is a homeomorphism of \overline{S} which permutes the points $\{P_0, P_{1n}, P_1\}$ as follows: $G(P_{1n}) = P_{1n}$, $G(P_1) = P_0$, and $G(P_0) = P_1$ - additionally, recall the following result given as Th.1, Th.2 and Remark 2.4 in [11]:

Theorem 3.17. *Let S be a surface (possibly a with boundary) and let $\phi : S \rightarrow S$ be Pseudo-Anosov homeomorphism - then, we have the following:*

- If x_1 is periodic of minimal period k for ϕ , then given any $\psi : S \rightarrow S$ which is isotopic to ϕ , when ϕ is isotoped to ψ the point x_1 is continuously deformed to x_2 , a periodic point for ψ of minimal period k . That is, the periodic dynamics of ϕ are **unremovable** - i.e., they are not destroyed by an isotopy.
- For every homeomorphism $\psi : S \rightarrow S$ isotopic to ϕ , there exists a closed $Y \subseteq S$ and a continuous surjection $\pi : Y \rightarrow S$ s.t. $\pi \circ \psi = \phi \circ \pi$. In particular, if $x \in S$ is periodic of minimal period n for ϕ , then $\pi^{-1}(x)$ includes a periodic orbit of minimal period n for ψ - i.e., the periodic dynamics are **uncollapsible**. In particular, when we isotope ϕ to ψ , no two periodic orbits of ϕ collapse into one another.

As a consequence of Th.3.17 and Th.1.8, every periodic orbit generated by G also persists as a periodic orbit for F - and moreover, since by the isotopy it follows H_p is continuously deformed to the rectangle $ABCD$, we conclude that when we return from G to F , the periodic orbits of G in $ABCD$ are all deformed to periodic orbits for F in $\overline{H_p}$ - and moreover, no two periodic orbits are destroyed, collapsed into one another, or change their minimal period. Consequentially, F generates infinitely many periodic orbits in its invariant set in $\overline{H_p}$ - and all in all, since $F|_{\overline{H_p}} = f_p$, the first-return map at trefoil parameter in Case A, we conclude:

Corollary 3.18. *Let $p \in P$ be a trefoil parameter s.t. Case A is satisfied - then, the first-return map $f_p : \overline{H_p} \rightarrow \overline{D_\alpha}$ generates infinitely many periodic orbits, of all minimal periods.*

Having proven Cor.3.18, it follows that in order to conclude the proof of Th.3.15 in Case A, we now need to define symbolic dynamics on some f_p -invariant $Q \subseteq H_p$, prove f_p is continuous on Q - and most importantly, show that the periodic orbits given by Cor.3.18 all lie in Q . We first prove we can define symbolic dynamics on a set I , some invariant set of f_p in $\overline{H_p}$. We do so as follows:

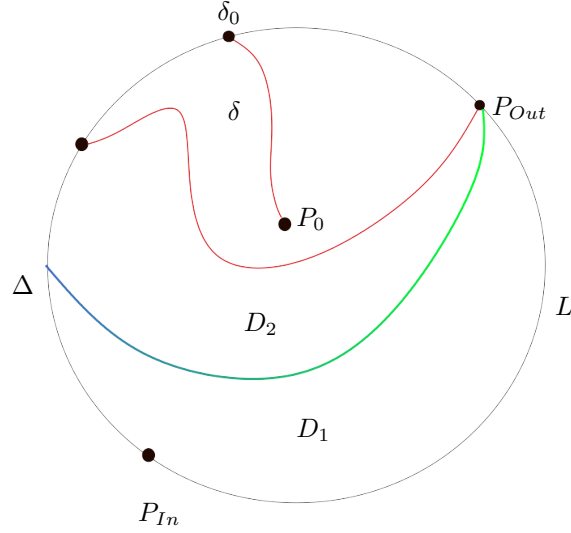
Lemma 3.19. *There exists a curve $\Delta \subseteq \overline{H_p}$, s.t. $\overline{H_p} \setminus \Delta$ includes two components - D_1 and D_2 . Consequentially, let I' denote the maximal invariant set in $\overline{H_p} \setminus \Delta$ - then, there exists a continuous $\pi' : I' \rightarrow \{1, 2\}^{\mathbb{N}}$ s.t. $\pi' \circ f_p = \sigma \circ \pi'$. Moreover, all the periodic orbits given by Cor.3.18 are in I' .*

Proof. Recall $G(ABCD)$ is a Smale Horseshoe, which implies there is a region R in the surface S (as indicated in Fig.54) s.t. $G^{-1}(R) \cap ABCD = V_1$ is a sub-rectangle of $ABCD$, connecting the AC and BD sides. Moreover, the different periodic orbits of G in $ABCD$ are separated by the pre-images of G . As we deform isotopically G back to F , because $ABCD$ is deformed to $\overline{H_p}$, the rectangle V_1 is deformed to Δ' , some subset of $\overline{H_p}$ - and as F coincides with f_p on $\overline{H_p}$, it follows the different periodic orbits given by Cor.3.18 are separated from one another by the pre-images of Δ' (w.r.t f_p). This proves there exists a curve $\Delta \subseteq \Delta'$ s.t. $\overline{H_p} \setminus \Delta$ is composed of two components: D_1 and D_2 (see the illustration in Fig.55).

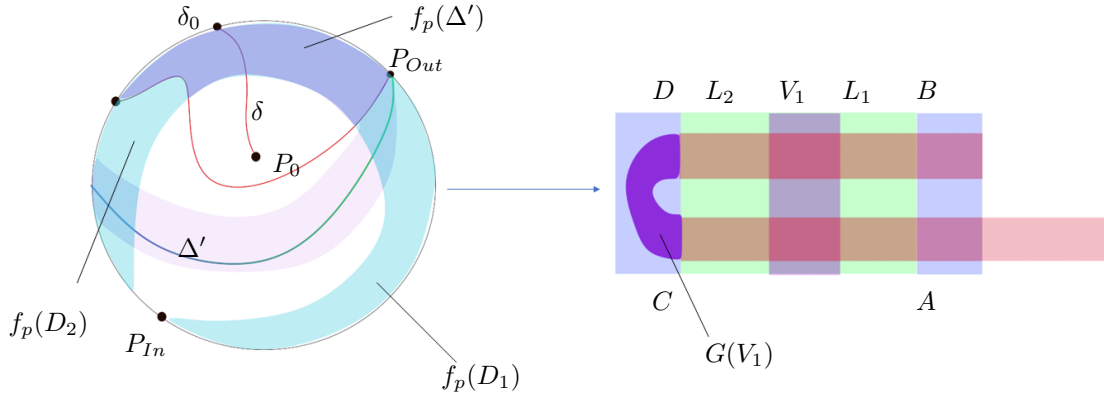
Note that I' , the maximal invariant set of f_p in $\overline{H_p} \setminus \Delta$, is a strict subset of the invariant set of f_p in $\overline{H_p}$ - therefore, because f_p is continuous on $\overline{H_p}$ it is also continuous on I' as well. Consequentially, there exists a continuous $\pi' : I' \rightarrow \{1, 2\}^{\mathbb{N}}$ s.t. both $\pi' \circ f_p = \sigma \circ \pi'$, and $\pi'(x) = \{s_n\}_{n \geq 0}$, where s_i is 1 whenever $f_p^i(x) \in D_1$ and 2 otherwise. Moreover, it follows by the discussion above that all the periodic orbits given by Cor.3.18 are in I' and Lemma 3.19 now follows. \square

Having proven Lemma 3.19, we now prove:

Lemma 3.20. *Let $p \in P$ be a trefoil parameter falling into case A. Then, given any periodic $s \in \{1, 2\}^{\mathbb{N}}$, we have $s \in \pi'(I')$.*


 FIGURE 55. The curve $\Delta \subseteq f_p^{-1}(\delta)$ in Case A.

Proof. The proof is similar to that of Lemma 3.19. As we isotopically deform $F : \overline{H_p} \rightarrow S$ to $G : ABCD \rightarrow S$, the set Δ' introduced in the proof of Lemma 3.19 is continuously deformed to the sub-rectangle V_1 inside $ABCD$, defined by $G(V_1) \cap ABCD = \emptyset$ (see the illustration in Fig.56). Recall the symbolic dynamics of G on its invariant set in $ABCD$ are defined by L_1 and L_2 , the sub-rectangles composing $ABCD \setminus V_1$ - and similarly to how Δ' is deformed to V_1 , the isotopy also deforms D_1 to L_1 and D_2 to L_2 . Consequentially, it follows that if the periodic orbit $\{x_1, \dots, x_k\}$ for G corresponds to some symbol in $\{1, 2\}^{\mathbb{N}}$, as it is deformed to $\{y_1, \dots, y_k\}$, a periodic orbit for $f_p = F|_{\overline{H_p}}$, its symbolic dynamics do not change - i.e., if $\{x_1, \dots, x_k\}$ corresponds to some periodic $s \in \{1, 2\}^{\mathbb{N}}$, the same is true for $\{y_1, \dots, y_k\}$. Lemma 3.20 now follows. \square


 FIGURE 56. The isotopy of $F|_{\overline{H_p}} = f_p$ on H_p to $G : ABCD \rightarrow S$ deforms the purple region Γ to the sub-rectangle L_3 .

We now conclude the proof of Th.3.15 for Case A. To do so, recall the factor map π' given by Lemma 3.19, and for any periodic $s \in \{1, 2\}^{\mathbb{N}}$ of minimal period k which is not the constant $\{1, 1, 1, \dots\}$, let us denote by D_s the component of $\pi'^{-1}(s)$ s.t. the following holds:

- D_s contains a periodic orbit of minimal period k , $\{x_1, \dots, x_k\}$.
- $\{x_1, \dots, x_k\}$ is deformed isotopically to a periodic orbit for G , of the same minimal period and the same symbol.

Such a D_s exists by both Th.3.17 and Cor.3.20. For the constant $s = \{1, 1, 1, \dots\}$, set $D_s = \{P_{In}\} \cup L$. Finally, let Q denote the collection of such D_s - by definition, $Q \subseteq I'$, where I' is as in Cor.3.19. Setting $\pi = \pi'|_Q$ and summarizing our results, we conclude the following:

- By Cor.3.19, the first-return map f_p is continuous on Q .
- Additionally, by Cor.3.19, there exists a continuous $\pi : Q \rightarrow \{1, 2\}^{\mathbb{N}}$ s.t. $\pi \circ f_p = \sigma \circ \pi$ (where $\sigma : \{1, 2\}^{\mathbb{N}} \rightarrow \{1, 2\}^{\mathbb{N}}$ denotes the one-sided shift).
- By Lemma 3.20, $\pi(Q)$ includes every periodic symbol in $\{1, 2\}^{\mathbb{N}}$.

- Moreover, by our construction of D_s above, if s is periodic of minimal period k , $\pi^{-1}(s)$ includes a periodic orbit of minimal period k for f_p .

All in all, we have completed the proof of Th.3.15 for Case A.

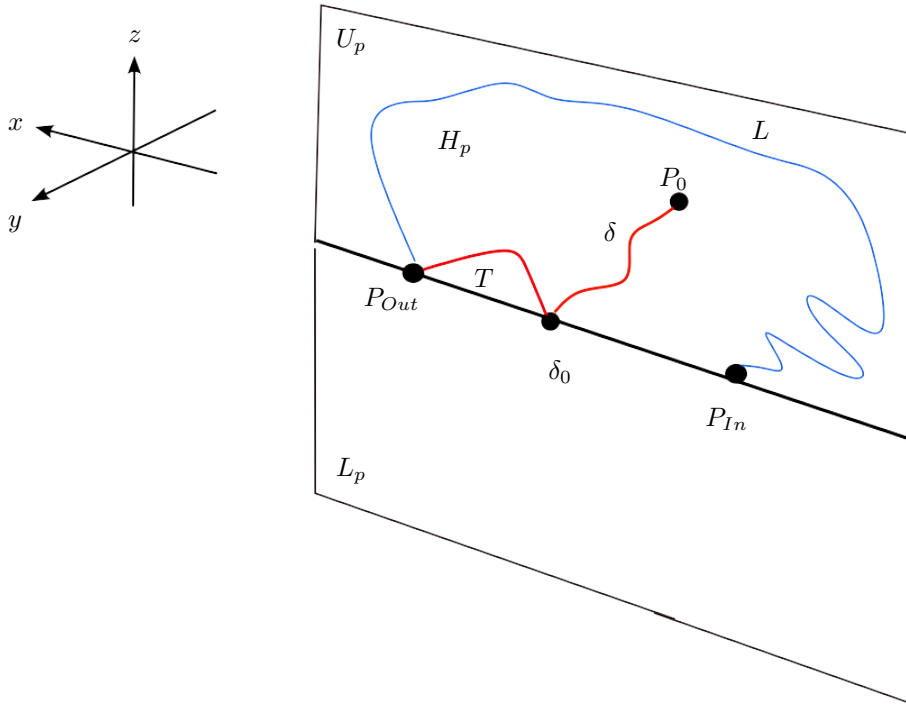


FIGURE 57. The cross-section H_p , in case B, with $f_p^{-1}(l)$ sketched as a curve.

3.3.2. *Stage II - proving Th.3.15 for Case B:* Having proven Th.3.15 for trefoil parameters $p \in P$ which fall into Case A, we now prove Th.3.15 for trefoil parameters which fall into Case B - that is, we now assume the curve δ and the cross-section H_p satisfy the following:

- Both δ and P_{In} lie in ∂H_p (see the illustration in Fig.57).
- Additionally, we assume δ_0 , the endpoint on δ in l , satisfies $\delta_0 \neq P_{Out}$.

Even though the heart of the proof will be essentially the same as in Case A, we will need to slightly adjust several of our arguments - if only because the first-return map f_p in Case B behaves somewhat differently. We begin with the following Lemma, which studies just how the first-return map folds H_p inside D_α :

Lemma 3.21. *Let $p \in P$ be a trefoil parameter falling into Case B. Then, there exists a curve $\gamma \subseteq H_p$ satisfying:*

- $\bar{\gamma} \cap \partial H_p = \{P_{In}, P_0\}$.
- $\overline{f_p(\gamma)}$ is a closed loop in D_α , s.t. $\overline{f_p(\gamma)} \cap \partial D_\alpha = \{P_{In}\}$ - i.e., $f_p(\gamma)$ begins and terminates at P_{In} .
- $\overline{f_p(\gamma)}$ winds once around P_0 - in particular, it separates P_0 from $\partial D_\alpha \setminus \{P_{In}\}$ (see the illustration in Fig.58).

Proof. By Prop.3.8, the components of $f_p^{-1}(l) \cap D_\alpha$ are either δ , or curves with at least two endpoints on l . Consequentially, since H_p is a component of $D_\alpha \setminus f_p^{-1}(l)$, by Prop.3.8 it follows H_p is a simply connected two-dimensional set, bounded by curves: i.e., a topological disc (see the illustration in Fig.57 - in Case B H_p is not a Jordan domain as ∂H_p is not homeomorphic to S^1). As such, since by Assumption 2 both P_{In}, δ lie on ∂H_p , because H_p is a topological disc and because $P_0 \in \delta$ there exists a curve $\gamma \subseteq H_p$ s.t. $\bar{\gamma} \cap \partial H_p = \{P_{In}, P_0\}$ - i.e., γ satisfies the following (see the illustration in Fig.58):

- γ is homeomorphic to an open interval.
- The endpoints of γ are simply P_{In} and P_0 .
- Every point on γ is strictly interior to H_p .

As a consequence, since H_p is a component of $D_\alpha \setminus f_p^{-1}(l)$, it trivially follows $\gamma \cap f_p^{-1}(l) = \emptyset$ - therefore, by Prop.3.8 f_p is continuous on γ . Now, recall the curve ρ given by Cor.3.10 lies on ∂H_p (see Lemma 3.12) - and that the sector T given by Cor.3.10 lies outside of H_p (see the illustration in Fig.57). Therefore, there is no sequence $\{x_n\}_n \subseteq \overline{H_p}$ s.t. $f_p(x_n) \rightarrow P_0$, which implies that for every sequence $\{s_n\}_n \subseteq \gamma$, $f_p(s_n) \not\rightarrow P_0$ - hence, $P_0 \notin \overline{f_p(\gamma)}$.

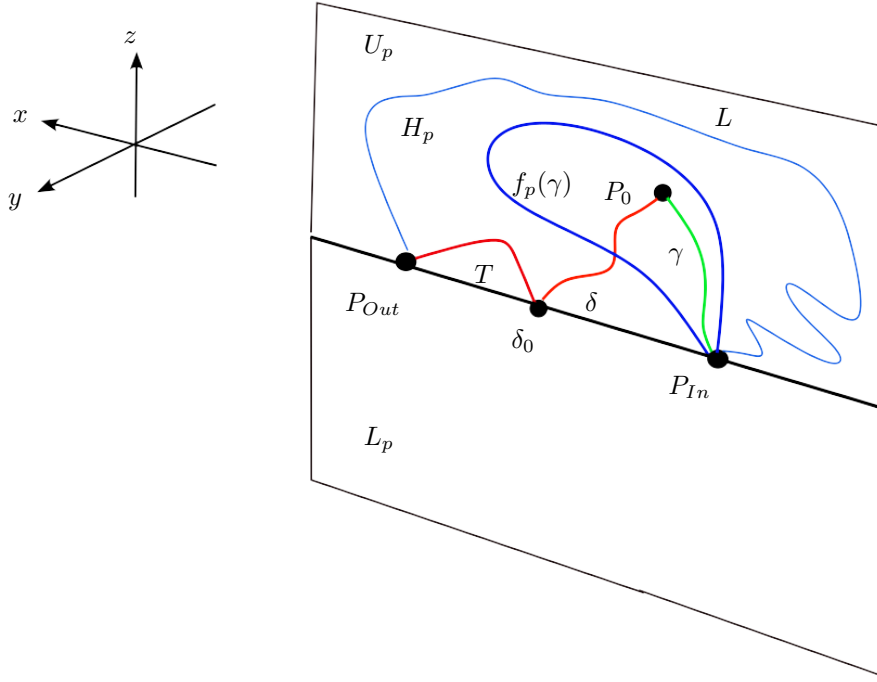


FIGURE 58. γ is the green curve inside H_p , which returns to the cross-section as $f_p(\gamma)$ - the closed blue loop, which begins and terminates at P_{In} and winds once around P_0 . Again, for simplicity we sketch $f_p^{-1}(l)$ as a curve.

Now, since the trajectory of P_0 tends to the fixed-point P_{In} (in infinite time), we conclude $f_p(\gamma)$ is a closed loop in D_α which begins and terminates at P_{In} . Moreover, by the existence of the heteroclinic trefoil knot (see Def.3.2), it follows we can now apply the argument given at the beginning of this section and conclude $f_p(\gamma)$ separates $P_0, \partial D_\alpha$ - i.e., $f_p(\gamma)$ is a closed loop in D_α as in Fig.45, Fig.46 and Fig.58. In particular, $\overline{f_p(\gamma)}$ is a curve which begins and terminates at the fixed-point P_{In} , winding once around P_0 . Lemma 3.21 is now proven. \square

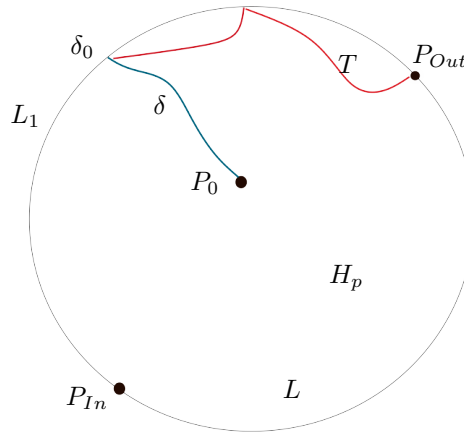


FIGURE 59. The cross section D_α , sketched as a topological disc (rather than a subset of a half-plane, as in Fig.58). The sub-arc L_1 denotes $[P_{In}, \delta_0)$, and L denotes $\partial B_\alpha \cap U_p$ - the boundary arc connecting P_{In}, P_{Out} (see Def.3.2.)

We are now ready to sketch $f_p(H_p)$ inside D_α . To do so, let us recall $f_p(L) = L$ (where $L = \partial B_\alpha \cap U_p$ is a curve connecting P_{In}, P_{Out} - see Def.3.2). Now, note the following facts:

- Replicating the argument in Cor.3.21 above, as the sector T lies outside H_p (and as T and H_p are separated by the curve ρ), for every $\{x_n\} \in H_p$, $f_p(x_n) \not\rightarrow P_0$ - that is, $P_0 \notin \overline{f_p(H_p)}$.
- Recall $f_p(\delta)$ is an arc on l connecting P_{In} and $f_p(\delta_0)$, and that $f_p^2(\delta)$ lies strictly inside D_α (see the proof of Prop.3.8) - i.e., $f_p^2(\delta)$ is an arc interior to D_α , beginning at P_{In} and terminating at $f_p^2(\delta_0)$.

- Finally, recall that in Case B the cross-section H_p is homeomorphic to a slit topological disc, with the slit corresponding to δ (see the discussion immediately after Lemma 3.12). As such, for every $s \in \delta$ there exists some $r > 0$ s.t. $B_r(s) \setminus \delta$ includes two components, C_1 and C_2 s.t. $C_i \subseteq H_p$, $i = 1, 2$, and for $\{s_n\}_n \subseteq C_i$, $s_n \rightarrow s$, $f_p(s_n) \rightarrow f_p^i(s)$, $i = 1, 2$ (where $B_r(s)$ denotes a planar disc on D_α).

As such, it follows $f_p(H_p)$ is as in Fig.60 - that is, the domain winds around P_0 , and encloses a domain $D_0 \subseteq D_\alpha$ s.t. $P_0 \in D_0$. Moreover, $f_p(\delta) \in \partial f_p(H_p)$ and $f_p^2(\delta)$ is at the interior of $\overline{f_p(H_p)}$ (see the illustration in Fig.60). In particular, the first-return map f_p tears H_p along δ , in accordance with the two-sided limits above.

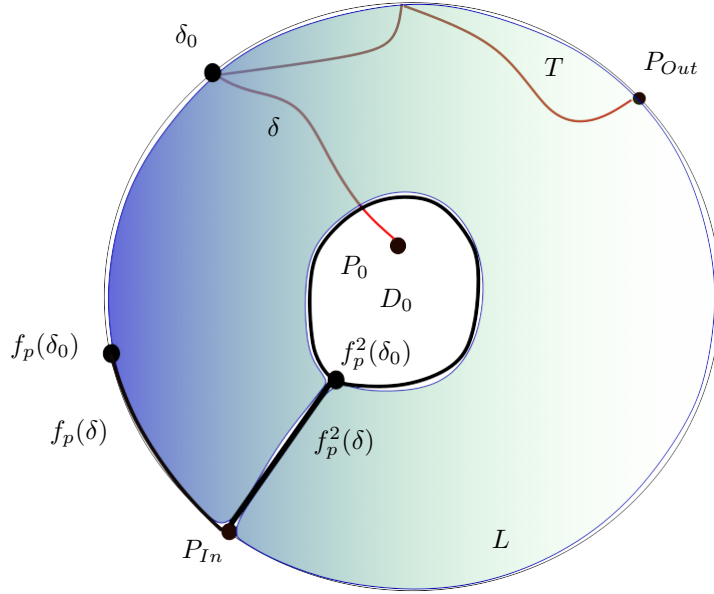


FIGURE 60. $f_p(H_p)$, imposed on the cross-section D_α . The red curve denotes $f_p^{-1}(l)$ - for simplicity, it is drawn as a curve.

Having sketched the first-return map for f_p , we see we cannot immediately apply the same arguments used to prove Case A - with the reason being that the fact $f_p(H_p)$ is glued to itself at $f_p^2(\delta_0)$ simply does not allow us to extend f_p to a disc homeomorphism as we did in Stage I . In order to overcome this difficulty, we begin by expanding the fixed point P_{In} to a directions sphere, with a fixed point P'_{In} on its boundary. Moreover, we open up the curve δ to an open sector δ' by splitting $\delta \cap \partial H_p$ to two curves, δ_1 and δ_2 , which enclose the said sector (see the illustration in Fig.61).

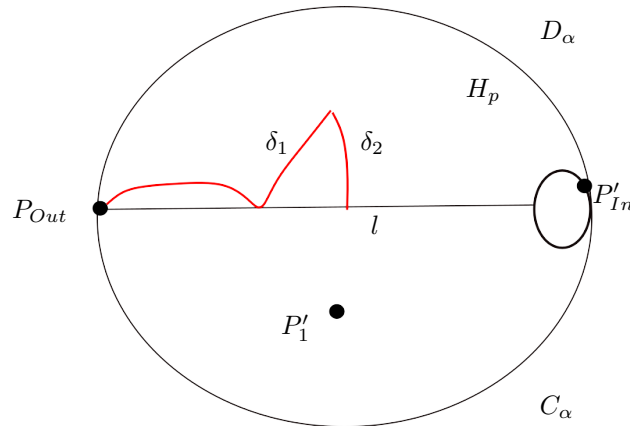


FIGURE 61. Amending $H_p - P_{In}$ is opened to a sphere of direction with a unique fixed point on its boundary, P'_{In} , while δ is opened to the sector trapped between δ_1, δ_2 and l . Again, we glue C_α to D_α at l .

Now, let $f_0 : \overline{H_p} \rightarrow \overline{D_\alpha}$ denote a continuous, injective function which is conjugate to f_p away from the open sector δ' , the set $\cup_{n \geq 0} f_0^{-n}(\delta')$, and the directions sphere P_{In} - in particular, we choose f_0 s.t. for $x \in H_p$, $x \rightarrow \delta_i$, we have $f_0(x) \rightarrow f_0(\delta_i)$, $i = 1, 2$. As such, we can sketch the graph of f_0 as in Fig.62. In other words, we obtain f_0 from f_p by opening the components of $\cup_{n \geq 0} f_p^{-n}(\delta)$ to open sets - and after this deformation, we are now able to extend f_0 to a homeomorphism of S , a twice-punctured disc, similarly to what we did in Case A.

To do so, choose some point, P'_0 , inside the sector δ' which lies away from $f_0(\overline{H_p}) \cap \delta'$, and make it a periodic point of period 2 (see the illustrations in Fig.62 and Fig.61) - i.e., similarly to Case A we extend f_0 to F , some homeomorphism of the disc, s.t. the following is satisfied:

- Similarly to Case A, we glue C_α to D_α at l , and generate a disc $V_\alpha = C_\alpha \cup D_\alpha$.
- We choose the extension F s.t. $F(P'_{In}) = P'_{In}$, and $F(P'_0) = P'_1$, $F(P'_1) = P'_0$.

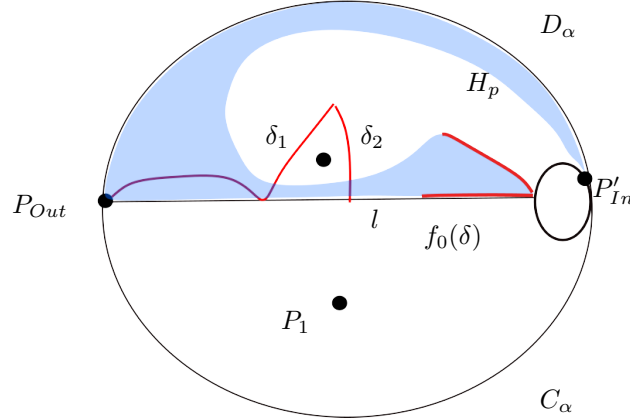


FIGURE 62. The new map f_0 - as can be seen, we can apply the logic of Case A to analyze it (the blue region denotes $f_0(H_p)$). Moreover, f_0 is conjugate to f_p away from δ_1, δ_2 and P'_{In} .

Consequentially, we reduced f_0 to the same situation as in Case A - as such, using the same arguments (and in particular, Th.3.17), we immediately conclude:

Corollary 3.22. *With the notations above, f_0 has infinitely many periodic orbits in $\overline{H_p}$ - of all minimal periods. Additionally, the dynamics of f_0 on its invariant are isotopically deformed to that of a Smale Horseshoe map $G : ABCD \rightarrow V_\alpha$ (where $ABCD$ is some topological rectangle in V_α) - in particular, we have the following:*

- As we isotopically deform F to G , $\overline{H_p}$ is isotoped to the rectangle $ABCD$.
- Every periodic orbit of minimal period k for G is isotopically deformed to a periodic orbit for f_0 in $\overline{H_p}$, of the same minimal period.
- If two periodic orbits $\{x_1, \dots, x_k\}$ and $\{y_1, \dots, y_j\}$ for G in $ABCD$ are deformed to the same periodic orbit $\{z_1, \dots, z_t\}$ for f_0 , then $k = j = t$ and $x_i = y_i$, $1 \leq i \leq k$.

We would now like to prove the analog of Lemmas 3.19 and 3.20 for the first-return map f_p - however, since f_0 is not exactly the same function as f_p we need to be a little bit more careful. We begin with the following fact:

Lemma 3.23. *Let $p \in P$ be a trefoil parameter falling into Case B. Then, f_p generates infinitely many periodic orbits, of every minimal period. Moreover, f_p is continuous at the said periodic orbits.*

Proof. We first claim that save perhaps for one periodic orbit, every periodic orbit for G of minimal period k , is deformed to a periodic orbit $\{x_1, \dots, x_k\}$ for f_0 which lies away from the sector δ' and the direction sphere P_{In} . To do so, let $G : ABCD \rightarrow ABCD$ denote the said Smale Horseshoe map from Cor.3.22, and consider a periodic orbit for G which is not deformed to P'_{In} , the fixed-point for f_0 - consequentially, by the the said orbit must lie away from the directions sphere P_{In} .

Now, let us remark that we can choose the isotopy from f_0 to G s.t. any point on $\partial\delta' = \delta_1 \cup \delta_2$ is eventually collapsed to an arc on the directions sphere P_{In} along the way (see the illustration in Fig.64) - and since P'_{In} is the only periodic orbit on the direction sphere P_{In} , it follows every periodic orbit on $\partial\delta'$ for f_0 can be destroyed or collapsed by the isotopy. Consequentially, as the periodic orbit $\{x_1, \dots, x_n\}$ is both unremovable and uncollapsible by Th.3.17, it must lie away from the curves δ_1, δ_2 and their pre-images in $\overline{H_p}$ - or, in other words, it lies away from the pre-images of the sector δ' in $\overline{H_p}$.

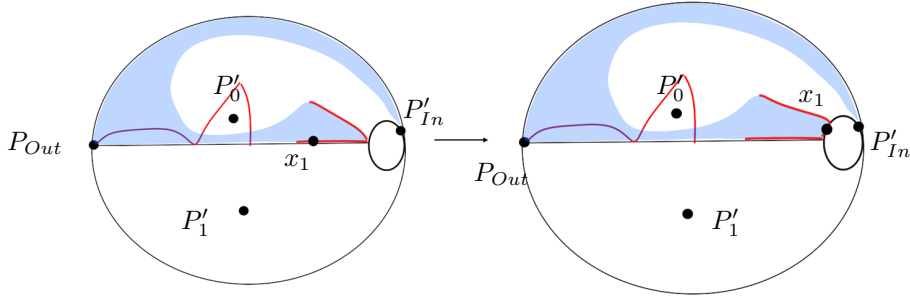


FIGURE 63. The isotopy collapsing points on $f_0(\delta_1 \cup \delta_2)$ like x_1 (or more generally, points $x_1 \in l \cup f_0(\delta_2)$) to P'_{In} .

All in all, we conclude that save for one periodic orbit for G which is deformed to P'_{In} , every other periodic orbit for G is deformed to a periodic orbit for f_0 , which lies away from P'_{In} and the pre-images of $\bar{\delta}$ in H_p . Consequentially, since f_p and f_0 are conjugate away from δ' , its pre-images, and the directions sphere P'_{In} we conclude $\{x_1, \dots, x_k\}$ is also a periodic orbit for f_p which lies away from the curve δ and its pre-images under f_p - as such, by Prop.3.8, f_p is continuous at the said periodic orbit. Finally, since this is true for every periodic orbit for the Smale Horseshoe map G (save perhaps for one), we conclude f_p generates infinitely many periodic orbits in H_p , of all minimal periods - and moreover, f_p is continuous at every such periodic orbit. \square

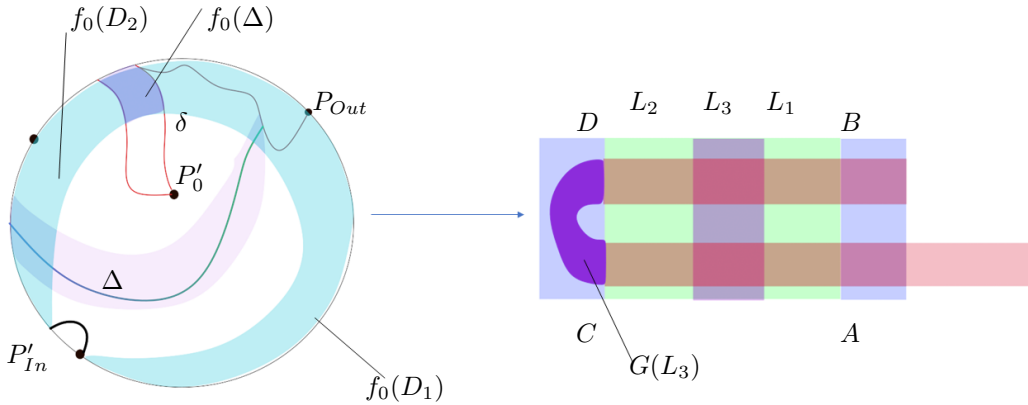


FIGURE 64. Similarly to Case A, the isotopy of $F|_{\overline{H_p}} = f_0$ on H_p to $G : ABCD \rightarrow S$ deforms the purple region Δ to the sub-rectangle L_3 .

Having proven Lemma 3.23, we can almost conclude the proof in Case B. To do so, we must first prove we can define symbolic dynamics for f_p - that, however, is immediate. By considering the curve δ and by recalling that when we deform f_p to the Smale Horseshoe map G we open δ to a sector and then continuously deform it to the CD side (see the illustration in Fig.64), using a similar argument to the one used to prove Lemma 3.19, we conclude:

Lemma 3.24. *Let $p \in P$ be a trefoil parameter falling into Case B. Then, there exists a curve $\Delta \subseteq f_p^{-1}(\delta)$ s.t. $\overline{H_p} \setminus \Delta$ includes two components - D_1 and D_2 , s.t. $P'_{In} \in \partial D_1 \setminus \Delta$ and $\delta \subseteq \partial D_2 \setminus \Delta$ (see the illustration in Fig.65). Consequentially, we can define symbolic dynamics on the invariant set of f_p in $\overline{H_p} \setminus f_p^{-1}(l)$, denoted by I' - i.e., there exists a continuous $\pi' : J \rightarrow \{1, 2\}^{\mathbb{N}}$ s.t. $\pi' \circ f_p = \sigma \circ \pi'$.*

Proof. By considering Fig.60, it immediately follows Δ exists and divides $\overline{H_p}$ to D_1 and D_2 , as in Fig.65. Now, it only remains to define symbolic dynamics on I' . Let us note that the set I' , by definition, is a subset of $\overline{D_\alpha} \setminus (\cup_{n \geq 1} f_p^{-n}(l))$, and it is also invariant under f_p - as such, since $\Delta \subseteq f_p^{-1}(\delta) \subseteq f_p^{-2}(l)$, any component C of I' either lies in D_1 or D_2 , and the same is true for $f_p(C)$. Furthermore, by Prop.3.8, f_p and all its iterates are continuous at initial conditions in I' - as such, given $x \in I'$, there exists a function $\pi' : I \rightarrow \{1, 2\}^{\mathbb{N}}$ s.t. $\pi'(x) = \{i_0, i_1, i_2, \dots\}$ where $i_k = 1$ when $f_p^k(x) \in D_1$ and 2 otherwise. It immediately follows that as f_p^k is continuous at x for every k , so is π' - and by definition, we also have $\pi' \circ f_p = \sigma \circ \pi'$, where $\sigma : \{1, 2\}^{\mathbb{N}} \rightarrow \{1, 2\}^{\mathbb{N}}$ is the one-sided shift. The proof of Lemma 3.24 is now complete. \square

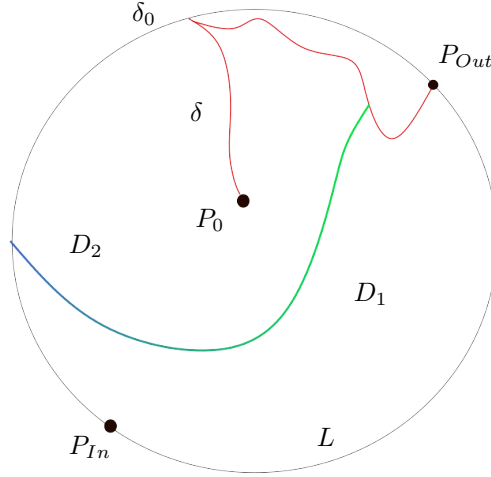


FIGURE 65. The curve Δ , partitioning $\overline{H_p}$ to D_1 and D_2 .

Now, having proven Cor.3.24, we now use it to conclude the following fact:

Corollary 3.25. *The periodic points given by Lemma 3.23 all lie in the set I' , given by Cor.3.24 - and consequentially, we can define symbolic dynamics on them. Moreover, $\pi'(I)$ includes every periodic symbol in $\{1, 2\}^{\mathbb{N}}$ that is not the constant $\{1, 1, 1, \dots\}$.*

Proof. Let $\{x_1, \dots, x_k\}$ be a periodic orbit given by Lemma 3.23 - by the proof of Lemma 3.23, we already know f_p is continuous on $\{x_1, \dots, x_k\}$, and that it lies away from δ . Hence, we have $\{x_1, \dots, x_k\} \subseteq \overline{H_p} \setminus (\cup_{n \geq 0} f_p^{-n}(\delta))$ and by $\Delta \subseteq f_p^{-1}(\delta)$ we conclude $\{x_1, \dots, x_k\}$ also lies in I' . Similarly to the argument in Lemma 3.20 for Case A, again the arc Δ is continuously deformed into the sub-rectangle L_3 of $ABCD$, defined by $G(L_3) \cap ABCD = \emptyset$ (see the illustration in Fig.64). As such, similarly to the proof of Lemma 3.20, it follows that when we deform $\{x_1, \dots, x_k\}$ to $\{y_1, \dots, y_k\}$, a periodic orbit for the Smale Horseshoe map G , the symbol corresponding to $\{x_1, \dots, x_k\}$ does not change. As such, since every periodic orbit for G (save the one corresponding to the constant $\{1, 1, 1, \dots\}$ - i.e., P'_{In}) can be continuously deformed to a periodic orbit for f_p , using a similar argument to the one used to prove Lemma 3.20 Cor.3.25 now follows. \square

We now conclude the proof of Th.3.15 for Case B. To do so, again, for every periodic $s \in \{1, 2\}^{\mathbb{N}}$ of minimal period k which is not the constant $\{1, 1, 1, \dots\}$, set D_s as the component of $\pi'^{-1}(s)$ in I' s.t.:

- D_s contains a periodic orbit of minimal period k , $\{x_1, \dots, x_k\}$ - by Cor.3.25, it exists.
- $\{x_1, \dots, x_k\}$ can be deformed isotopically to a periodic orbit of G , the Smale Horseshoe map.

Now, similarly to Case A, when $s = \{1, 1, 1, \dots\}$ set $D_s = \{P'_{In}, P'_{Out}\} \cup L$ (where $L = \partial B_\alpha \cap U_p$ - see Def.3.2) - and let Q denote the collection of such D_s , for periodic s . Setting $\pi = \pi'|_Q$ and summarizing our results, we conclude:

- The first-return map f_p is continuous on Q .
- Also, there exists a continuous $\pi : Q \rightarrow \{1, 2\}^{\mathbb{N}}$ s.t. $\pi \circ f_p = \sigma \circ \pi$ (where $\sigma : \{1, 2\}^{\mathbb{N}} \rightarrow \{1, 2\}^{\mathbb{N}}$ denotes the one-sided shift).
- $\pi(Q)$ includes every periodic symbol in $\{1, 2\}^{\mathbb{N}}$.
- If s is periodic of minimal period k , $\pi^{-1}(s)$ includes a periodic orbit of minimal period k for f_p .

All in all, we have completed the proof of Th.3.15 for Case B.

3.3.3. Stage III - proving Th.3.15 for Case C: Having proven Th. 3.15 holds for Cases A and B, we now prove the same for Case C. In this case we have $\delta_0 = P_{Out}$, as illustrated in Fig.66. Consequentially, in this scenario, by $f_p(P_{Out}) = P_{Out}$ we have $\delta = f_p^{-1}(l)$, and as such H_p is homeomorphic to a slit disc - see the illustration in Fig.66. However, this implies $f_p(l) = f_p^2(\delta)$ is a curve in D_α , beginning at P_{In} and terminating at P_{Out} - see the illustration in Fig.67.

Since $f_p(\delta) = l$ for every $s_0 \in \delta$ the limit $\lim_{s \rightarrow s_0} f_p(s)$ is either $f_p(s_0)$ or $f_p^2(s_0)$ - depending on the direction from which s tends to s_0 . This remains true even when $s_0 = P_{Out}$ - it is therefore easy to see that when $s \in H_p$ tends to P_{Out} from above δ , $f_p(s) \rightarrow P_{Out}$, and when it does so from below δ (i.e., from the sector T given by Cor.3.10 - see Fig.66), we'd have $f_p(s) \rightarrow P_0$.

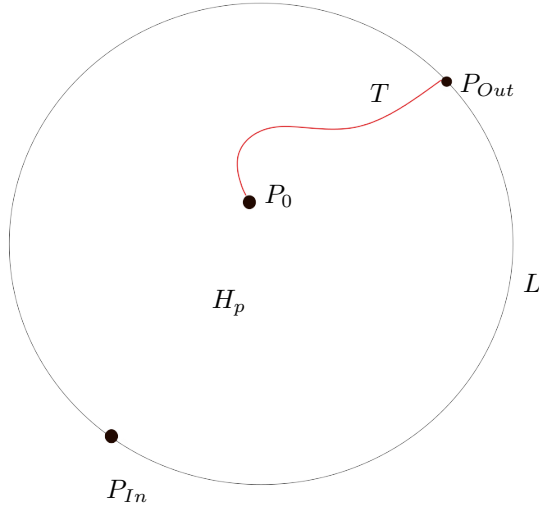


FIGURE 66. Case C - $\delta_0 = P_{Out}$, and δ is the red curve connecting P_0 and P_{Out} .

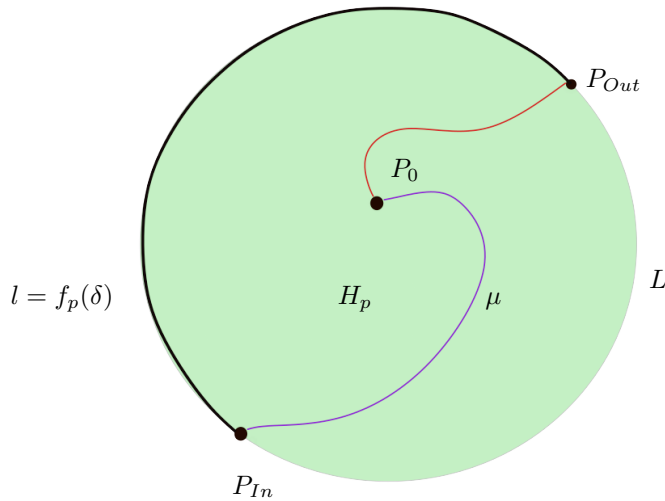


FIGURE 67. The first-return map in Case C - the curve μ denotes $f_p^2(\delta) = f_p(l)$. μ begins at P_{In} and terminates at P_0 .

By this entire discussion we see that Case C is very similar to Case B - only that in Case B the point P_0 was away from $f_p(\overline{H_p})$. In this scenario this is not the case - as such, making P_0 a periodic point w.r.t. to any extension of f_p to a homeomorphism of a disc would have to be done more carefully.

To do so, we deform the cross-section H_p as follows - first, note that by Fig.67 and Lemma 3.2 (and by Remark 3.9), every $s \in \delta$ which is not P_0 has a unique n -th pre-image in $\overline{D_\alpha}$. Now, begin deforming H_p by opening P_{Out} to a direction sphere (see the illustration in Fig.68). Then, open up the curve δ into an open sector, as in Fig.68 - and do the same simultaneously for every component $\cup_{n \geq 0} f_p^{-n}(\delta)$ in D_α . Much like Case B, after this deformation δ becomes a sector δ' , whose boundary includes two curves, terminating at P_0 - δ_1 and δ_2 , as illustrated in Fig.68.

Now, open up P_{In} to a directions sphere with a unique fixed-point on it, P'_{In} , and let f_0 denote some homeomorphism $f_0 : \overline{H_p} \rightarrow \overline{D_\alpha}$ s.t. f_0 is conjugate to f_p on $\overline{H_p} \setminus \cup_{n \geq 0} f_0^{-n}(\delta')$, and behaves as in Fig.69. In particular, when $x \rightarrow \delta_i$, we have $f_0(x) \rightarrow f_0(\delta_i)$, $i = 1, 2$. Consequentially, $f_0(\delta)$ is a sector whose boundary intersects the directions sphere P_{In} and includes P_0 on its vertex (see the illustration in Fig.68) - as such, because $f_p^2(\delta)$ is an arc beginning at P_{In} and terminating at P_0 , when we deform f_p to f_0 we can arrange for the intersection $f_0(\delta') \cap \delta'$ to include an open disc D as in Fig.69.

Similarly to Cases A and B, glue some half-disc C_α to D_α at l to create a disc V_α as illustrated in Fig.68 and Fig.69, and choose some $P'_0 \in f_0(\delta) \cap \delta$ and another P_1 , interior to C_α . Finally, extend f_0 to a disc homeomorphism $F : V_\alpha \rightarrow V_\alpha$ s.t. F coincides with f_0 on $\overline{H_p}$ and $F(P_{In}) = P_{In}$, $F(P'_0) = P_1$ and $F(P_1) = P'_0$. Now, consider

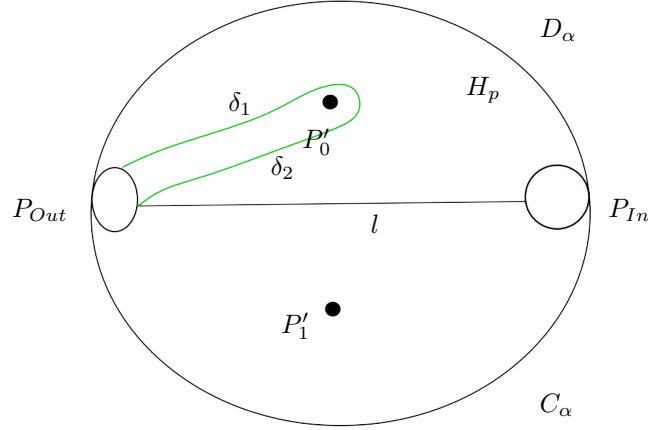


FIGURE 68. H_p after the deformation - δ is blown to a sector, while P_{In} and P_{Out} are both opened to direction spheres. Similarly to cases A and B, we glue C_α to D_α at l .

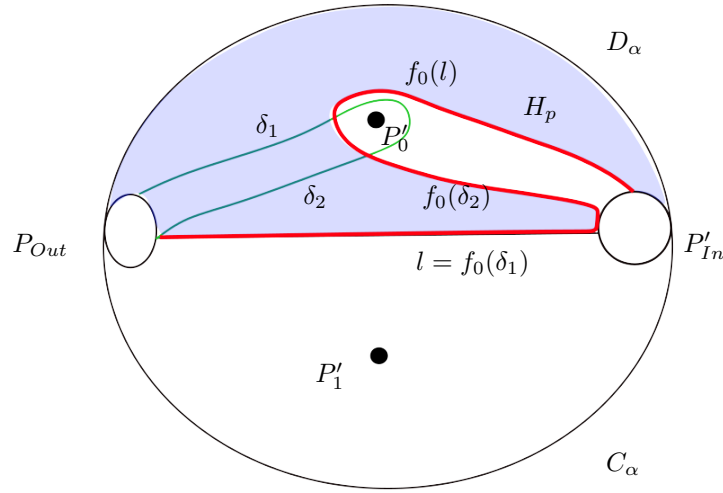


FIGURE 69. $f_0(H_p)$ imposed on H_p - the red curve denotes $f_0(l \cup \partial\delta)$. D is the region trapped between $f_0(\partial\delta)$ and $\partial\delta$.

a graph T inside H_p connecting P'_1, P_0 and P_{In} as in Fig.70, and then consider its image under f_0 (see Fig.70) - again, applying the same procedures used to prove Cases A and B we see the resulting graph map is essentially the same as the one obtained for Cases A and B.

As such, all in all, we have shown Case C can be reduced to Case B - now, recalling Cor.3.22, Lemma 3.23, Cor.3.24 and their corollaries did not depend on the location of δ_0 in the curve \bar{l} , we see their conclusions extend to Case C as well. All in all, using similar arguments to those used in B, Th.3.15 similarly follows for Case C. The proof of Th.3.15 is now complete. \square

At this point, let us remark the proof of Th.3.15 can probably be generalized to other heteroclinic parameters for the Rössler system, which generate knots more complex than a trefoil (see Def.3.1) - however, much like Th.3.15, the proof of any such generalization would greatly depend on the topology of the heteroclinic knot involved.

Let us also remark Th.3.15 can be reformulated in a somewhat simpler way (the proof, of course, remains the same). To begin, recall the cross-section U_p (see the discussion before Lemma 2.1), the curve Δ and the regions D_1, D_2 from the proof of Th.3.15 (as defined per Case A, B or C). Let ρ denote some curve in \bar{D}_α s.t. the following is satisfied (see the illustration in Fig.71):

- $\Delta \subseteq \rho$.
- ρ is homeomorphic to a closed interval - in particular, the endpoints of ρ are in \bar{l} .
- $\bar{U}_p \setminus \rho$ is composed of two components, U_1, U_2 - indexed by $D_i \subseteq U_i, i = 1, 2$.

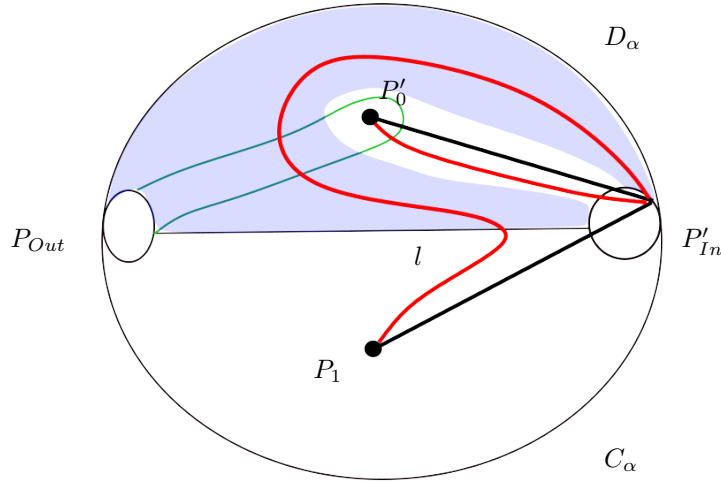


FIGURE 70. The image of the black graph T under F is the red curve - the image of one edge connects P'_{In} and P'_0 , while the image of the second begins at P'_{In} , loops around P_0 and then enters C_α and connects with P_1 .

Now, set I as the maximal invariant set of f_p in $\overline{U_p} \setminus \rho$ - that is, I is the collection of initial conditions in the cross-section U_p whose trajectories both never hit ρ and never escape to ∞ . It is easy to see the set Q constructed in the proof of Th.3.15 is a subset of I . We now restate Th.3.15 as follows:

Corollary 3.26. *Let $p \in P$ be a trefoil parameter for the Rössler system and let $f_p : \overline{U_p} \rightarrow \overline{U_p}$ denote the first-return map. Let I be as above and denote by $\sigma : \{1, 2\}^{\mathbb{N}} \rightarrow \{1, 2\}^{\mathbb{N}}$ the one-sided shift - then, there exists an f_p -invariant $Q \subseteq I$, s.t. the following holds:*

- f_p is continuous on Q .
- There exists a continuous $\pi : Q \rightarrow \{1, 2\}^{\mathbb{N}}$ s.t. $\pi \circ f_p = \sigma \circ \pi$.
- $\pi(Q)$ includes every periodic $s \in \{1, 2\}^{\mathbb{N}}$.
- If $s \in \{1, 2\}^{\mathbb{N}}$ is periodic of minimal period $k > 0$, $\pi^{-1}(s)$ includes at least one periodic point for f_p of minimal period k .

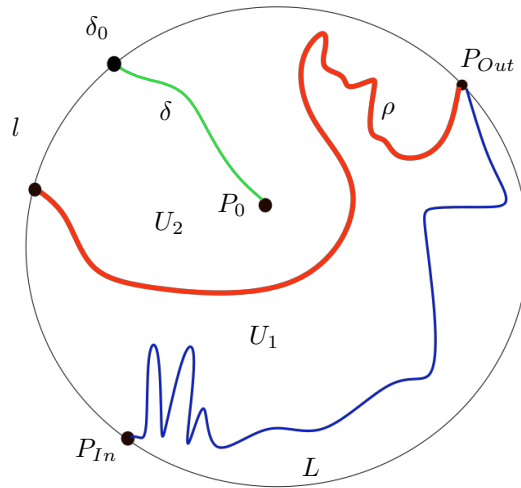


FIGURE 71. The cross-section U_p , sketched as a disc instead of a half-plane. The curve ρ bisects U_p to U_1, U_2 , with L denoting the curve $\partial B_\alpha \cap U_p$ (see Def.3.2).

One final remark before we conclude this section is that the periodic orbits in Q given by Th.3.15 are isotopy stable and uncollapsible, in a sense which is somewhat different than that of Th.3.17. To state it, let us recall the curve Δ from the proof of Th.3.15 and the curve δ from Prop.3.8. Now, let $g : \overline{H_p} \setminus \delta \rightarrow \overline{D_\alpha}$ be a homeomorphism isotopic to $f_p : \overline{H_p} \setminus \delta \rightarrow \overline{D_\alpha}$, s.t. the following is satisfied (see the illustrations in Fig.72 and 73):

- $g(P_{In}) = P_{In}$ and $g(P_{Out}) = P_{Out}$.

- $g(H_p) \setminus \Delta$ includes at least two components.
- Whenever $P_0 \in \partial H_p$, we have $\lim_{s \rightarrow P_0} g(s) = P_{In}$.
- $P_0 \notin \bar{g}(\overline{H_p} \setminus \delta)$.

Applying a similar logic used to prove Th.3.15, we have the following result:

Corollary 3.27. *Let $p \in P$ be a trefoil parameter, and let $g : \overline{H_p} \setminus \delta \rightarrow \overline{D_\alpha}$ be as above. Then, if $s \in \{1, 2\}^{\mathbb{N}}$ is periodic of minimal period k and $x \in D_s \subseteq Q$ is periodic of minimal period k , we have the following:*

- x is continuously deformed to y , a periodic orbit of minimal period k for g . In particular, y is in the invariant set of g in $\overline{H_p} \setminus \Delta$.
- Let $s, \omega \in \{1, 2\}^{\mathbb{N}}$ be periodic orbits of minimal periods k_1 and k_2 , and let $x_1 \in D_s$ and $x_2 \in D_\omega$ be periodic for f_p of minimal periods k_1 and k_2 . If the isotopy deforms x_i to y_i , $i = 1, 2$, then $y_1 = y_2$ if and only if $s = \omega$ - that is, the periodic dynamics are also uncollapsible.

Proof. Recall the disc $S = V_\alpha \setminus \{P_0, P_1\}$ introduced in the proof of Th.3.15, and let us recall that the set Q given by Th.3.15 lies in the invariant set of f_p in $\overline{H_p} \setminus \Delta$. Since g is isotopic to f_p as described above, similarly to how we extend f_p to $F : S \rightarrow S$ we can extend g to $G' : S \rightarrow S$, and moreover, we can do so s.t. F and G' are isotopic on S (see the illustration in Fig.72 and 73). Since by Th.3.17 the periodic orbits in Q are unremovable and uncollapsible it follows that as we isotope F to G' , the periodic orbits for $f_p = F|_{\overline{H_p} \setminus \Delta}$ are continuously deformed to the periodic orbits of $g = G'|_{\overline{H_p} \setminus \Delta}$ without changing their minimal periods or collapse into one another. Cor.3.27 now follows. \square

Remark 3.28. *The function g from Cor.3.27 need not necessarily be a first-return map for a flow. That is, it need only be a homeomorphism of $\overline{H_p} \setminus \delta$.*

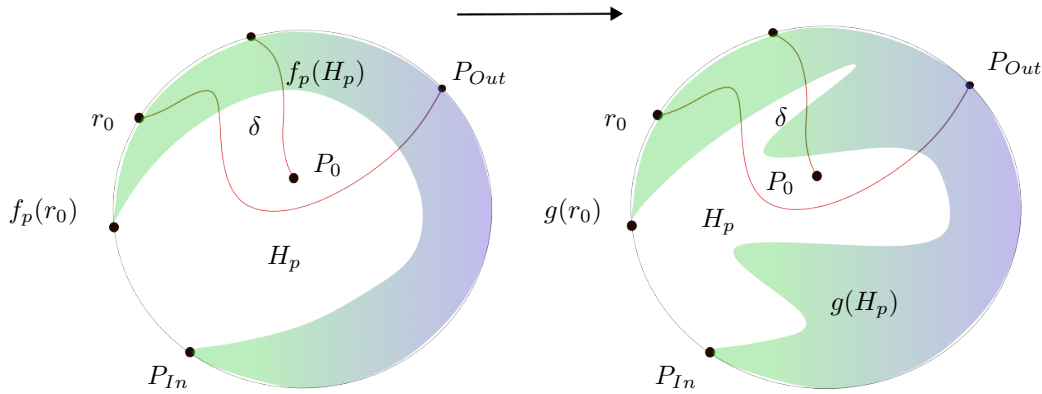


FIGURE 72. Since g (on the right) and f_p (on the left) are isotopic and g satisfies the assumptions of Cor.3.27, the periodic orbits in Q all persist when f_p is isotoped to g . As can be seen, in this scenario $p \in P$ is a trefoil parameter falling into Case A (see Fig.47).

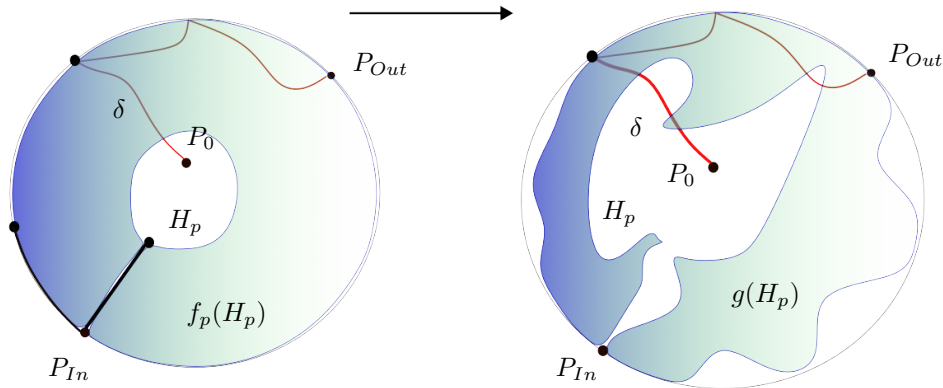


FIGURE 73. Again, here we see an isotopy between f_p and g , when p is a trefoil parameter corresponding to Case B (see Fig.57), where again g is on the right and f_p is on the left. As g satisfies the assumptions of Cor.3.27, the periodic orbits in Q all persist when f_p is isotoped to g .

4. THE IMPLICATIONS:

Th.3.15 teaches us that at trefoil parameters, the dynamics of the Rössler system are complex essentially like those of a Smale Horseshoe, suspended around a heteroclinic trefoil knot. Motivated by the theory of homoclinic bifurcations (and in particular, Shilnikov's Theorem - see [2]), in this section we use Th.3.15 to prove several results about the dynamical complexity of the Rössler system and its bifurcations around trefoil parameters.

To begin, recall P always denote the parameter space introduced in page 3, and that given a parameter $v \in P$ we denote by F_v the vector field corresponding to $v = (a, b, c)$ (see Eq.1.5). This section is organized as follows - first we study the question of hyperbolicity of the dynamics at trefoil parameter: namely, in Prop.4.1 we prove the flow at trefoil parameters $p \in P$ are non-hyperbolic. Following that, we prove that in the space of C^∞ vector fields (on \mathbf{R}^3), trefoil parameters are inseparable from period-doubling and saddle-node bifurcation sets (for a more precise formulation, see Prop.4.2). Finally, we conclude this Section with the following result: given a trefoil parameter $p \in P$, a positive $n > 0$ and $v \in P$, provided v is sufficiently close to p the vector field F_v generates at least n distinct periodic trajectories (see Th.4.4).

To begin, let us first recall the notion of hyperbolicity:

Definition 4.1. *Let M be a smooth 3-manifold, let F be a C^∞ vector field on M , and denote by ϕ_t the resulting flow on M . An invariant set $\Lambda \subseteq M$ w.r.t. the flow is said to **have a hyperbolic structure on Λ** or in short, **hyperbolic on Λ** , provided at every $x \in \Lambda$ one can split the tangent space, $T_x M = E_x^s \oplus E_x^u \oplus E^c(x)$ s.t. the following is satisfied:*

- $E^c(x)$ is spanned by $F(x)$.
- E_x^s, E_x^u and E_x^c vary continuously to $E_{\phi_t(x)}^s, E_{\phi_t(x)}^u$ and $E_{\phi_t(x)}^c$ (respectively) as x flows to $\phi_t(x)$, $t \in \mathbf{R}$ - in particular, $D_{\phi_t(x)} E_x^j = E_{\phi_t(x)}^j$ where $j \in \{s, u, c\}$ and $D_{\phi_t(x)}$ is the differential of the flow at time t .
- There exist constants $C > 0$ and $\lambda > 1$ s.t. for every $t > 0$ and every $x \in \Lambda$ we have:
 - (1) For $v \in E_x^s$, we have $\|D_{\phi_t(x)} v\| < C e^{-\lambda t} \|v\|$.
 - (2) For $v \in E_x^u$, we have $\|D_{\phi_t(x)} v\| > C e^{\lambda t} \|v\|$.

In other words, the flow expands (or stretches) in one direction along the trajectories on Λ , and contracts in another direction.

Now, let us recall that in Cor.3.11 we defined I as the maximal invariant set of the first-return map $f_p : \overline{D_\alpha} \setminus \{P_0\} \rightarrow \overline{D_\alpha} \setminus \{P_0\}$ in $\overline{D_\alpha} \setminus l$ - as proven in Th.3.15, the set I includes infinitely many periodic orbits for f_p . We now prove:

Proposition 4.1. *Let $p \in P$ be a trefoil parameter. Then, the Rössler system at trefoil parameters does not satisfy any hyperbolicity condition on I .*

Proof. To begin, let p be a trefoil parameter, and let Λ be the closure in \mathbf{R}^3 of trajectories (both forward and backwards) for initial conditions in I - it follows Λ is also F_p -invariant. By Cor.3.11, it follows Λ is inseparable from P_{In} - since p is a trefoil parameter the two dimensional manifolds W_{In}^u, W_{Out}^s coincide (see Def.17), which implies Λ is also inseparable from P_{Out} . Now, recall P_{In}, P_{Out} are hyperbolic saddle-foci of opposing indices, connected by a bounded heteroclinic trajectory Θ (see Def.3.2) - with Θ being a component of both one-dimensional invariant manifolds W_{In}^s, W_{Out}^u . Consequentially, by the density of I in D_α it must also be dense around P_0 , which, by previous discussion and the compactness of Λ , implies Θ, P_{In}, P_{Out} all lie in Λ .

Now, assume by contradiction we can decompose $T\Lambda$ as in the definition above - with previous notations, this implies the unstable subspace $E^u(P_{Out})$ of the tangent space $T_{P_{Out}} \mathbf{R}^3$ is one-dimensional, while the unstable subspace $E^u(P_{In})$ of $T_{P_{In}} \mathbf{R}^3$ is two dimensional. Hence, for a point $x \in \Theta$, the subspace $E^u(x)$ cannot vary continuously as x flows from P_{Out} to P_{In} and we have a contradiction. This proves the vector field F_p cannot be hyperbolic on Λ , and Prop.4.1 follows. \square

Having proven the non-hyperbolic nature of the flow, we proceed to study the bifurcations around trefoil parameters. To begin, let $p \in P$ be a trefoil parameter and recall we denote the saddle-indices for the saddle-foci P_{In}, P_{Out} by ν_{In}, ν_{Out} - respectively (see the definition at page 3). Additionally, recall that we assume that we assume the saddle-indices corresponding to v always satisfy either $\nu_{In} < 1$ or $\nu_{Out} < 1$ (see the discussion in page 3). Plugging in this assumption, we derive the following result:

Proposition 4.2. *Let $p \in P$ be a trefoil parameter for the Rössler system. Then, the vector field F_p is an accumulation point for infinitely many period-doubling and saddle-node bifurcation sets in the space of C^∞ vector fields on \mathbf{R}^3 .*

Proof. For completeness, let us first recall Sections 3.2 and 3.1 of [10]. In that paper, the setting is that of a smooth, two-parameter family of vector fields $\{X_{(a_1, a_2)}\}_{(a_1, a_2) \in O}$, with (a_1, a_2) varying smoothly in some open set $O \subseteq \mathbf{R}^2$. Assume there exists a curve $\gamma \subseteq O$ corresponding to the existence of homoclinic trajectories. Also assume the saddle indices along γ are all strictly lesser than 1. As proven in [10], under these assumptions there exists a family of spirals, $\{\delta_o\}_{o \in \gamma}$ satisfying:

- δ_o is a curve in O , spiralling towards o .
- δ_o is a subset of O corresponding to the existence of a periodic trajectory T for the vector field X_s , $s \in \delta_o$.
- Provided the saddle index along γ is bounded, there exists some $c > 0$ s.t. $\forall o \in \gamma$, $\text{diam}(\delta_o) > c$ (with that diameter taken w.r.t. the Euclidean metric in O)
- As $s \in \delta_o$ goes to o along δ_o , T undergoes a cascade of period-doubling and saddle node bifurcations. Consequentially, the period-doubling and saddle-node bifurcation sets in O are dense around every point in $o \in \gamma$.

Now, back to the Rössler system. To begin, recall we denote by F_p the corresponding vector field and assume first that $\nu_{In} < 1$ - additionally, recall that since $p \in P$ is a trefoil parameter, by Def.3.2 we know the two dimensional manifolds W_{Out}^s, W_{In}^u coincide. Therefore, we can perturb F_p at some small neighborhood of P_{Out} and combine the heteroclinic trajectory Θ and some flow line in $W_{In}^u = W_{Out}^s$ to create a homoclinic trajectory to P_{In} - and moreover, we can choose this perturbation to be arbitrarily close to F_p in the C^∞ metric. In other words, we have just proven there exists an arbitrarily small C^∞ approximation of F_p , V s.t. V generates a homoclinic trajectory to the fixed point P_{In} . Consequentially, there exists a smooth curve γ_{In} in the space of C^∞ vector fields on \mathbf{R}^3 , s.t. for every $\omega \in \gamma_{In}$, the vector field corresponding to ω generates a homoclinic curve to P_{In} . Moreover, by the description of these perturbations above, we can choose the curve γ_{In} s.t. for every $\omega \in \gamma_{In}$, the vector fields ω, F_p coincide around the fixed point P_{In} - consequentially, the saddle index ν_{In} is constant along γ_{In} .

As $\nu_{In} < 1$ the discussion above implies the period-doubling and saddle node bifurcations sets are dense around every vector field on γ_{In} (in the space of C^∞ vector fields on \mathbf{R}^3) - and since $F_p \in \overline{\gamma_{In}}$, it follows these bifurcation sets are also dense around F_p . The argument for the case $\nu_{Out} < 1$ is symmetric, and Prop.4.2 now follows. \square

Remark 4.3. Assume both $\nu_{In}, \nu_{Out} < 1$. In that case, the proof of Prop.4.2 essentially proves the bifurcations around trefoil parameters in the space of C^∞ vector fields on \mathbf{R}^3 are doubly as complicated when compared to homoclinic bifurcations. This should be contrasted with the results of [16], where it was proven a two-dimensional parameter space cannot be used to completely describe the bifurcations around heteroclinic vector fields like F_p .

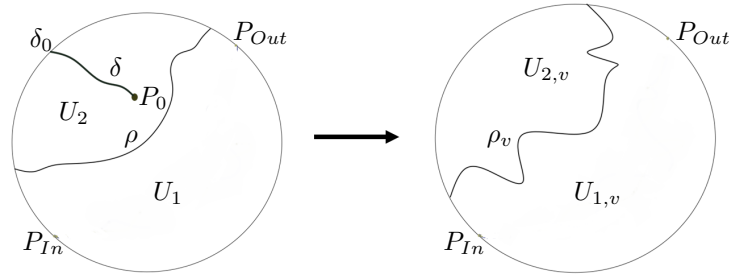


FIGURE 74. the deformation of U_p (on the left) to U_v (on the right). The curve ρ is deformed to ρ_v . For simplicity, U_p and U_v are sketched as discs rather than half-planes.

We now study how the dynamical complexity given by Th.3.15 wears off on nearby vector fields in the parameter space P . That is, we will now prove that given a trefoil parameter p in P and given any $n > 0$, provided a parameter v in the parameter space P is sufficiently close to p , the Rössler system corresponding to v generates at least n periodic trajectories. This has the following heuristic meaning - the closer the parameter v is to a trefoil parameter p , the more complex are the dynamics of the Rössler system corresponding to v - or, in other words, the dynamical complexity given by Th.3.15 "wear off" on nearby vector fields.

Despite the simple formulation, the proof would be very technical - as it would rely on constructing explicit (local) homotopies of the first-return map f_p , and proving these homotopies satisfy very specific topological conditions. However, the idea behind the proof is relatively simple, and based off the following intuition - if $p \in P$ is a trefoil parameter, by Th.3.15 the dynamics of the flow are essentially those of a suspended Smale Horseshoe map. As such, since suspended Smale Horseshoes are hyperbolic on their periodic trajectories (see, for example, [3]), we would expect every periodic trajectory given by Th.3.15 to persist under sufficiently small perturbations

of the vector field.

In practice, due to Prop.4.1 we cannot assume any hyperbolicity condition on any of the periodic trajectories given by Th.3.15. Therefore, to prove the persistence of periodic dynamics we will take a different route, and apply the notion of the Fixed-Point Index to the first-return map of the flow (see Ch.VII.5 in [4]). The reason we do so is because the Fixed-Point Index allows us to "ignore" the non-hyperbolic nature of the flow, and treat the periodic dynamics as a homotopy-invariant of the first-return map. In more detail, whenever the Fixed-Point Index is non-zero, it serves as a homotopy-invariant indicator for the existence of periodic points - as such, it allows us to study the persistence of periodic dynamics in the absence of hyperbolicity conditions.

To begin, let us first recall several facts and notations. First, given a trefoil parameter $p \in P$, $p = (a, b, c)$, recall $f_p : \overline{U_p} \rightarrow \overline{U_p}$ always denotes the first-return map generated by the Rössler system on the half-plane $U_p \subseteq \{y = 0\}$ (wherever defined - see Lemma 2.1) - in particular, recall $U_p = \{(x, -\frac{x}{a}, z) \mid -z + \frac{x}{a} < 0\}$. Additionally, recall the curve ρ given by Cor.3.26 which partitions $\overline{U_p} \setminus \rho$ into two components, U_1 and U_2 - and further recall we denote the one-sided shift by $\sigma : \{1, 2\}^{\mathbb{N}} \rightarrow \{1, 2\}^{\mathbb{N}}$. Now, let $v \in P$, $v = (a', b', c')$ be some parameter - by the parameterization of U_p , as we smoothly deform the vector field F_p to F_v through the parameter space, the half-plane U_p is smoothly deformed to the half-plane U_v . Consequentially, the curve $\rho \subseteq \overline{U_p}$ is deformed to some curve $\rho_v \subseteq \overline{U_v}$ - which implies U_1 and U_2 are continuously deformed to $U_{1,v}$ and $U_{2,v}$, the components of $\overline{U_v} \setminus \rho_v$ (see the illustration in Fig.74).

To continue, denote by $f_v : \overline{U_v} \rightarrow \overline{U_v}$ the first-return map corresponding to the vector field F_v (wherever defined in $\overline{U_v}$ - see Lemma 2.1), and set I_v as the maximal invariant set of f_v in $\overline{U_v} \setminus \rho_v$ - that is, I_v is the maximal collection of initial conditions $x \in \overline{U_v} \setminus \rho_v$ whose forward trajectory never hits ρ_v or diverges to ∞ . Finally, since by definition $I_v \subseteq (U_{1,v} \cup U_{2,v})$ it follows there exists a symbolic coding $\pi_v : I_v \rightarrow \{1, 2\}^{\mathbb{N}}$ s.t. $\pi_v \circ f_v = \sigma \circ \pi_v$. With these ideas and notations in mind, we now prove the following:

Theorem 4.4. *Let $p \in P$ be a trefoil parameter, and let $s \in \{1, 2\}^{\mathbb{N}}$ be periodic of minimal period k that is not the constant $\{1, 1, 1, \dots\}$. Then, for all parameters $v \in P$ sufficiently close to p we have:*

- $s \in \pi_v(I_v)$.
- $\pi_v^{-1}(s)$ contains at least one periodic point x_s for f_v , of minimal period k .
- The functions f_v, f_v^2, \dots, f_v^k are all continuous at x_s .
- π_v is continuous at $x_s, f_v(x_s), \dots, f_v^{k-1}(x_s)$.

Consequentially, given any n , provided v is sufficiently close to p the Rössler system corresponding to v generates at least n distinct periodic trajectories.

Proof. From now on to the end of the proof, for any parameter v in the parameter space P , denote by F_v the corresponding vector field (see Eq.1.5) - moreover, from now on, p would always denote a trefoil parameter. The proof of Th.4.4 would be technical and based on direct topological analysis of the first-return map. Therefore, before giving an outline of the proof, we first recall several facts from Section 3 (and in particular, the proof of Th.3.15). To begin, recall the topological disc $D_\alpha \subseteq U_p$, bounded by the curve $L \cup l \cup \{P_{In}, P_{Out}\}$ - as proven in Prop.3.4, D_α is a topological disc on U_p , and as shown in Lemma 3.1, the heteroclinic trefoil knot intersects $\overline{D_\alpha}$ in precisely one interior point, P_0 , thus making $D_\alpha \setminus \{P_0\}$ homeomorphic to a punctured disc (see the illustration in Fig.32). Moreover, as proven in Lemma 3.2, the first-return map $f_p : \overline{D_\alpha} \setminus \{P_0\} \rightarrow \overline{D_\alpha} \setminus \{P_0\}$ is well defined (by Remark 3.9, we also know f_p is surjective).

Now, recall there exists another cross-section $H_p \subseteq D_\alpha$, also a topological disc (as defined in Lemma 3.12) - and that we proved Th.3.15 by studying the map $f_p : \overline{H_p} \setminus \overline{\delta} \rightarrow D_\alpha$ (recall f_p is continuous on H_p - see Lemma 3.12). In more detail, we proved the existence of an invariant set Q for f_p in $\overline{H_p} \setminus \overline{\delta}$ (where δ is as in Prop.3.8) s.t. the following is satisfied:

- $Q \subseteq \overline{U_p} \setminus \rho$, and f_p is continuous on Q - in particular, Q is a subset of the invariant set I given by Cor.3.26.
- Q includes infinitely many periodic orbits for f_p .
- There exists a continuous map $\pi : Q \rightarrow \{1, 2\}^{\mathbb{N}}$ s.t. $\pi \circ f_p = \sigma \circ \pi$ (where $\sigma : \{1, 2\}^{\mathbb{N}} \rightarrow \{1, 2\}^{\mathbb{N}}$ denotes the one-sided shift).
- $\pi(Q)$ includes every periodic sequence $s \in \{1, 2\}^{\mathbb{N}}$
- For every periodic $s \in \{1, 2\}^{\mathbb{N}}$ of minimal period k , $D_s = \pi^{-1}(s)$ is connected - and includes a periodic point x_s of minimal period k for f_v . Moreover, whenever s is not the constant $\{1, 1, 1, \dots\}$, x_s is not a fixed-point for the flow.

With these ideas in mind, we are now ready to give a general outline of the proof of Th.4.4. The general idea is as follows - we begin by constructing an isotopy of $f_p : \overline{H_p} \setminus \overline{\delta} \rightarrow \overline{D_\alpha}$ to a Smale Horseshoe map, which we use to prove

the Fixed-Point Index (as defined below) on periodic orbits in Q is non-zero. Following that, we prove that for any parameter $v \in P$ sufficiently close to p , the perturbation of F_p to F_v generates a homotopy between the first-return maps for F_v and F_p - then, using the the invariance of the Fixed-Point Index under homotopies Th.4.4 would follow.

To begin, fix some periodic $s \in \{1, 2\}^{\mathbb{N}}$ which is not the constant $\{1, 1, 1, \dots\}$ - by the construction of Q in the proof of Th.3.15 in Stages *I*, *II* and *III*, this implies D_s lies away from the fixed-point P_{In} . Now, define $Per(s) = \{x \in D_s \mid f_p^k(x_s) = x_s\}$ - it is easy to see $Per(s)$ is compact in $\overline{H_p}$. Moreover, since for every $0 \leq j < k$ we have $f_p^j(D_s) \cap D_s = \emptyset$, it is also immediate that if $x \in Per(s)$, then x is periodic of minimal period k for f_p . We first prove the following technical (yet useful) fact:

Lemma 4.5. *Let $p \in P$ be a trefoil parameter, and let $s \in \{1, 2\}^{\mathbb{N}}$ be periodic of minimal period k s.t. s is not the constant $\{1, 1, 1, \dots\}$. Then, there exists a connected open set $V_s \subseteq H_p$, $Per(s) \subseteq V_s$ s.t. the following is satisfied:*

- f_p^k has no fixed points in $V_s \setminus Per(s)$.
- $Per(s)$ is compact in V_s .
- For every $0 \leq i < j \leq k - 1$, $f_p^j(V_s) \cap f_p^i(V_s) = \emptyset$.
- f_p, \dots, f_p^k is continuous on V_s .

Proof. We first make some general observations. Let us first recall we have $\partial D_\alpha = L \cup \{P_{In}, P_{Out}\}$ (see Prop.3.4), and that since the curve L is the intersection between the two-dimensional invariant manifold W_{Out}^s and the half-plane U_p (see the illustration in Fig.75) - consequentially, there are no periodic orbits for f_p in L . Additionally, using a similar argument to the one used to prove Prop.3.8, it follows every component of $f_p^{-k}(l)$, $k \geq 0$ is a curve in $\overline{D_\alpha}$ with two endpoints on $\cup_{0 \leq j \leq k-1} f_p^{-j}(l)$ - see the illustration in Fig.75.

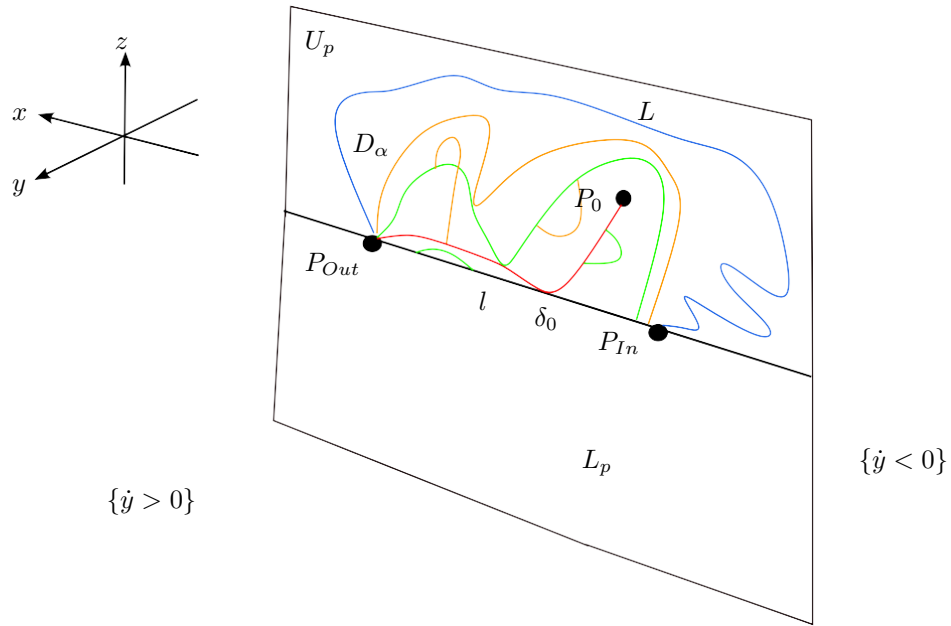


FIGURE 75. The cross-section U_p . L is the blue curve, l is the straight line connecting P_{In} and P_{Out} , while $f_p^{-1}(l)$, $f_p^{-2}(l)$ and $f_p^{-3}(l)$ are the red, green and orange arcs (respectively). Every component in $f_p^{-j}(l)$ is a curve with endpoints on $\cup_{i=0}^{j-1} f_p^{-i}(l)$. In this scenario, H_p is the sub-region of D_α trapped between l , $f_p^{-1}(l)$ and L . δ is the red arc connecting P_0 and δ_0 - see Prop.3.8.

We now claim that $Per(s) \cap (\cup_{n \geq 0} f_p^{-n}(l)) = \emptyset$. To see why, assume by contradiction this is not the case - which implies there exists some $x \in Per(s)$ and $j \geq 0$ s.t. $f_p^j(x) \in l$. Using a similar argument to the proof of Lemma 3.23, this implies there exists an isotopy of $f_p : \overline{H_p} \rightarrow \overline{D_\alpha}$ which collapses x to P_{In} , similarly to as illustrated in Fig.63. Since all the periodic points in Q given by Th.3.15 are uncollapsible (per Th.3.17 and Cor.3.27), by $Per(s) \subseteq Q$ we derive a contradiction. Consequentially, it follows $Per(s) \cap (\cup_{n \geq 0} f_p^{-n}(l)) = \emptyset$.

To continue, consider $\{x_n\}_n$, a sequence of periodic points in $\overline{D_\alpha} \setminus Per(s)$ which tends to some $x \in Per(s)$ - we now claim the minima period of f_p on elements in $\{x_n\}_n$ is unbounded. To do so, assume by contradiction the assertion is incorrect, i.e., that the period of x_n is bounded - since $x \in Per(s)$, by the continuity of the flow this would imply the minimal period of x_n has to be k (for any sufficiently large n). Since $\{1, 2\}^{\mathbb{N}}$ only has a finite number of

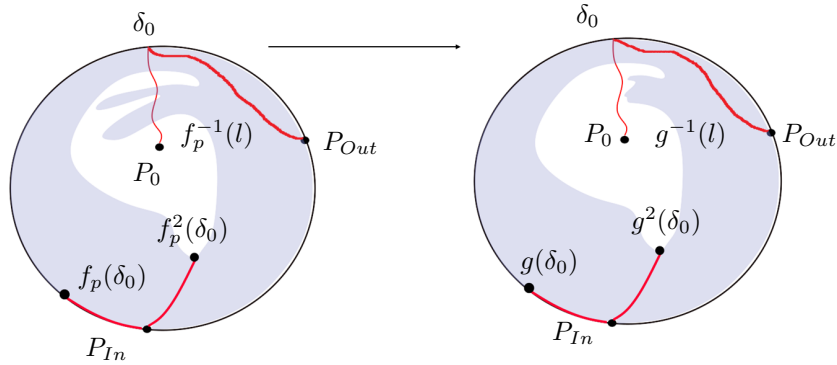


FIGURE 76. l is the left-arc on the circle connecting P_{In} and P_{Out} , the shaded region is $f_p(\overline{H_p} \setminus \delta)$ (where $\delta \subseteq f_p^{-1}(l)$ is the red curve connecting P_0 and δ_0), while the red arcs are $f_p(\delta)$ and $f_p^2(\delta)$. As $\delta \subseteq f_p^{-1}(l)$, it is easy to see the isotopy of $f_p : \overline{H_p} \setminus \delta \rightarrow \overline{D_\alpha}$ to $g : \overline{H_p} \setminus \delta \rightarrow \overline{D_\alpha}$ above removes periodic orbits not in Q , while preserving Q due to Cor.3.27.

periodic symbols of minimal period k , and because for every periodic $\omega, s \in \{1, 2\}^{\mathbb{N}}$ both $Per(s)$ and $Per(\omega)$ are compact and disjoint, it follows that for any sufficiently large n , $x_n \notin Q$ - therefore, without any loss of generality, we may assume $\{x_n\}_n \cap Q = \emptyset$. Consequentially, $x \in \partial D_s$ - and since $Per(s) \cap (\cup_{n \geq 0} f_p^{-n}(l)) = \emptyset$, by $\{x_n\}_n \cap Q = \emptyset$ it follows x is separated from $\{x_n\}_n$ by the components of $\cup_{n \geq 0} f_p^{-n}(l)$, hence the set $\cup_{n \geq 0} f_p^{-n}(l)$ accumulates on x .

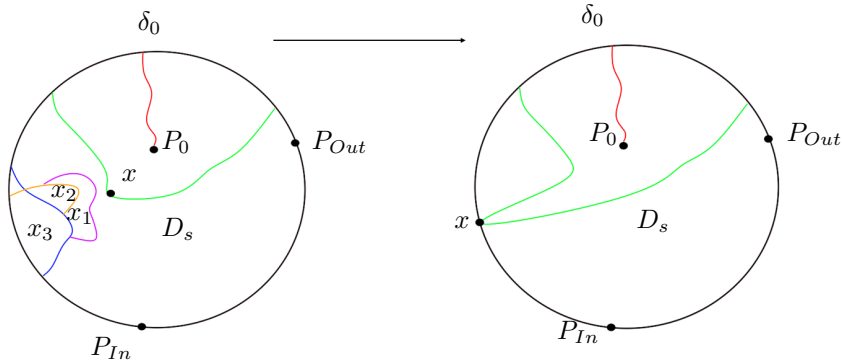


FIGURE 77. l is the left-arc on the circle connecting P_{In} and P_{Out} , the shaded region is $f_p(\overline{H_p} \setminus \delta)$ (where δ is the red curve connecting P_0 and δ_0), while the red arcs are $f_p(\delta)$ and $f_p^2(\delta)$. As $\{x_n\}_n$ accumulates on x , the isotopy described in the proof of Lemma 4.5 and depicted in Fig.76 pushes the sequence $\{x_n\}_n$ towards l , thus pushing $g^j(x)$ to l as well (for some j - in this illustration, we chose $j = 1$).

Now, deform $f_p : \overline{H_p} \setminus \delta \rightarrow \overline{D_\alpha}$ isotopically to some $g : \overline{H_p} \setminus \delta \rightarrow \overline{D_\alpha}$ by destroying all the periodic orbits generated by $\{x_n\}$ as illustrated in Fig.76 and 77 - moreover, we do so s.t. the assumptions in Cor.3.27 are satisfied. In more detail, we do so by collapsing to singletons the arcs in $\cup_{n \geq 0} f_p^{-n}(l)$ and domains in $\overline{D_\alpha} \setminus (\cup_{n \geq 0} f_p^{-n}(l))$ which include elements of $\{x_n\}_n$ (we can do so by $\{x_n\}_n \cap Q = \emptyset$). Because x is separated from $\{x_n\}_n$ by the set $\cup_{n \geq 0} f_p^{-n}(l)$, as x is inseparable from $\{x_n\}_n$ it follows the isotopy described above pushes x to some arc γ on $f_p^{-j}(l)$ - which, consequentially, implies $g^j(x) \in l$ (see the illustration in Fig.77). However, this implies we can isotopically deform $g : \overline{H_p} \setminus \delta \rightarrow \overline{D_\alpha}$ to $g' : \overline{H_p} \setminus \delta \rightarrow \overline{D_\alpha}$ by collapsing x to P_{In} as in Fig.76 - and again, using an argument similar to Lemma 3.23, we have a contradiction. Therefore, by this contradiction we conclude that if $\{x_n\}_n$ is a sequence of periodic orbits for f_p which approximates $x \in Per(s)$, the minimal periods of $\{x_n\}_n$ have to be unbounded.

Consequentially, since $Per(s) \cap \partial H_p = \emptyset$, it follows there exists an open, connected neighborhood $V_s \subseteq H_p$ s.t. $Per(s) \subseteq V_s$ s.t. there are no fixed points for f_p^k in $V_s \setminus Per(s)$ - hence $Per(s)$ is compact in V_s . Now, recall f_p, \dots, f_p^k are all continuous on D_s , and that for every $0 \leq i < j \leq k-1$ we have $f_p^j(D_s) \cap f_p^i(D_s) = \emptyset$ - moreover, recall that D_s is in the invariant set of f_p in $\overline{H_p} \setminus \delta$, which implies it also lies away from $H_p \cap (\cup_{n \geq 1} f_p^{-n}(l))$. By $Per(s) \subseteq D_s$ and because D_s is connected, it follows we can choose V_s s.t. the flow lines emanating from V_s and it to $f_p(V_s), \dots, f_p^k(V_s)$ never hit l , i.e., they are all transverse to the half-plane U_p - consequentially, by Prop.3.8 it follows f_p, \dots, f_p^k are all continuous on V_s . Moreover, by $f_p^j(D_s) \cap f_p^i(D_s) = \emptyset$ we may also choose V_s s.t. for every $0 \leq i < j \leq k-1$ we have $f_p^j(V_s) \cap f_p^i(V_s) = \emptyset$. The proof of Lemma 4.5 is now complete. \square

To continue, we now recall the notion of the Fixed-Point Index (see [4]). To do so, let $O \subseteq \mathbf{R}^2$ be an open set, and let $f : O \rightarrow \mathbf{R}^2$ be continuous s.t. the set $\{x \in O | f(x) = x\}$ is compact in O . The **Fixed-Point Index** of f would be defined as the degree of $f(x) - x$ on O - it is well-known that when f has no fixed points in O its Fixed-Point Index is 0 (see Lemma VII.5.5 in [4]). Now, let $f_t : O \rightarrow \mathbf{R}^2$, $t \in [0, 1]$ be a homotopy of continuous maps, and for every $t \in [0, 1]$ set $F_t = \{x \in O | f_t(x) = x\}$. As proven in Th.VII.5.8 in [4] (termed "homotopy invariance"), provided $\cup_{t \in [0, 1]} F_t \times \{t\}$ is compact in $O \times [0, 1]$, the fixed point index is invariant under the homotopy. Or in other words, given a homotopy as described above, if the Fixed-Point Index for f_0 is non-zero, the same is true for f_1 - that is, if f_0 has a fixed point in O of non-zero index, f_1 also has at least one fixed point in O .

We now proceed to compute the Fixed Point Index of f_p^k on V_s . We begin by isotopically deforming $f_p : \overline{H_p} \rightarrow \overline{D_\alpha}$ by an isotopy $g_t : \overline{H_p} \rightarrow \overline{D_\alpha}$, $t \in [0, 1]$ s.t. $g_0 = f_p$, and g_1 is a Smale Horseshoe map $H : ABCD \rightarrow \overline{D_\alpha}$ as appears below in Fig.78 (i.e., we deform H_p to a topological rectangle $ABCD$). Moreover, we do so s.t. every g_t satisfies the assumptions of Lemma 3.27.

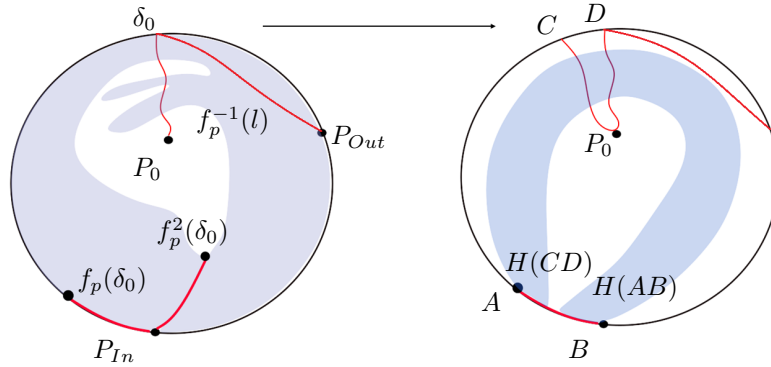


FIGURE 78. The isotopy deforming $f_p : \overline{H_p} \setminus \delta \rightarrow \overline{D_\alpha}$ to the Smale Horseshoe map $H : ABCD \rightarrow \overline{D_\alpha}$. $ABCD$ is obtained from $\overline{H_p} \setminus \delta$ by opening P_{In} to the AB side and δ to the CD side.

Consequentially, since $Per(s) \subseteq Q$, by Cor.3.27 the periodic orbits in $Per(s)$ persist and vary continuously throughout the isotopy - i.e., for every $1 \geq t > 0$ the set $Per(s) = Per_0(s)$ is continuously deformed to $Per_t(s) = \{x \in V_s | g_t^k(x) = x\}$, a collection of periodic points of minimal period k for g_t . It is easy to see the conclusion of Lemma 4.5 also holds for every g_t - and since the set $Per(s)$ varies continuously with t , it follows we can choose the isotopy s.t. we have the following:

- g_s^k has no fixed points in $V_s \setminus Per_t(s)$.
- $Per_t(s)$ is compact in V_s .
- For every $0 \leq i < j \leq k - 1$, $g_t^j(V_s) \cap g_t^i(V_s) = \emptyset$.
- g_t, \dots, g_t^k is continuous on V_s .

Consequentially, it follows there exist an isotopy of continuous maps $g_t^k : V_s \rightarrow \overline{D_\alpha}$, $t \in [0, 1]$ s.t. for every t , g_t^k has no fixed points in $V_s \setminus Per_t(s)$. Consequentially, the set $\cup_{t \in [0, 1]} Per_t(s) \times \{t\}$ is compact in $V_s \times [0, 1]$. Applying the invariance of the Fixed-Point Index under homotopies to the isotopy $g_t^k : V_s \rightarrow \overline{D_\alpha}$, $t \in [0, 1]$, we now conclude:

Corollary 4.6. *With the notations above, the fixed-point index of f_p^k on V_s is negative.*

Proof. By the invariance of the Fixed-Point Index under homotopies mentioned above, it immediately follows the Fixed-Point Index of $g_t^k = f_p^k$ on V_s is the same as that of $g_1^k = H^k$ on V_s (where H is a Smale Horseshoe) - therefore, provided we prove the Fixed Point Index of H^k on V_s is negative, we are done. To do so, first note H is a \cap -Horseshoe map (see Fig.78), which implies it is orientation-preserving - hence its differential on its invariant set has one eigenvalue in $(1, \infty)$ and another at $(0, 1)$. It therefore follows that given any periodic orbit for H of minimal period k , the degree of $H^k - Id$ is -1 .

Since for every $k > 0$ the Smale Horseshoe map H has only a finite number of periodic orbits of period k (minimal or not), it follows $Per_1(s)$ is finite. Consequentially, by the additivity of the Fixed-Point Index (see Lemma VII.5.6 in [4]), it follows the Fixed-Point Index of H^k in V_s is given by $\sum_{x \in Per_1(s)} -1 = I_1$. It follows I_1 is negative, and Cor.4.6 now follows. \square

Remark 4.7. *With just a little bit of work, one can prove $I_1 = -1$. We, however, will not need it.*

Having proven Cor.4.6, we now use it to conclude the proof of Th.4.4. To do so, recall we assume $p = (a, b, c)$ is a trefoil parameter, and consider v , another parameter in P s.t. $v \neq p$, $v = (a', b', c')$. Additionally, recall that given

any $v \in P$, the cross-section $\overline{U}_p = \{(x, -\frac{x}{a}, z) | -z + \frac{x}{a} \leq 0\}$ is smoothly deformed to $\overline{U}_v = \{(x, -\frac{x}{a'}, z) | -z + \frac{x}{a'} \leq 0\}$ (see the discussion before Lemma 2.1) - therefore, since V_s is an open, connected set inside U_p it follows that when the vector field F_p is perturbed to F_v , the set V_s (which is a subset of H_p , that in itself is a subset of U_p) is continuously deformed to V_v , an open subset of the half-plane U_v (see the illustration in Fig.79).

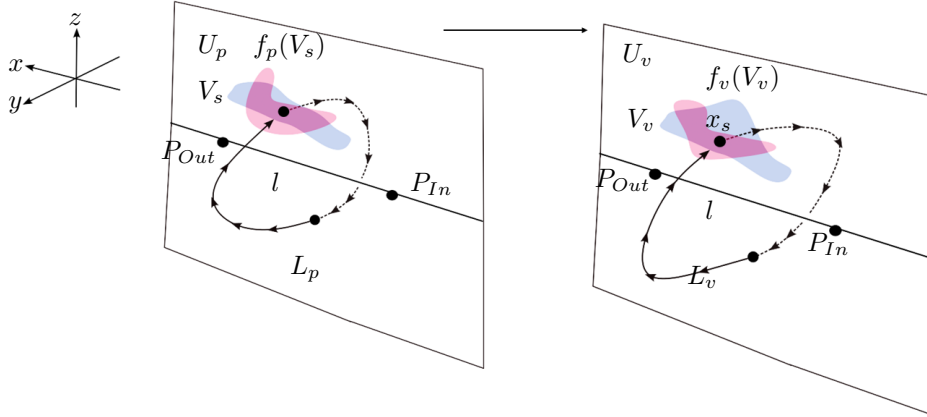


FIGURE 79. The sets V_s and V_v in blue, with $f_p(V_s)$ and $f_v(V_v)$ in red (for simplicity, we assume $s \in \{1, 2\}^{\mathbb{N}}$ is periodic of minimal period 1). As the vector field F_p is smoothly deformed to F_v through P , it induces a homotopy between $f_p : V_s \rightarrow U_p$ and $f_v : V_v \rightarrow U_v$.

To continue, recall we constructed V_s in Lemma 4.5 s.t. the flow lines connecting $V_s, f_p(V_s), \dots, f_p^k(V_s)$ are all transverse to U_p . Recalling the cross-section H_p is bounded in U_p , it follows V_s is pre-compact - and therefore, whenever v is sufficiently close to the trefoil parameter p the first-hit map $f_v : V_v \rightarrow U_v$ w.r.t. the vector field F_v is well defined, and so are its iterates f_v^2, \dots, f_v^k . Consequentially, it follows that given any $x \in \overline{V}_v$ whenever v is sufficiently close to p , the flow lines for F_v connecting $V_v, f_v(V_v), \dots, f_v^k(V_v)$ are all transverse to U_v (see the illustration in Fig. 79) - which implies f_v, \dots, f_v^k are all continuous on V_v . Similarly, since by Lemma 4.5 for every $0 \leq i < j \leq k-1$ we have $f_p^j(V_s) \cap f_p^i(V_s) = \emptyset$, it follows that provided v is sufficiently close to p , for every $0 \leq i < j \leq k-1$ we also have $f_v^j(V_v) \cap f_v^i(V_v) = \emptyset$. Summarizing our results, we conclude:

Corollary 4.8. *Let $p \in P$ be a trefoil parameter, let V_s be as in Lemma 4.5, and let V_v be as above. Then, provided $v \in P$ is sufficiently close to p , we have the following:*

- f_v, \dots, f_v^k are all continuous on V_v .
- For every $0 \leq i < j \leq k-1$, $f_v^i(V_v) \cap f_v^j(V_v) = \emptyset$.
- $f_p^k : V_s \rightarrow U_p$ are homotopic (see the illustration in Fig.79).

Consequentially, if $x \in V_v$ is periodic for f_v , its minimal period is at least k .

Our next goal is to compute the Fixed-Point Index of f_v^k in V_v - provided we show it is non-zero, by Cor.4.8 it would immediately follow f_v has a periodic point of minimal period k in V_v . To this end, we first prove:

Lemma 4.9. *Let $p \in P$ be a trefoil parameter. Then, there exists an neighborhood $O \subseteq P$, s.t. $p \in O$, and for every $v \in O$, f_v^k has no fixed points in ∂V_v .*

Proof. We prove Lemma 4.9 by contradiction. To this end, assume the Lemma is incorrect - that is, assume there exists a sequence $\{(x_n, v_n)\}_n \subseteq \cup_{v \in P} V_v \times \{v\}$ s.t. the following holds:

- $(x_n, v_n) \in \cup_{v \in P} V_v \times \{v\}$ for every n .
- $v_n \rightarrow p$.
- $f_{v_n}^k(x_n) = x_n$.
- $(x_n, v_n) \rightarrow \partial V_s \times \{p\}$.

Let $x \in \partial V_s$ be the limit (or partial limit) of x_n . Since by construction $\overline{V}_s \subseteq \overline{H}_p$, from $\overline{H}_p \subseteq \overline{D}_\alpha$ and by both Prop.3.4 and Lemma 3.2 it follows the trajectory of x is bounded. Now, note the vector fields $\{F_{v_n}\}_n$ converge to F_p in the C^∞ metric on vector fields in \mathbf{R}^3 - therefore, because every x_n lies on a periodic trajectory for F_{v_n} which intersects the half-plane U_{v_n} at most k times, it follows x must lie on T , a periodic trajectory for F_p , and satisfy $f_p^k(x) = x$. However, this contradicts Lemma 4.5 where we proved that for all $x \in \partial V_s$, $f_p^k(x) \neq x$ - hence no such sequence exists and the assertion follows. \square

As a consequence of Lemma 4.9, Cor.4.6, and Cor.4.8, it follows that for every $v \in P$ sufficiently close to a trefoil parameter $p \in P$, we have:

Corollary 4.10. *Let $p \in P$ be a trefoil parameter - then, provided $v \in P$ is sufficiently close to p the Fixed Point Index of $f_v^k : V_v \rightarrow \overline{U_v}$ is negative - hence, f_v has a periodic point x_s in V_v of minimal period k . Moreover, f_v, \dots, f_v^k are continuous on x_s (see the illustration in Fig.79).*

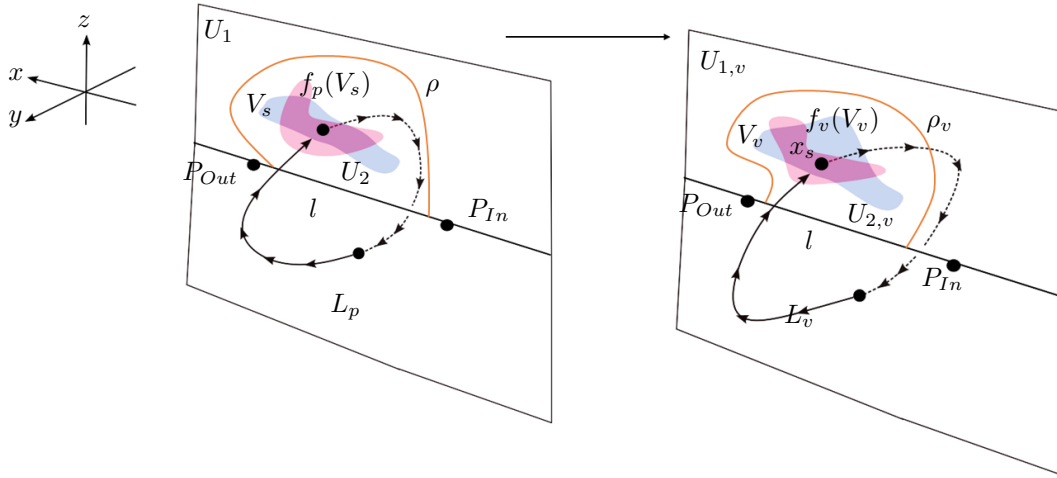


FIGURE 80. The sets V_s and V_v in blue, with $f_p(V_s)$ and $f_v(V_v)$ in red (for simplicity, we assume $s \in \{1, 2\}^{\mathbb{N}}$ is periodic of minimal period 1). The curves ρ and ρ_v are sketched in orange - as ρ is continuously deformed to ρ_v , U_i is continuously deformed to $U_{i,v}$, $i = 1, 2$. Provided v is sufficiently close to p , $\pi_v(x_s) = s$.

We can now conclude the proof of Th.4.4. To do so, first recall we originally chose $s \in \{1, 2\}^{\mathbb{N}}$ s.t. it is periodic of minimal period k , $s = \{i_0, i_1, i_2, \dots, i_k, i_0, \dots\}$ and not the constant $\{1, 1, 1, \dots\}$. Additionally, recall the curve $\rho \subseteq U_p$ and the curve ρ_v which divides the cross-section U_v to $U_{1,v}, U_{2,v}$ - and additionally, recall the invariant set I_v , and the map $\pi_v : I_v \rightarrow \{1, 2\}^{\mathbb{N}}$ (see the discussion before Th.4.4 and the illustration in Fig.74 and Fig.80). Having proven Cor.4.10, all that remains to conclude the proof of Th.4.4 is to prove the point x_s given by Cor.4.10 lies inside I_v , that $\pi_v(x_s) = s$, and that π_v is continuous on the finite sequence $\{x_s, f_v(x_s), \dots, f_v^{k-1}(x_s)\}$. Note that since f_v, \dots, f_v^k are continuous at x_s by Cor.4.10, provided $x_s \in I_v$ then π_v is automatically continuous at $x_s, f_v(x_s), \dots, f_v^{k-1}(x_s)$ - therefore, we need only prove that $x_s \in I_v$, and that $\pi_v(x_s) = s$.

However, that is immediate - recall that by Cor.3.26, for every $0 \leq j \leq k$ we have $f_p^j(D_s) \subseteq U_{i_j}$ - where $s = \{i_0, i_1, \dots, i_k, i_0, \dots\}$. It therefore follows by $Per(s) \subseteq D_s$ that we can choose V_s to be a sufficiently small neighborhood of $Per(s)$ s.t. for every $0 \leq j \leq k$, $f_p^j(V_s) \subseteq U_{i_j}$. Because U_p is continuously deformed to U_v (and consequentially, the curve ρ is continuously deformed to ρ_v) it follows that provided $v \in P$ is sufficiently close to the trefoil parameter p , the set V_v also satisfies $f_v^j(V_v) \subseteq U_{i_j,v}$ for all $0 \leq j \leq k$ (see the illustration in Fig.80). By $x_s \in V_v$, $f_v^k(x_s) = x_s$ and because the minimal period of x_s w.r.t. f_v is k , this implies $\pi(x_s) = s$ - and Th.4.4 now follows. \square

Remark 4.11. *Given $v \in P$, the set $\pi_v(I_v)$ is never empty. It is easy to see the curve ρ from Cor.3.26 does not include the fixed point P_{In} . As such, the same is true for ρ_v - or in other words, for every $v \in P$, $P_{In} \in U_{1,v}$. Since P_{In} is a fixed-point, it follows $P_{In} \in I_v$ and consequentially that the constant $\{1, 1, 1, \dots\}$ is in $\pi_v(I_v)$.*

Remark 4.12. *In [15], the Fixed-Point Index was applied to prove the existence of infinitely many periodic trajectories in the Rössler system.*

Remark 4.13. *Given a trefoil parameter $p \in P$ with its corresponding vector field F_p , it is easy to see the proof of Th.4.4 above can be generalized for sufficiently small C^k perturbations of F_p , where $k \geq 1$.*

5. DISCUSSION:

Before we conclude this paper, we would like to make several remark. To begin, first note both Th.3.15 and Th.4.4 are essentially facts about the periodic dynamics of the Rössler system - and that their proof is essentially two-dimensional. It is well-known in the theory of two-dimensional dynamics that one can study the topological dynamics of a surface homeomorphism by studying its class of essential periodic dynamics (see [12] for a review of the topic). This leads us to ask the following question: can we describe the dynamics (and bifurcations) of the Rössler system in and around trefoil parameters by studying its periodic trajectories?

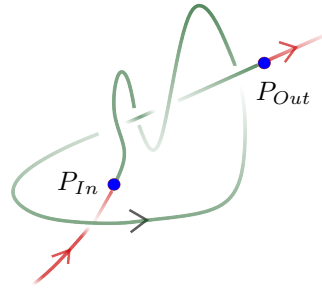


FIGURE 81. A heteroclinic knot more complex than a trefoil.

This question can and will be studied rigorously. In a series of future papers it will be proven that by applying ideas from [9],[6] and [7], it is possible to classify the knot-types of periodic trajectories in the set Q - and prove their persistence under perturbations in the parameter space P . This would allow to reduce the flow in and around trefoil parameters to a one-dimensional model, which also acts as a geometrical model describing the flow.

Another natural question arising from both Th.4.4 and Th.3.15 is the following - can these results be extended to other heteroclinic knots in the Rössler system? At the moment, we do not have an answer for this question - and moreover, the our knowledge, no study (numerical or analytical) attempted to study which heteroclinic knots are generated by the Rössler system. Therefore we will be content with the following conjecture:

Conjecture 5.1. *Let $p \in P$ be a heteroclinic parameter for the Rössler system (not necessarily a trefoil parameter - see Def.3.1). Then, provided the heteroclinic knot it generates is complex at least like a trefoil knot, it generates infinitely many periodic trajectories.*

Finally, another interesting question which arises from both Th.3.15 and Th.4.4 is their possible connection with the theory of homoclinic bifurcations. The theory of homoclinic bifurcations had been extensively applied to numerically study and analyze the onset of chaos in the Rössler system (see [30] and the references therein) - and yet, surprisingly, save for Prop.4.2 and Prop.3.14, none of the results proven in this paper depend on that theory. Therefore, one is motivated to ask the following open questions, with which we conclude this paper:

- (1) Motivated by Cor.3.14 and Prop.4.2, we first ask the following - what is the connection between heteroclinic trajectories in the Rössler system and homoclinic bifurcation phenomena in the Rössler system?
- (2) Let us now further note that in Th.3.15 (and to a lesser extent, also in Th.4.4) the bounded heteroclinic trajectory serves a somewhat analogous role to that of the homoclinic trajectory in the proof of Shilnikov's Theorem. This motivates us to ask the following - does there exist a general theory of heteroclinic bifurcations, s.t. Th.3.15 and Th.4.4 are special instances of facts within it?
- (3) Finally, if the answer to the question above is positive, how much of this theory is analogous to the theory of homoclinic bifurcations?

REFERENCES

- [1] E.N Lorenz. "Deterministic Nonperiodic Flow". In: *Journal of the Atmospheric Sciences* 20 (1963), pp. 130–141.
- [2] L. Shilnikov. "A case of the existence of a denumerable set of periodic motions". In: *Sov. Math. Dok.* 6 (1967), pp. 163–166.
- [3] S. Smale. "Differentiable dynamical systems". In: *Bull. Amer. Math. Soc.* 73 (1967), pp. 747–817.
- [4] A. Dold. *Lectures on Algebraic Topology*. Springer, 1972.
- [5] O.E. Rössler. "An equation for continuous chaos". In: *Physics Letters A* 57 (1976), pp. 397–398.
- [6] K.T. Alligood, J.M. Paret, and J.A. Yorke. "Geometric Dynamics". In: Springer Verlag, 1983. Chap. 1 - *An index for the continuation of relatively isolated sets of periodic orbits*.
- [7] J.S. Birman and R.F. Williams. "Knotted periodic orbits in dynamical systems II: Knot holders for fibered knots". In: *Contemporary Mathematics* 20 (1983), pp. 1–60.
- [8] O.E. Rössler. "The Chaotic Hierarchy". In: *Zeitschrift für Naturforschung A* 38 (1983), pp. 788–801.
- [9] K.T. Alligood and J.A. Yorke. "Families of periodic orbits: Virtual periods and global continuability". In: *Journal of Differential Equations* 55 (1984), pp. 59–71.
- [10] P. Gaspard, R. Kapral, and G. Nicolis. "Bifurcation Phenomena near Homoclinic Systems: A Two-Parameter Analysis". In: *Journal of Statistical Physics* 35 (5/6) (1984), pp. 597–727.

- [11] M. Handel. “Global shadowing of pseudo-Anosov homeomorphisms”. In: *Ergodic Theory and Dynamical Systems* 5 (3) (1985), pp. 373–377.
- [12] P. Boyland. “Topological methods in surface dynamics”. In: *Topology and its Applications* 58 (3) (1994).
- [13] M. Betsvina and M. Handel. “Train-tracks for surface homeomorphisms”. In: *Topology* 34 (1) (1995), pp. 109–140.
- [14] C. Letellier, P. Dutertre, and B. Maheu. “Unstable periodic orbits and templates of the Rössler system: Toward a systematic topological characterization”. In: *Chaos* 5, 271 (1995).
- [15] P. Zgliczynski. “Computer assisted proof of chaos in the Rössler equations and in the Hénon map”. In: *Nonlinearity* 10(1) (1997), pp. 243–252.
- [16] V.V Bykov. “On systems with separatrix contour containing two saddle-foci”. In: *Journal of Mathematical Sciences* 95 (1999), pp. 2513–2522.
- [17] M.T. Teryokhin and T.L. Paniflova. “Periodic Solutions of the Rössler System”. In: *Russian Mathematics* 43 (8) (1999), pp. 66–69.
- [18] L.O. Chua et al. *Methods of Qualitative Theory in Nonlinear Dynamics, Part II*. New Jersey: World Scientific, 2001.
- [19] J. Kennedy and J.A. Yorke. “Topological Horseshoes”. In: *Transactions of the American Mathematical Society* 353 (2001), pp. 2513–2530.
- [20] John W. Milnor. *Topology from the Differentiable viewpoint*. New Jersey: World Scientific, 2001.
- [21] L. Perko. *Differential Equations and Dynamical Systems, Third Edition*. Springer, 2001.
- [22] X.S. Yang, Yu Y., and Zhang S. “A new proof for existence of horseshoe in the Rössler system”. In: *Chaos, Solitons, and Fractals* 18 (2003), pp. 223–227.
- [23] J.C. Gallas. “The Structure of Infinite Periodic and Chaotic Hub Cascades in Phase Diagrams of Simple Autonomous Flows”. In: *International Journal of Bifurcation and Chaos* 20(2) (2010), pp. 197–211.
- [24] M.F.S. Lima and J. Llibre. “Global dynamics of the Rössler system with conserved quantities”. In: *J. Phys. A: Math. Theor.* 44 (2011).
- [25] R. Barrio, F. Blesa, and S. Serrano. “Topological Changes in Periodicity Hubs of Dissipative Systems”. In: *Phys. Rev. Lett.* 108, 214102 (2012).
- [26] R. Barrio, A. Shilnikov, and L.P. Shilnikov. “Chaos, CNN, Memristors and beyond – a festschrift for Leon Chua”. In: World Scientific, 2013. Chap. 33 - *Symbolic Dynamics and Spiral Structures due to the Saddle Focus Bifurcations*.
- [27] R. Barrio, F. Blesa, and S. Serrano. “Unbounded dynamics in dissipative flows: Rössler model”. In: *Chaos* 242 (2014).
- [28] M. Rosalie. “Templates and subtemplates of Rössler attractors from a bifurcation diagram”. In: *Journal of Physics A: Mathematical and Theoretical, IOP Publishing* 49(31) (2016).
- [29] M.R. Cândido, D. D. Novaes, and C. Valls. “Periodic solutions and invariant torus in the Rössler system”. In: *Nonlinearity* 33 4512 (2020), pp. 66–69.
- [30] S. Malykh et al. “Homoclinic chaos in the Rössler model”. In: *Chaos* 30 (2020).
- [31] T. Pinsky. “Analytical study of the Lorenz system: Existence of infinitely many periodic orbits and their topological characterization”. In: *Proceedings of the National Academy of Sciences* 120 (2023).